UCLA
COMPUTATIONAL AND APPLIED MATHEMATICS

Magnetoconvection in Rapidly Rotating Boussinesq and Compressible Fluids

C. A. Jones
P. H. Roberts

October 1989

CAM Report 89-30

Department of Mathematics
University of California, Los Angeles
Los Angeles, CA. 90024-1555

Magnetoconvection in rapidly rotating Boussinesq and compressible Fluids

C. A. Jones[1] and P. H. Roberts
Department of Mathematics
University of California
Los Angeles
California, CA 90024

Received:

Finite amplitude convection is considered in a plane fluid layer rotating with angular velocity Ω about a horizontal axis in the y-direction. The fluid is electrically conducting, and a uniform horizontal magnetic field of strength B_0 is applied horizontally, in the x-direction, perpendicular to the rotation axis. The gravitational acceleration, g is parallel to Oz. The layer is infinite in x-extent but is bounded laterally in the y-direction by vertical walls, which may be either be stress-free or be rigid, i.e. prevent fluid motion. The model is intended to simulate crudely conditions near the equator of the solar convection zone.

At the onset of convection in a stagnant layer, a Lorentz force, F, is created in the x-direction which, though weak, has a nonzero horizontal average that cannot be balanced by any other forces in the equation of motion. This force sets up a geostrophic flow, U, in the x-direction, i.e. a flow that depends on z alone. This flow affects F, and in a so-called "Taylor State" obliterates F. Such Taylor states are here shown to occur at small Elsasser numbers, $\Lambda = \sigma B_0^2/2\Omega\rho$, where ρ is density, σ is the electrical conductivity. At larger values of Λ, the amplitude of the geostrophic flow is determined by viscous friction, either at the vertical walls of the duct when these are rigid, or by viscous friction throughout the bulk of the fluid when the vertical walls are stress-free.

Numerical solutions are presented for both these cases for several values of the Rayleigh number, $r = g\alpha\beta d^2/2\Omega\kappa$, where α is the coefficient of volume expansion, β is the applied adverse temperature gradient, and κ is the thermal diffusivity. A symmetry-breaking bifurcation is located at large r in the case of stress-free side walls and sufficiently large Λ. For smaller r the solutions are steady and symmetric about the horizontal mid-level; for larger r they progress in opposite x-directions as horizontal waves hugging one horizontal boundary or the other.

All these results were obtained for a Boussinesq fluid, but it is shown that a compressible layer exhibits analagous behaviour. As demonstrated by Jones *et al.* (1990), convection is necessarily unsteady and unsymmetric in this case but, as r is increased at sufficiently large Λ, solutions develop that also progress in opposite x-directions as horizontal waves hugging one horizontal boundary or the other. The unfolding of the symmetry-breaking bifurcation of the Boussinesq model as the compressibility is increased from zero is elucidated.

The final summary of the paper includes some astrophysical speculations about the possible bearing of this work on the regime of convection in the outer regions of the Sun.

[1]Permanent address: Department of Mathematics and Statistics, University of Newcastle upon Tyne, Newcastle upon Tyne NE1 7RU, England

1. INTRODUCTION

Rapidly rotating magnetoconvection is believed to occur in the outer core of the Earth and in the convection zones of many stars. By 'rapidly rotating magnetoconvection', we mean that the Coriolis, Lorentz and buoyancy forces dominate the motions and are comparable in magnitude, so that the corresponding dimensionless measures of these forces, the Taylor, Chandrasekhar and Rayleigh numbers, are all large. The problem of understanding the nature of convection in these circumstances is not a simple one, and in this paper were shall restrict our attention to some particular aspects.

The study of rapidly rotating magnetoconvection has close links, of both a mathematical and physical nature, with dynamo theory. It is widely believed that planetary and stellar magnetic fields originate from convection-driven dynamos. A natural preliminary to the study of the full dynamo problem is the analysis of convection in an imposed magnetic field, the magnetoconvection problem.

We shall adopt a plane Cartesian geometry in this paper. Although all applications have the spherical geometry of naturally-occurring bodies, the use of a planar model greatly simplifies the mathematics, while still allowing us, we believe, to increase our understanding of the fundamentals of the dynamics of rapidly rotating magnetoconvection in general geometries.

An issue that arises almost immediately is the role of viscosity. In the linear problem of marginal convection (Eltayeb, 1972), self-consistent solutions could be obtained when the viscous terms were entirely omitted. This is an attractive feature as, in the applications to the planets and stars, the viscosity is very uncertain, although almost certainly small. The molecular viscosity of stellar material is too tiny to be significant, and the turbulent viscosity can only be crudely guessed. The philosophy generally adopted in numerical simulations (Gilman, 1983; Glatzmaier, 1984, 1985a, 1985b) is to select the smallest value of the viscosity for which numerical instabilities are absent. The viscosity of the Earth's core is generally believed to be small, although its actual value is uncertain to many orders of magnitude.

Further support to the idea that viscosity may be irrelevant in the planetary and stellar contexts has come from a suggestion by Taylor (1963). He pointed out that, if the magnetic field satisfies a certain restriction, which has come to be known as *Taylor's Constraint*, solutions of the magnetohydrodynamic dynamo problem might be possible that are independent of the viscosity. This idea was developed further for α^2-dynamos by Malkus and Proctor (1975) and Soward and Jones (1983), and for $\alpha\omega$-dynamos by Braginsky (1975, 1978), Braginsky and Roberts (1988), Abdel-Aziz and Jones (1988) and Roberts (1989). These authors considered the nonlinear axisymmetric dynamos in which viscous friction, acting through Ekman layers at the walls, balanced the mean azimuthal component of the Lorentz force. In all these models, Taylor's constraint was not satisfied by the field predicted by the linear stability analysis so that, when the dynamo number, D, slightly exceeded its critical value, D_c, for field generation, the amplitude of the solution was limited by Ekman suction. Nevertheless, in several of the papers cited above, the fields increasingly approached a Taylor configuration as D was increased. At some particular value, D_T, of D, the field satisfied Taylor's constraint exactly, and Ekman pumping was no longer needed to balance the mean azimuthal Lorentz force. As D approached D_T,

the amplitude of the solution rapidly increased in magnitude, from a value of order $E^{1/4}$, where E is the Ekman number, to O(1). If D is increased beyond D_T, meridional circulation terms become significant, and these new nonlinearities determine the amplitude in this "ageostrophic regime".

The question arises, "Does a similar behaviour occur in the magnetoconvection problem?" In general, the solutions of the linearized, convective instability problem do not satisfy Taylor's constraint, so that an azimuthal *geostrophic flow* is set up. Since the mean Lorentz force must balance the viscous force generated by the geostrophic flow, the smaller the viscosity the larger the associated geostrophic flow. At a given Rayleigh number, r, a nonlinear balance is achieved when the geostrophic flow impedes convection so that it is marginal for that value of r.

We should note that this type of nonlinearity is rather different from those normally associated with convecting systems. This is a consequence of assuming that the Taylor number, T, and the Chandrasekhar number, Q, are both large. The problem of slowly rotating magnetoconvection, where T and Q are of order 1 (or actually a few hundred, because of factors of π) has been considered by many authors, e.g. Zhang (1987), Zhang and Busse (1988) and Merryfield (1990), and has also provided the basis for the simulations of solar convection by Gilman and Glatzmaier referenced above. These authors find that convection induces a general differential rotation in their models, whereas only the geostrophic wind is significant in our model; however, when T = O(1), other nonlinearities, principally the advection of angular momentum through the $\mathbf{u}.\nabla\mathbf{u}$ term in the equation of motion, and the advection of heat through the $\mathbf{u}.\nabla T$ term in the energy equation (where $\mathbf{u}$ is fluid velocity and T is temperature), occur simultaneously with the Ekman nonlinearity, so that the non-geostrophic part of the differential rotation is as significant as the geostrophic part. In the rapidly rotating case, the feedback associated with the geostrophic wind occurs at smaller Rayleigh numbers than does the feedback associated with the advective nonlinearities. Naturally, if the the Rayleigh number is increased sufficiently, in a sense that we shall make more precise below, the advective terms will become significant even in the rapidly rotating case, and the problem is then considerably more difficult to solve.

Rapidly rotating magnetoconvection in a plane layer was first discussed in the nonlinear regime by Roberts and Stewartson (1974, 1975), for the particular case of a plane layer with rotation axis parallel to gravity and a horizontal applied magnetic field. In this geometry, convecting motions having the planform of unidirectional rolls are possible, but are atypical in that they satisfy Taylor's constraint exactly. However, if planforms consisting of a combination of rolls in two different directions are present (and, in their geometry, such a combination is typically the most relevant one), a geostrophic wind is set up. The Roberts-Stewartson model was studied further by Soward (1980, 1986), who confined their layer horizontally by bounding vertical walls parallel to the applied field; in this duct model, the single roll planform of the unbounded layer is disallowed, and two roll systems are generally necessary. Soward showed that, for a wide range of parameters, the magnetic field moved towards a Taylor configuration as the Rayleigh number was increased, and that Taylor's constraint was exactly satisfied at some second critical Rayleigh number, r_T. He also noted that, at small values of the ratio $q = \kappa/\eta$ of magnetic to thermal diffusivities, the nature of the Taylor solution became rather complicated.

The motivation for the present paper came from a wish to extend our previous paper (Jones *et al*, 1990; hereafter this paper will be called "Paper I") on the linear compressible layer to nonlinear regimes, and indeed in §7 below this will be done. Paper I was motivated by the observationally based claim that toroidal rolls occur in the solar convection zone (Ribes *et al*, 1985; Beckers, 1978; Wilson, 1988). Since the toroidal magnetic field of the Sun, as evidenced by sunspots, appears to be most important near the equatorial region of the solar surface, we adopted a geometry in which rotation, $\mathbf{\Omega}$, magnetic field, $\mathbf{B}_0$, and gravity, $\mathbf{g}$, were mutually perpendicular. We discovered that compressibility adds a qualitative difference to the linear stability problem, since it requires that convection occurs in the form of travelling waves, and cannot be steady. We therefore wanted to investigate whether solutions satisfying Taylor's constraint occur in compressible magnetoconvection. But as a first step it was natural to reconsider the Boussinesq case.

We did not anticipate that changing the geometry from the Roberts-Stewartson case of parallel rotation and gravity to the present case in which they are perpendicular would have a significant effect on Boussinesq convection. This expectation was, as we shall show below, not borne out by our findings. When the Elsasser number, $\Lambda = B_0^2/2\Omega\mu\rho\eta$, is greater than a value of about 4 (where ρ is density and μ is magnetic permeability; SI units are used throughout), the wavelength in the direction of $\mathbf{B}_0$ exceeds that in the direction of $\mathbf{\Omega}$, according to linear theory; this was expected, since the larger the Λ the greater the constraint of the Faraday-Maxwell stresses. We show below that, for such values of Λ and associated wavelengths, no Taylor state is possible. As the Rayleigh number is increased, the geostrophic wind produced by the mean Lorentz force increases without limit, and a boundary layer structure develops. The induced field in the direction parallel to gravity becomes much smaller than the induced field parallel to the rotation axis, so that the 'meridional' field created is principally parallel to the rotation axis, as for Braginsky's *Model-Z* dynamos (Braginsky, 1975, 1978; Braginsky and Roberts, 1988; Roberts, 1989).

We have also investigated the differences that occur in the case of a rigid boundary and a slippery boundary normal to the rotation axis. In geophysical applications, the core-mantle boundary provides a rigid "lid" to the convecting layer, but in the astrophysical contexts no such lid exists, convecting regions usually being confined by stably stratified layers. In such situations Ekman layers are unlikely to be important, and the force balancing the mean azimuthal Lorentz force will be provided by a turbulent viscosity, effective throughout the bulk of the layer. This means that the gradient of the geostrophic wind, rather than the absolute value of the wind itself, provides the required balance. We show in §6 below that this leads to a significant difference in behaviour; a symmetry-breaking bifurcation occurs when Ekman layers are absent. This symmetry-breaking means that two travelling wave solutions are possible, one associated with convection that occurs mainly in the upper half of the layer, and the other with convection that occurs mainly in the lower half of the layer.

The effect of compressibility, included in the analysis of §7, is that of perturbing the symmetry-breaking bifurcation, since compressibility itself introduces asymmetry between the upper and lower halves of the layer. As we shall see, the solution bifurcating from the lowest critical Rayleigh number connects onto a solution where convection is predominantly in the lower half of the layer, whereas the solution bifurcating from the second lowest critical

Rayleigh number connects to a solution with convection occuring mainly in the tenuous region near the top of the layer. This separation of the convection zone into two parts is of some interest. It was conjectured in Paper I that the observations of Ribes *et al* (1985) might be explained as follows: the importance of the toroidal field, as measured by the local Elsasser number, becomes large as the density falls near the solar surface, and such a toroidal field may be expected to "channel" the fluid motion to be predominantly zonal, so favouring the formation of "doughnut" convection cells; at depth, however, where the local Elsasser number is small and Coriolis forces dominate Lorentz forces, "banana" convection cells might be preferred. It is hard to discern from linear theory any reason why there should be a separation of the convection zone into two independent convective regimes, unless of course one selects a two-layer model to represent the convection zone. In the present nonlinear study, we find that the convective layer *naturally* divides into two zones, even in a homogeneous Boussinesq model.

2. BASIC EQUATIONS AND BOUNDARY CONDITIONS

The basic equations of this study are the continuity equation, the equation of motion, the electromagnetic induction equation, the energy equation, the gas law, and the equation that rules out magnetic monopoles:

$$\frac{\partial \rho}{\partial t} + \nabla.(\rho \mathbf{u}) = 0, \tag{2.1}$$

$$\rho\left(\frac{\partial \mathbf{u}}{\partial t} + \mathbf{u}.\nabla\mathbf{u}\right) + 2\rho\mathbf{\Omega}\times\mathbf{u} = -\nabla p + g\rho\mathbf{1}_z + \frac{1}{\mu}(\nabla\times\mathbf{B})\times\mathbf{B} + \rho\nu\left[\nabla^2\mathbf{u} + \tfrac{1}{3}\nabla(\nabla.\mathbf{u})\right], \tag{2.2}$$

$$\frac{\partial \mathbf{B}}{\partial t} = \nabla\times(\mathbf{u}\times\mathbf{B} - \eta\nabla\times\mathbf{B}), \tag{2.3}$$

$$\frac{\mathcal{R}\rho}{\gamma-1}\left(\frac{\partial T}{\partial t} + \mathbf{u}.\nabla T\right) = K\nabla^2 T + \frac{p}{\rho}\left(\frac{\partial \rho}{\partial t} + \mathbf{u}.\nabla\rho\right), \tag{2.4}$$

$$p = \mathcal{R}\rho T, \tag{2.5}$$

$$\nabla.\mathbf{B} = 0, \tag{2.6}$$

where T is temperature, p is pressure, ρ is density, $\mathbf{u}$ is fluid velocity, and $\mathbf{B}$ is magnetic field. The angular velocity $\mathbf{\Omega}$, the acceleration due to gravity $g\mathbf{1}_z$, the gas constant $\mathcal{R}$, the ratio of specific heats γ, the thermal conductivity K, the viscosity $\rho\nu$, the magnetic diffusivity η and the magnetic permeability μ are all assumed to be constant; ν is the kinematic viscosity and $\eta = 1/\mu\sigma$, where σ is the electrical conductivity. The coefficient of bulk viscosity is assumed to be zero.

Equations (2.1) – (2.6) admit the polytropic solution:

$$T_0 = \beta_0 z, \qquad p_0 = \bar{P}\left(\frac{z}{d}\right)^{m+1}, \qquad \rho_0 = \frac{\bar{P}(m+1)}{gd^{m+1}}z^m, \qquad \mathbf{u}_0 = 0, \qquad \mathbf{B}_0 = \text{const.}, \tag{2.7}$$

where $\bar{P}$ is a constant pressure and

$$\beta_0 = \frac{g}{\mathcal{R}(m+1)}$$

is the temperature gradient. The fluid is confined to a horizontal layer of depth d.

We now consider a convective state in which

$$T = T_0 + T_1,$$

and similarly for other variables. Substitute into (2.1) – (2.6) to obtain

$$\frac{\partial \rho_1}{\partial t} + \nabla.(\rho_0 \mathbf{u}) + \nabla.(\rho_1 \mathbf{u}) = 0, \tag{2.8}$$

$$(\rho_0 + \rho_1)\left[\frac{D\mathbf{u}}{Dt} + 2\boldsymbol{\Omega} \times \mathbf{u}\right] = -\nabla p_1 + g\rho_1 \mathbf{1}_z + \frac{1}{\mu}(\nabla \times \mathbf{B}_1) \times (\mathbf{B}_0 + \mathbf{B}_1) + \rho\nu\left[\nabla^2 \mathbf{u} + \tfrac{1}{3}\nabla(\nabla.\mathbf{u})\right], \tag{2.9}$$

$$\frac{\partial \mathbf{B}_1}{\partial t} = \nabla \times [\mathbf{u} \times (\mathbf{B}_0 + \mathbf{B}_1) - \eta \nabla \times \mathbf{B}_1], \tag{2.10}$$

$$\frac{(\rho_0 + \rho_1)}{\gamma - 1}\left[\mathcal{R}\frac{DT_1}{Dt} + \frac{g}{m+1}u_z\right] = K\nabla^2 T_1 - (p_0 + p_1)\nabla.\mathbf{u}, \tag{2.11}$$

$$p_1 = \mathcal{R}(T_0\rho_1 + \rho_0 T_1 + \rho_1 T_1), \tag{2.12}$$

$$\nabla.\mathbf{B}_1 = 0, \tag{2.13}$$

where D/Dt stands for the motional derivative:

$$\frac{D}{Dt} = \frac{\partial}{\partial t} + \mathbf{u}.\nabla .$$

We may carry out the process of thermodynamic linearization commonly called *the anelastic approximation*. As a first step, we transform to dimensionless variables by writing

$$\mathbf{x} \to d\mathbf{x}, \qquad t \to \frac{d^2}{\eta}t, \qquad \mathbf{u} \to \frac{\eta}{d}\mathbf{u}, \qquad \mathbf{B} \to B_0\mathbf{B}. \tag{2.14}$$

In these units the layer occupies the region

$$z_0 \le z \le 1 + z_0.$$

It is often convenient to relate variables to their values at the centre, $z = z_0 + \frac{1}{2}$, of the layer, and also to write

$$\zeta = z/(z_0 + \tfrac{1}{2}).$$

Then (2.7) gives

$$T_0 = [\beta_0 d(z_0 + \tfrac{1}{2})]\,\zeta, \quad p_0 = \left[\bar{P}(z_0 + \tfrac{1}{2})^{m+1}\right]\zeta^{m+1}, \quad \rho_0 = \left[\frac{\bar{P}(m+1)}{gd}(z_0 + \tfrac{1}{2})^m\right]\zeta^m,$$

suggesting similar dimensionless groupings for T_1, p_1 and ρ_1:

$$T_1 \to \alpha[\beta_0 d(z_0 + \tfrac{1}{2})]\,T_1, \quad p_1 \to \alpha\left[\bar{P}(z_0 + \tfrac{1}{2})^{m+1}\right]p_1, \quad \rho_1 \to \alpha\left[\frac{\bar{P}(m+1)}{gd}(z_0 + \tfrac{1}{2})^m\right]\rho_1,$$

where

$$\alpha = \frac{2\Omega\eta}{gd}.$$

Equations (2.8) – (2.13) may now be written as

$$\alpha\left[\frac{\partial\rho_1}{\partial t} + \nabla.(\rho_1\mathbf{u})\right] + \nabla.(\zeta^m\mathbf{u}) = 0, \tag{2.15}$$

$$(\zeta^m + \alpha\rho_1)\left[\mathrm{Ro}\frac{D\mathbf{u}}{Dt} + \mathbf{1}_\Omega \times \mathbf{u}\right] = -\frac{(z_0+\frac{1}{2})}{m+1}\nabla p_1 + \rho_1\mathbf{1}_z + \Lambda(\nabla\times\mathbf{B}_1)\times(\mathbf{1}_B + \mathbf{B}_1) + E\left[\nabla^2\mathbf{u} + \tfrac{1}{3}\nabla(\nabla.\mathbf{u})\right], \tag{2.16}$$

$$\frac{\partial\mathbf{B}_1}{\partial t} = \nabla\times[\mathbf{u}\times(\mathbf{1}_B + \mathbf{B}_1) - \nabla\times\mathbf{B}_1], \tag{2.17}$$

$$\frac{1}{q\gamma}(\zeta^m + \alpha\rho_1)\frac{DT_1}{Dt} = \frac{(\gamma-1)}{q\gamma}(\zeta + \alpha T_1)\frac{D\rho_1}{Dt} - \left[r\zeta^m + \frac{1}{\gamma q\left(z_0+\frac{1}{2}\right)}\left\{\rho_1 - m(\gamma-1)\zeta^{m-1}T_1\right\}\right]u_z + \nabla^2 T_1, \tag{2.18}$$

$$p_1 = \zeta^m T_1 + \zeta\rho_1 + \alpha\rho_1 T_1, \tag{2.19}$$

$$\nabla.\mathbf{B}_1 = 0, \tag{2.20}$$

where E, Ro, Λ and r are Ekman, Rossby, Elsasser and Rayleigh numbers:

$$E = \frac{\rho\nu}{2\Omega d^2\rho_m}, \qquad \mathrm{Ro} = \frac{\eta}{2\Omega d^2}, \qquad \Lambda = \frac{B_0^2}{2\Omega\rho_m\mu\eta}, \qquad r = \frac{g\beta d}{2\Omega\beta_0\kappa\left(z_0+\frac{1}{2}\right)},$$

and $\mathbf{1}_\Omega$ and $\mathbf{1}_B$ are unit vectors in the directions of $\mathbf{\Omega}$ and $\mathbf{B}_0$, ρ_m is the density at the centre of the layer, κ is the thermal diffusivity at the centre of the layer, and β is the superadiabatic temperature gradient:

$$\rho_m = \frac{\bar{P}(m+1)}{gd}\left(z_0+\tfrac{1}{2}\right)^m, \qquad \kappa = \frac{(\gamma-1)\beta_0 d}{\gamma\left(z_0+\frac{1}{2}\right)^m\bar{P}}K, \qquad \beta = \beta_0\left(\frac{m+1}{\gamma} - m\right);$$

$q = \kappa/\eta$ is a ratio of diffusivities. [Usually the Rossby number is defined as $U/2\Omega d$, a dimensionless measure of a typical fluid velocity U. Here U is replaced by the unit of velocity introduced in (2.14). The Rayleigh number is often taken to be $g\alpha\beta d^4/\nu\kappa$, where α is the coefficient of volume expansion; we therefore use a different letter, r for our dimensionless measure of the buoyancy force.]

The anelastic approximation consists in taking the limit in which the superadiabatic gradient, β is small compared with the total gradient, β_0; since $\beta/\beta_0 = \alpha r q\left(z_0+\frac{1}{2}\right)$ and since r, q and $z_0 + \frac{1}{2}$ are all O(1) quantities, this is tantamount to taking the limit

$$\alpha \to 0. \tag{2.21}$$

In addition we shall confine attention to vanishing Rossby numbers

$$\mathrm{Ro} \rightarrow 0. \tag{2.22}$$

Equations (2.15) – (2.20) then become

$$\boldsymbol{\nabla}.(\zeta_m \mathbf{u}) = 0, \tag{2.23}$$

$$\zeta^m \mathbf{1}_\Omega \times \mathbf{u} = -\frac{(z_0+\frac{1}{2})}{m+1}\boldsymbol{\nabla} p + \rho \mathbf{1}_z + \Lambda(\boldsymbol{\nabla}\times\mathbf{B})\times(\mathbf{1}_B+\mathbf{B}) + E\left[\nabla^2\mathbf{u} + \tfrac{1}{3}\boldsymbol{\nabla}(\boldsymbol{\nabla}.\mathbf{u})\right], \tag{2.24}$$

$$\frac{\partial \mathbf{B}}{\partial t} = \boldsymbol{\nabla}\times[\mathbf{u}\times(\mathbf{1}_B+\mathbf{B}) - \boldsymbol{\nabla}\times\mathbf{B}], \tag{2.25}$$

$$\frac{\zeta^m}{q\gamma}\frac{DT}{Dt} = \frac{(\gamma-1)}{q\gamma}\zeta\frac{D\rho}{Dt} - \left[r\zeta^m + \frac{1}{\gamma q\left(z_0+\frac{1}{2}\right)}\left\{\rho - m(\gamma-1)\zeta^{m-1}T\right\}\right]u_z + \nabla^2 T, \tag{2.26}$$

$$p = \zeta^m T + \zeta\rho, \tag{2.27}$$

$$\boldsymbol{\nabla}.\mathbf{B} = 0. \tag{2.28}$$

We are able here and below to omit the suffix $_1$ without causing confusion.

Equations (2.23) – (2.28) are the basic starting point of this study. They are closely related to those on which paper I was based. There are however two differences. First, we are interested here in the nonlinear developments of paper I. We have therefore retained all nonlinear terms apart from those that were removed by (2.22) and the anelastic approximation (2.21). Second, we will retain the viscous term in (2.24). In paper I, we assumed that

$$E = 0. \tag{2.29}$$

We suppose instead that

$$E \rightarrow 0. \tag{2.30}$$

The solution can then usually be thought of as a "mainstream", in which (2.29) holds to leading order in the limit (2.30), but in which (and this is essential for what follows in §3 onwards) E enters at higher orders, and boundary layers at the walls, whose thicknesses vanishes in the limit (2.30), but in which viscous forces are important even at leading order. In these layers, the solution matches the mainstream to wall conditions.

A large part of this paper will be devoted to the Boussinesq limit,

$$z_0 \rightarrow \infty,$$

under which equations (2.23) – (2.28) simplify further to

$$\boldsymbol{\nabla}.\mathbf{u} = 0, \tag{2.31}$$

$$\mathbf{1}_\Omega \times \mathbf{u} = -\boldsymbol{\nabla} p + T\mathbf{1}_z + \Lambda(\boldsymbol{\nabla}\times\mathbf{B})\times(\mathbf{1}_B+\mathbf{B}) + E\nabla^2\mathbf{u}, \tag{2.32}$$

$$\frac{\partial \mathbf{B}}{\partial t} = \boldsymbol{\nabla}\times[\mathbf{u}\times(\mathbf{1}_B+\mathbf{B}) - \boldsymbol{\nabla}\times\mathbf{B}], \tag{2.33}$$

$$\frac{1}{q}\frac{DT}{Dt} = \nabla^2 T - r u_z, \tag{2.34}$$

$$\boldsymbol{\nabla}.\mathbf{B} = 0. \tag{2.35}$$

The basic equations (2.23) - (2.28) or (2.31) - (2.35) are of twelfth order, and six boundary conditions are required at each of the horizontal boundaries. These conditions are mechanical, magnetic and thermal. The surfaces may be "rigid" or "free", which means that the mechanical conditions are of one of two types: no-slip or stress-free:

$$\text{no-slip}: \quad u_x = u_y = u_z = 0,$$
$$\text{stress-free}: \quad \frac{\partial u_x}{\partial z} = \frac{\partial u_y}{\partial z} = u_z = 0.$$

We shall find it more convenient to use the equivalent demands

$$\text{no-slip}: \quad u_z = \frac{\partial u_z}{\partial z} = \omega_z = 0, \quad \text{at} \quad z = z_0,\ 1 + z_0, \tag{2.36r}$$

$$\text{stress-free}: \quad u_z = \frac{\partial^2}{\partial z^2}(\zeta^m u_z) = \frac{\partial \omega_z}{\partial z} = 0, \quad \text{at} \quad z = z_0,\ 1 + z_0, \tag{2.36f}$$

where

$$\boldsymbol{\omega} = \nabla \times \mathbf{u}$$

is the vorticity. The magnetic conditions depend on the electrical properties (and extent) of the regions $z < z_0$ and $z > 1 + z_0$. We shall consider only the two extreme cases in which these regions are perfect electrical insulators or are perfect electrical conductors. In the former case all conditions are satisfied by making $\mathbf{B}$ continuous; in the latter case $\mathbf{n}.\mathbf{B}$ and $\mathbf{n} \times \mathbf{E}$ must vanish at a wall, where $\mathbf{n}$ is the normal to the wall and $\mathbf{E}$ is the electric field: in dimensional units

$$\mathbf{E} = -\mathbf{u} \times \mathbf{B} + \eta \nabla \times \mathbf{B},$$

so that at a perfectly conducting boundary

$$\frac{\partial B_x}{\partial z} = \frac{\partial B_y}{\partial z} = B_z = 0.$$

Using (2.6) we see that only two of these three conditions are independent. Introducing the (dimensionless) electric current density $\mathbf{J}$, by

$$\mathbf{J} = \nabla \times \mathbf{B},$$

we see that

$$\text{perfect conductor:} \quad B_z = \frac{\partial J_z}{\partial z} = 0, \quad \text{at} \quad z = z_0,\ 1 + z_0, \tag{2.37p}$$

$$\text{insulator:} \quad \langle B_z \rangle = \langle \frac{\partial B_z}{\partial z} \rangle = J_z = 0, \quad \text{at} \quad z = z_0,\ 1 + z_0, \tag{2.37i}$$

Evidently (2.37p) place two restrictions on the solution, but apparently (2.37i) places three. This is because we have yet to impose the condition that no sources of field exist in the insulator (except for the current sources that create $\mathbf{B}_0$). When we add this demand,

we shall find that (2.36i) also embodies only two restrictions on the solution. Finally we consider the thermal conditions, which also depend on the nature of the containing walls. We shall make the usual assumption, that the walls are perfect thermal conductors, so that

$$T = 0, \qquad \text{at} \quad z = z_0,\ 1 + z_0. \tag{2.38}$$

Following the geometry of paper I, in which $\mathbf{\Omega}$ and $\mathbf{B}_0$ are horizontal and perpendicular to one another, we shall take $\mathbf{1}_B = \mathbf{1}_x$ and $\mathbf{1}_\Omega = \mathbf{1}_y$. In the limit (2.30), the mainstream is governed by the $E = 0$ forms of (2.23) - (2.28) or (2.31) - (2.35), which are then systems of only sixth order ($l \neq 0$) or fourth order ($l = 0$). The mainstream is therefore capable of satisfying only three conditions at each of the horizontal walls ($l \neq 0$) or two conditions ($l = 0$), the remaining conditions being met by boundary layers. For ($l \neq 0$), the analysis of these "side-wall" layers (so-called because in the theory of rotating fluids $\mathbf{\Omega}$ is often regarded as being "vertical") has been undertaken by Condi (1978); see also Fearn (1983). We state here only the final result of his analysis. In the case in which solutions are proportional to

$$\exp[i(kx + ly + \omega t)], \tag{2.39}$$

the case we shall consider below, conditions (2.36) - (2.38) require that the mainstream solutions obey

$$\text{perfect cond.:} \qquad B_z = \frac{\partial J_z}{\partial z} \mp (k\,\mathrm{sgn}\,l)\,u_z = T = 0, \quad \text{at} \quad z = z_0 + \tfrac{1}{2} \pm \tfrac{1}{2}, \tag{2.40p}$$

$$\text{insulator:} \qquad J_z = \frac{\partial B_z}{\partial z} \pm \sqrt{(k^2 + l^2)}\,B_z = T = 0, \quad \text{at} \quad z = z_0 + \tfrac{1}{2} \pm \tfrac{1}{2}, \tag{2.40i}$$

where upper and lower signs are to be taken together. The mechanical conditions, whether for a no-slip or a stress-free boundary, are irrelevant; they affect only the structure of the side-wall layers, which are of thickness $O(E^{1/3}d)$. In what follows (2.40i) will be adopted.

When $l = 0$, Coriolis forces can be absorbed into the pressure gradient, and the boundary layers on $z = z_0$ and $z_0 + 1$ are essentially the Shercliff layers familiar from the theory of magnetohydrodynamic duct flow. Their thickness is $M^{-1/2}d$, where $M = B_0 d/\sqrt{(\mu\rho_0\eta\nu)}$ is the Hartmann number, whose square (the Chandrasekhar number) measures the relative strength of Lorentz and viscous forces. From the theory of these layers, it emerges that the mainstream is required to obey

$$\text{perfect cond.:} \qquad B_z = T = 0, \quad \text{at} \quad z = z_0,\ 1 + z_0, \tag{2.41p}$$

$$\text{insulator:} \qquad \frac{\partial B_z}{\partial z} \pm \sqrt{(k^2 + l^2)}\,B_z = T = 0, \quad \text{at} \quad z = z_0 + \tfrac{1}{2} \pm \tfrac{1}{2}. \tag{2.41i}$$

Except in parts of §§3 and 5, we shall no longer employ Eltayeb's (1972) illustrative conditions

$$T = u_z = B_z = 0, \qquad \text{at} \quad z = z_0,\ 1 + z_0, \tag{2.42}$$

which were used exclusively in paper I.

Finally, we shall later (for reasons given in §3) limit our system horizontally, by plane vertical walls at $y = \pm \frac{1}{2}L$. The boundary conditions to be applied at these walls will be discussed in §§4 and 5.

3. SMALL AMPLITUDE BOUSSINESQ SOLUTIONS

In this and subsequent sections, we consider only the Boussinesq limit; compressibility will be reinstated in §7. The basic conduction solution replacing (2.7) is

$$T_0 = \beta z, \quad p_0 = g\rho_0\left(z - \tfrac{1}{2}\alpha_0\beta z^2\right) + \text{const.}, \quad \rho_0 = \text{const.}, \quad \mathbf{u}_0 = 0, \quad \mathbf{B}_0 = \text{const.}, \tag{3.1}$$

or in dimensionless units

$$T_0 = z, \qquad p_0 = z - \tfrac{1}{2}z^2 + \text{const.}, \qquad \rho_0 = \text{const.}, \qquad \mathbf{u}_0 = 0, \qquad \mathbf{B}_0 = \mathbf{1}_z. \tag{3.2}$$

We may now take the layer to be

$$0 \leq z \leq 1,$$

(where, for consistency with the compressible case, $z = 0$ is the top of the layer) and E, Ro, Λ and r reduce to

$$E = \frac{\nu}{2\Omega d^2}, \qquad \mathrm{Ro} = \frac{\eta}{2\Omega d^2}, \qquad \Lambda = \frac{B_0^2}{2\Omega\rho_0\mu\eta}, \qquad r = \frac{g\alpha_0\beta d^2}{2\Omega\kappa},$$

where α_0 is the coefficient of volume expansion.

Departures from state (3.2) are governed by (2.31) – (2.35):

$$\nabla.\mathbf{u} = 0, \tag{3.3}$$

$$\mathbf{1}_\Omega \times \mathbf{u} = -\nabla p + T\mathbf{1}_z + \Lambda(\nabla\times\mathbf{B})\times(\mathbf{1}_B + \mathbf{B}), \tag{3.4}$$

$$\frac{\partial\mathbf{B}}{\partial t} = \nabla\times[\mathbf{u}\times(\mathbf{1}_B + \mathbf{B}) - \nabla\times\mathbf{B}], \tag{3.5}$$

$$\frac{1}{q}\frac{DT}{Dt} = \nabla^2 T - ru_z, \tag{3.6}$$

$$\nabla.\mathbf{B} = 0. \tag{3.7}$$

We have omitted the viscous term in (3.4), i.e. (3.3) – (3.7) govern the mainstream solution. In paper I, we assumed for simplicity the simple boundary conditions (2.42):

$$T = u_z = B_z = 0, \qquad \text{at} \quad z = 0, 1, \tag{3.8}$$

rather than one of the physically-motivated conditions (2.40). It transpires however that, in the linear Boussinesq theory that follows, the equation and boundary condition determining B_z factor out from the fourth-order system determining u_z and T, i.e. the latter determine the onset of convection, and B_z can be determined later (if desired). In this restricted sense, the results of linear Boussinesq theory are independent of the conditions placed on B_z on the walls. This is however not true of finite amplitude, or of non-Boussinesq convection.

The linear stability of state (3.2) is examined by writing

$$T = z + T', \tag{3.9}$$

and similarly for other variables. Substitute into (3.3) – (3.7), and neglect squares and products of the primed variables, to obtain a set of linear equations:

$$\nabla.\mathbf{u} = 0, \tag{3.10}$$

$$\mathbf{1}_y \times \mathbf{u} = -\nabla p' + T'\mathbf{1}_z + \Lambda(\nabla \times \mathbf{B}') \times \mathbf{1}_x, \tag{3.11}$$

$$\frac{\partial \mathbf{B}'}{\partial t} = \nabla \times (\mathbf{u} \times \mathbf{1}_x) + \nabla^2 \mathbf{B}', \tag{3.12}$$

$$\frac{1}{q}\frac{\partial T'}{\partial t} = \nabla^2 T' - r u_z, \tag{3.13}$$

$$\nabla.\mathbf{B}' = 0. \tag{3.14}$$

The solution to (3.8) and (3.10) – (3.14) may be found in Eltayeb (1972) or in §4 of Paper I. It is there shown that, for solutions depending on x, y and t as in (2.39), i.e.

$$T'(x,y,z,t) = \tilde{T}'(z)\exp[i(kx + ly + \omega t)] + \text{c.c.}, \tag{3.15}$$

where c.c. stands for the complex conjugate, the marginal state ($r = r_m$) is direct ($\omega = 0$), and has the Reynolds number

$$r_m = \frac{l^2\left(k^2 + l^2 + \pi^2\right)^2}{\Lambda k^2\left(k^2 + l^2\right)} + \frac{\Lambda k^2\left(k^2 + l^2 + \pi^2\right)}{k^2 + l^2}. \tag{3.16}$$

The critical state ($r_m = r_c$) is the one that minimizes r_m over k and l. [The functions $\tilde{T}'$, $\tilde{\mathbf{u}}'$, and $\tilde{\mathbf{B}}'$ are complex, and their conjugates will be denoted by $\tilde{T}'^*$, etc. Where possible, the tilde and the prime will be omitted from $\tilde{T}'$ etc.]

If $\Lambda < 4$, the critical mode is a single convection roll parallel to the rotation axis and of indefinitely large x-dimension:

$$k_c \to 0, \qquad l_c \equiv 0, \qquad r_c = \pi^2\Lambda.$$

If $\Lambda > 4$, there are two convective rolls, equally inclined to both $\boldsymbol{\Omega}$ and $\mathbf{B}_0$, which are the first to convect when, starting from state (3.2), r is increased from zero:

$$k_c = \pm\pi\sqrt{\left(\frac{\chi(1-2\chi)}{1-\chi}\right)}, \quad l_c = \pm\pi\sqrt{\left(\frac{\chi^2}{1-\chi}\right)}, \quad r_c = \frac{\pi^2\chi}{1-\chi}\left(\frac{1+\chi}{\chi}\right)^{\frac{3}{2}}, \tag{3.17a}$$

where χ ($< \frac{1}{2}$) is the larger of the two positive roots of

$$(4\Lambda^2 - 1)(\chi^3 - \chi^2) + (\Lambda^2 + 1)\chi - 1 = 0,$$

i.e.

$$\Lambda = \frac{1-\chi}{1-2\chi}\sqrt{\left(\frac{1+\chi}{\chi}\right)}. \tag{3.17b}$$

If, holding k and l fixed, one increases r slightly beyond r_m, the convective state acquires a small but finite amplitude, which can be determined by a so-called "weakly nonlinear analysis", in which (3.9) is taken to be the first two terms in an amplitude expansion of solutions to (3.3) – (3.8):

$$T = z + T' + T'' + \ldots, \tag{3.18}$$

and similarly for the other variables. In the present problem, it is not at once apparent how the dynamical balance is achieved in this state. A difficulty arises from the term,

$$\Lambda(\nabla \times \mathbf{B}') \times \mathbf{B}', \tag{3.19}$$

which appears in the equation of motion $(3.4)''$ from the set $(3.3)''$ – $(3.8)''$ determining the $''$ variables. The horizontal part (denoted by the suffix $_H$) of the horizontal average (denoted by an overbar) of (3.19),

$$\mathbf{F}(z) = \Lambda\left[\overline{(\nabla \times \mathbf{B}') \times \mathbf{B}'}\right]_H, \tag{3.20}$$

is nonzero for all Λ [even when single rolls with $(l \neq 0)$ are excited], but there is no other term in $(3.4)''$ that can balance this force!

This type of difficulty was first described by Taylor (1963) in the context of geodynamo theory. It was encountered first in the theory of magnetoconvection by Roberts and Stewartson (1975); see also Soward (1980). The weak horizontal force (3.20) is independent of x and y, and this suggests that it will, acting over a sufficiently long time (dependent on the amplitude of the force, i.e. on the degree of supercriticality), set up a horizontal motion independent of x and y. This *geostrophic velocity* shear will affect the convective motions; in other words, its presence invalidates the formulation (3.10) – (3.14) of the linear stability problem. In particular, (3.11) and (3.12) should be replaced by

$$\frac{\partial \mathbf{B}'}{\partial t} + \mathbf{U}.\nabla\mathbf{B}' = \nabla \times (\mathbf{u} \times \mathbf{1}_x) + \nabla^2\mathbf{B}', \tag{3.21}$$

$$\frac{1}{q}\frac{\partial T'}{\partial t} + \mathbf{U}.\nabla T' = \nabla^2 T' - r u_x. \tag{3.22}$$

We might intuitively expect that, for the ultimate equilibrated $\mathbf{U}(z)$, the force $\mathbf{F}(z)$ will vanish, and this suggest a definite numerical procedure: iterate on $\mathbf{U}(z)$ until $\mathbf{F}(z) = 0$, i.e. until, in terms of the representation (3.15),

$$\frac{d}{dz}(u_x B_x^* - u_x^* B_x) = 0, \tag{3.23}$$

$$\frac{d}{dz}\left(B_x \frac{dB_x^*}{dz} - B_x^* \frac{dB_x}{dz}\right) = 0, \tag{3.24}$$

When such a solution can be found, it is appropriate to call it a *Taylor State*, since as envisaged by Taylor (1963) it resolves the dilemma of the unbalanced force, $\mathbf{F}(z)$, without invoking coupling to the walls (e.g. without introducing viscous friction). If, however, a solution can be found only when some form of coupling is restored (in our case viscous friction), it would be appropriate to describe it as of *Model-Z form*, following the suggestion and terminology of Braginsky (1975), also made in the context of geodynamo theory.

We shall now show by a *reductio ad absurdum* argument that, when convection occurs as the single roll (3.15), a Taylor state is impossible. Suppose a Taylor state exists, so that (3.23) holds. On integrating, using (3.8), we see that

$$u_z(z)B_z^*(z) \; - \; u_z^*(z)B_z(z) \; = \; 0. \tag{3.25}$$

Introduce the polar representation,

$$u_z(z) \; = \; \alpha(z)\mathrm{e}^{i\theta(z)}, \qquad B_z(z) \; = \; \beta(z)\mathrm{e}^{i\phi(z)}, \tag{3.26}$$

where α, β, θ, and ϕ are real functions. Then (3.25) gives

$$\alpha\beta\sin(\theta \, - \, \phi) \; = \; 0, \qquad \text{for all } z,$$

so that, either $\alpha \; \equiv \; 0$ or $\beta \; \equiv \; 0$, or (as we shall now suppose) for some integer n,

$$\theta \; \equiv \; \phi \; + \; n\pi. \tag{3.27}$$

On substituting (3.26) into the z-component of the induction equation (3.21), multiplying by $\exp(-i\phi)$, and making use of (3.27), we obtain

$$\frac{d^2\beta}{dz^2} \; - \; \left[k^2 \; + \; l^2 \; + \; \left(\frac{d\phi}{dz}\right)^2\right]\beta \; = \; 0. \tag{3.28}$$

Multiplying through by β, integrating across the layer, and making use of the fact that, by (3.8), $\beta \; = \; 0$ on the walls, we obtain

$$\int_0^1 \left\{\left(\frac{d\beta}{dz}\right)^2 \; + \; \left[k^2 \; + \; l^2 \; + \; \left(\frac{d\phi}{dz}\right)^2\right]\beta^2\right\} dz \; = \; 0. \tag{3.29}$$

It follows that

$$\beta \equiv \; 0, \qquad \text{i.e. } B_z' \; \equiv 0,$$

from which it also follows that $u_z' \; \equiv \; 0$.

The case when two rolls of the form (3.15) are simultaneously present, one with $kl \; > \; 0$ the other with $kl \; < \; 0$, is more intricate. We shall suppose that these two rolls are excited to equal amplitude, a case relevant to the duct models of §§4-6. Then (3.15) is replaced by

$$T'(x,y,z,t) \; = \; \tilde{T}'(z)\exp[i(kx \; + \; \omega t)]\cos ly \; + \; \text{c.c.}, \tag{3.30}$$

and similarly for u_z, and B'_z; $\sin ly$ appears in place of $\cos ly$ in the representations of u_x, u_y, ω'_z, B'_x, B'_y, and J'_z. In this case $F_y \equiv 0$ and therefore $U_y \equiv 0$; the existence of a Taylor state is decided by whether or not U_x can be found such that $F_x = 0$. This requires that

$$\frac{d}{dz}\left\{(u_z B_z^* - u_z^* B_z) + \frac{k^2\Lambda}{l^2}\left(B_z\frac{dB_z^*}{dz} - B_z^*\frac{dB_z}{dz}\right)\right\} = 0. \tag{3.31}$$

When boundary conditions (3.8) apply, (3.31) may be integrated to give

$$(u_z B_z^* - u_z^* B_z) + \frac{k^2\Lambda}{l^2}\left(B_z\frac{dB_z^*}{dz} - B_z^*\frac{dB_z}{dz}\right) = 0. \tag{3.32}$$

Multiplying the z component of the induction equation (3.21) by B_z^* and taking the real part, we find that

$$B_z^*\frac{d^2B_z}{dz^2} + B_z\frac{d^2B_z^*}{dz^2} - 2\left(k^2 + l^2\right)B_z B_z^* = -ik\left(u_z B_z^* - u_z^* B_z\right). \tag{3.33}$$

Now suppose that a Taylor state exists, and use (3.32) to rewrite the right-hand side of (3.33), so obtaining

$$\frac{d}{dz}\left(B_z^*\frac{dB_z}{dz}\right) + \frac{d}{dz}\left(B_z\frac{dB_z^*}{dz}\right) - 2\left[\frac{dB_z}{dz}\frac{dB_z^*}{dz} + \left(k^2 + l^2\right)B_z B_z^*\right] = \frac{ik^3\Lambda}{l^2}\left(B_z\frac{dB_z^*}{dz} - B_z^*\frac{dB_z^*}{dz}\right). \tag{3.34}$$

Using again the polar representation (3.26) and integrating (3.33) across the layer, making use of the fact that, by (3.8), $\beta = 0$ on the walls, we obtain in place of (3.29)

$$\int_0^1 \left\{\left(\frac{d\beta}{dz}\right)^2 + \left[k^2 + l^2 + \frac{k^3\Lambda}{l^2}\left(\frac{d\phi}{dz}\right) + \left(\frac{d\phi}{dz}\right)^2\right]\beta^2\right\} dz = 0. \tag{3.35}$$

Since $\beta = 0$ at $x = 0$ and 1, a variational inequality gives

$$\int_0^1 \left(\frac{d\beta}{dz}\right)^2 dz \geq \pi^2 \int_0^1 \beta^2\, dz, \tag{3.36}$$

so that by (3.35)

$$\int_0^1 \left[\pi^2 + k^2 + l^2 + \frac{k^3\Lambda}{l^2}\left(\frac{d\phi}{dz}\right) + \left(\frac{d\phi}{dz}\right)^2\right]\beta^2\, dz \leq 0. \tag{3.37}$$

The integrand in (3.37) is non-negative for all $d\phi/dz$ if

$$k^6\Lambda^2 \leq 4l^4\left(\pi^2 + k^2 + l^2\right). \tag{3.38}$$

Confining attention to the critical mode for which (3.17) holds, we may translate (3.38) into

$$2\chi^2 + 3\chi - 1 \geq 0, \tag{3.39}$$

or

$$\chi \geq \tfrac{1}{4}(\sqrt{17} - 3),$$

so that (3.37) cannot be satisfied if

$$\Lambda \geq 3.5035.... \tag{3.40}$$

and so for this value of Λ no Taylor state is possible. For this value of Λ it is the $l = 0$ single roll, and not the double rolls, that are preferred at marginal stability. This suggest that the Taylor states, if they exist, are irrelevant. This inference may, however, be too simplistic. It is by no means clear that the wavenumbers of the preferred mode at marginal stability will correspond to a stable finite amplitude mode at supercritical Rayleigh numbers. Ideally only the k and l of stable modes should be inserted into (3.38), and at large values of r it may happen that such Taylor states will exist at values of Λ greater than 4.

In the main bulk of this paper we shall apply, not (3.8), but the physically more realistic conditions (2.40i) that apply when the walls $z = 0, 1$ are insulating:

$$T = u_z = \frac{\partial B_z}{\partial z} \pm \sqrt{(k^2 + l^2)}\, B_z = 0, \quad \text{at} \quad z = \tfrac{1}{2} \pm \tfrac{1}{2}. \tag{3.41}$$

We have here used the z-component of the curl of (3.11), namely

$$\frac{\partial J_z}{\partial x} = -\frac{1}{\Lambda}\frac{\partial u_z}{\partial y},$$

to replace the condition on J_z in (2.40i) by a like condition on u_z.

Very similar conclusions may be drawn about the Taylor states when (3.41) apply. Consider first the case of the single roll system. Equation (3.28) is again valid, but β no longer vanishes on the walls, so that in place of (3.29) we have

$$\int_0^1 \left\{ \left(\frac{d\beta}{dz}\right)^2 + \left[k^2 + l^2 + \left(\frac{d\phi}{dz}\right)^2\right]\beta^2 \right\} dz + \sqrt{(k^2 + l^2)}\,[\beta^2(0) + \beta^2(1)] = 0. \tag{3.42}$$

The impossibility of Taylor states is as obvious as before.

Turning now to the double-roll case, (3.35) is replaced by

$$\int_0^1 \left\{ \left(\frac{d\beta}{dz}\right)^2 + \left[k^2 + l^2 + \frac{k^3\Lambda}{l^2}\left(\frac{d\phi}{dz}\right) + \left(\frac{d\phi}{dz}\right)^2\right]\beta^2 \right\} dz + \sqrt{(k^2 + l^2)}\,[\beta^2(0) + \beta^2(1)] = 0. \tag{3.43}$$

The variational inequality appropriate to the boundary condition (3.41) is not (3.36) but

$$\int_0^1 \left(\frac{d\beta}{dz}\right)^2 dz + \sqrt{(k^2+l^2)}\,[\beta^2(0)+\beta^2(1)] \geq \lambda^2 \int_0^1 \beta^2\,dz, \tag{3.44}$$

where λ is the smallest positive root of

$$\tan\lambda = \frac{2\lambda\sqrt{(k^2+l^2)}}{\lambda^2 - k^2 - l^2}. \tag{3.45}$$

Inequality (3.36) is now replaced by

$$\int_0^1 \left[\lambda^2 + k^2 + l^2 + \frac{k^3\Lambda}{l^2}\left(\frac{d\phi}{dz}\right) + \left(\frac{d\phi}{dz}\right)^2\right]\beta^2\,dz \leq 0, \tag{3.46}$$

so that there are no Taylor states when

$$k^6\Lambda^2 \leq 4l^4\left(\lambda^2 + k^2 + l^2\right). \tag{3.47}$$

Again confining attention to the critical wavenumbers (3.17), we may translate (3.45) and (3.47) into

$$\tan\lambda = \frac{2\pi\lambda\chi^{1/2}}{\lambda^2 - \pi^2\chi}, \tag{3.48}$$

$$2\chi^3 + \left(1 + \frac{4\lambda^2}{\pi^2}\right)\chi^2 + 2\chi - 1 \geq 0. \tag{3.49}$$

¿From these relations it follows that

$$\chi \geq 0.339\ldots, \tag{3.50}$$

so that no Taylor state can exist when

$$\Lambda \geq 4.080\ldots \tag{3.51}$$

This is the replacement of (3.40) for insulating walls.

For values of Λ not satisfying inequality (3.51) Taylor states cannot be ruled out, and indeed, our numerical scheme has found Taylor states for values of Λ below 4. The situation is as indicated in Figure 1, where the (Λ, r)-plane for insulating walls is displayed. The solid lines give the critical Rayleigh number at which convection onsets: for $\Lambda \leq 4$ this is governed by the $l = 0$ mode, and for $\Lambda > 4$ by modes with both k and l non-zero; this is why the solid curve has a discontinuity in slope at $\Lambda = 4$. The two curves which comprise this stability boundary can be extended above and below $\Lambda = 4$, and these extensions appear as dashed curves in Figure 1: they lie above the solid curve, of course, so they do not define the critical Rayleigh number. The $l = 0$ linear solutions satisfy

Taylor's constraint automatically, so the criteria (3.40) and (3.51) are not relevant for these modes. The dashed curve labelled r_T in Figure 1 gives the Taylor states with wavenumbers corresponding to the dashed extension of the $l \neq 0$ linear curve below $\Lambda = 4$. These wavenumbers are given by (3.17) with $\frac{1}{5} \leq \chi \leq \frac{1}{3}$. In this range, the linear $l \neq 0$ solutions are at a local minimum of the Rayleigh number, but not at a global minimum, which is given by $l = 0$ modes. If one adopts the simple philosophy that the wavenumbers selected should be those that give the smallest Rayleigh number at onset, and that these wavenumbers should be retained as the Rayleigh number is increased, these Taylor states will never occur. Nevertheless, we have included them as a dashed curve in Figure 1 because it may be that stability considerations will indicate that the wavenumbers that actually arise as r is increased move away from their values at onset. It is also interesting to note how closely the inequality (3.51) is approached by the Taylor solutions shown in Figure 1.

4. BOUSSINESQ SCALINGS

Rather than attempting to eliminate the unbalanced force, $\mathbf{F}$, defined in (3.20), we shall, for the remainder of this paper, include an equal but opposite viscous force set up by the geostrophic shear, $\mathbf{U}$.

This dynamical balance can be demonstrated by scaling solutions of (2.31) – (2.35) in the following way:

$$\begin{aligned} T &= -z + E^{1/2}T', & p &= P + E^{1/2}p', \\ \mathbf{u} &= \mathbf{U} + E^{1/2}\mathbf{u}', & \mathbf{B} &= \mathbf{1}_z + E^{1/2}\mathbf{B}', \end{aligned} \tag{4.1}$$

where the geostrophic velocity, $\mathbf{U}(z)$ is the horizontal average of $\mathbf{u}$, so that $\overline{\mathbf{u}'} = 0$. On substituting (4.1) into (2.31) – (2.35) and equating like powers of E, we find that the dominant balance involves only the geostrophic flow:

$$U_z = \frac{dP}{dz}. \tag{4.2}$$

At order $E^{1/2}$, we recover (3.11), (3.21) and (3.22), and at order E we find

$$\nabla^2\mathbf{U} + \Lambda \left[\overline{(\nabla\times\mathbf{B}')\times\mathbf{B}'}\right]_H = 0. \tag{4.3}$$

This equation is obtained from the geostrophic part of (2.32), i.e. its horizontal average. [The remaining (non-geostrophic) part, of $(\nabla\times\mathbf{B}')\times\mathbf{B}'$ creates an order E velocity, which is negligible to the approximation to which we are working. The vertical component of $\overline{(\nabla\times\mathbf{B}')\times\mathbf{B}'}$ can of course be balanced by a vertical pressure gradient.]

We have now transformed our problem into that of solving the fully nonlinear (4.3) and

$$\nabla.\mathbf{u} = 0, \tag{4.4}$$

$$\mathbf{1}_y \times \mathbf{u} = -\nabla p' + T'\mathbf{1}_z + \Lambda(\nabla \times \mathbf{B}') \times \mathbf{1}_z, \tag{4.5}$$

$$\frac{\partial \mathbf{B}'}{\partial t} + \mathbf{U}.\nabla \mathbf{B}' = \nabla \times (\mathbf{u} \times \mathbf{1}_z) + \nabla^2 \mathbf{B}', \tag{4.6}$$

$$\frac{1}{q}\frac{\partial T'}{\partial t} + \mathbf{U}.\nabla T' = \nabla^2 T' - r u_z, \tag{4.7}$$

$$\nabla.\mathbf{B}' = 0, \tag{4.8}$$

subject to appropriate boundary conditions. By re-introducing the viscosity (into the determination of the geostrophic flow) we have not automatically ruled out the possibility of a Taylor state. As such a state is approached, the magnitude of $\mathbf{B}'$ tends to infinity while $\left[\overline{(\nabla \times \mathbf{B}') \times \mathbf{B}'}\right]_H$ and $\mathbf{U}$ tend to finite limits.

Supplemental to the derivation of boundary conditions in §2, we note here that the geostrophic flow should obey

$$\text{no-slip}: \quad \mathbf{U} = 0, \quad \text{at} \quad z = z_0,\ 1 + z_0, \tag{4.9r}$$

$$\text{stress-free}: \quad \frac{\partial \mathbf{U}}{\partial z} = 0, \quad \text{at} \quad z = z_0,\ 1 + z_0, \tag{4.9f}$$

the latter of which determines $\mathbf{U}$ only to an additive constant. Since, however, the excitation of convection in the layer cannot create horizontal momentum, we can supplement (2.36f) by

$$\text{stress-free}: \quad \int_0^1 \mathbf{U}\, dz = 0, \tag{4.10}$$

which removes the arbitrary constant.

As for the system (3.10) - (3.14), solutions exist of the form (3.15). The basic idea is that the solution will, through the nonlinearity of (4.3), equilibrate to a steady ($\omega = 0$) or a periodic ($\omega \neq 0$) state. And it is the determination of this state that provides the main theoretical challenge.

We shall henceforward consider only *duct models*, by which we mean that the convecting layer will be confined horizontally in the direction defined by $\mathbf{\Omega}$ by vertical walls, $y = 0, L$ in dimensionless variables; the layer is still unbounded in the x-direction (i.e. parallel to $\mathbf{B}_0$). We shall at first consider the case in which the vertical walls are slippery, but later in this section and throughout §5 we shall suppose instead that they are no-slip surfaces. In either case the preferred $l = 0$ modes (the "bananas") are still possible when $\Lambda < 4$ though, in the case of no-slip surfaces, the nonzero y-vorticity of the $l = 0$ roll creates an Ekman pumping at the walls; this pumping is insignificant, as we shall see below. The walls make themselves felt when $\Lambda > 4$: a single oblique roll is no longer a possibility. The two preferred rolls must be excited to equal amplitude as otherwise u_y would be nonzero on the walls. This has the consequence that $U_y \equiv 0$, and in future we shall write

$$\mathbf{U} = U(z)\mathbf{1}_x,$$

ignoring the suffix $_x$ on U_x.

The motivations for studying convective ducts are twofold. First, with stellar and planetary applications in mind (see §1), we wish to model only the equatorial regions of a spherical convection zone, and we therefore wish to impose a "cut-off" that simulates the limited latitudinal extent of the applications. The longitudinal wavelength of convection in an equatorial belt can only take discrete values, dictated by the circumference of the star or planet. The axisymmetric "doughnut" mode, $k = 0$ is still possible. Second, we wish to introduce vertical walls to explore in a planar model the differences that might be expected in the convective regimes of bodies like stars, that have free surfaces, and planets, whose convective cores are confined by surrounding mantles (see §1). We therefore wish to consider both the case of slippery vertical walls (§6) and no-slip vertical walls (§5). From the expressions for u_y, B_y' and $\partial T'/\partial y$ corresponding to (3.30), we see that these quantities vanish simultaneously whenever y is an integral multiple of π/l. We therefore find it convenient to suppose that the vertical walls of the duct are impermeable, perfectly electrically conducting and thermally insulating, and that they are placed at $y = 0$ and π/l. In Paper I, we chose $L = \pi$, so that l was an integer (or zero) for all solutions considered. For most of the numerical examples presented in this paper, however, $\Lambda = 6$ and for this choice $k = 1.117$ and $l = 1.668$ define the preferred mode of marginal Boussinesq convection in an unbounded layer. We shall therefore concentrate here on these values of k and l, and we shall therefore take $L = \pi/1.668 \approx 1.883$. In what follows, we shall, for B_x alone, modify (3.30), writing instead

$$B_x'(x,y,z,t) = ik\tilde{B}'(z)\exp[i(kx + \omega t)]\cos ly + \text{c.c.}. \tag{4.11}$$

By (4.11) and the u_x' given by (3.30), we see that, if l is an odd integer (we shall always take $l = 1$), u_x' and B_x' vanish together on the vertical walls. Implicit in (4.11) is therefore the presumption that these walls are perfect electrical conductors.

After eliminating u_x, u_y, B_x, and B_y from (4.4) – (4.8) (and after omitting the $'$ and the $\tilde{}$ as before), we obtain

$$\left(\frac{d^2}{dz^2} - k^2 - l^2\right) u_z = i(\omega + kU)\left[u_z - \frac{\Lambda^2 k^4}{l^2}B\right] + \Lambda k^2 \frac{dU}{dz}B + \frac{\Lambda k^2 (k^2 + l^2)}{l^2}T + \frac{\Lambda^2 k^4}{l^2}u_z, \tag{4.12}$$

$$\left(\frac{d^2}{dz^2} - k^2 - l^2\right) B = i(\omega + kU)B - u_z, \tag{4.13}$$

$$\left(\frac{d^2}{dz^2} - k^2 - l^2\right) T = \frac{i(\omega + kU)}{q}T + ru_z. \tag{4.14}$$

In the case of slippery vertical walls, we have from (4.3)

$$\frac{d^2U}{dz^2} = \frac{1}{2(k^2 + l^2)}\frac{d}{dz}\left\{l^2(u_z B^* + u_z^* B) + ik^3\Lambda\left(B\frac{dB^*}{dz} - B^*\frac{dB}{dz}\right)\right\}. \tag{4.15}$$

Bearing in mind (4.9f) and (4.10f), we see that in the case of stress-free walls

$$U = \frac{1}{2(k^2+l^2)} \int_0^z \left\{ l^2 (u_z B^* + u_z^* B) + ik^3 \Lambda \left(B \frac{dB^*}{dz} - B^* \frac{dB}{dz} \right) \right\} dz + C, \tag{4.16f}$$

where the constant C is chosen so that dU/dz vanishes at the walls. If however there is no-slip at the walls, we see from (4.9f) that

$$U = \frac{1}{2(k^2+l^2)} \int_0^z \left\{ l^2 (u_z B^* + u_z^* B) + ik^3 \Lambda \left(B \frac{dB^*}{dz} - B^* \frac{dB}{dz} \right) \right\} dz + Dz, \tag{4.16r}$$

where the constant D is chosen so that U vanishes on the walls. We consider only the case of free horizontal boundaries in this paper.

The system of equations (4.3) – (4.8) is also relevant to another scaling of the solutions other than (4.1), namely that appropriate to no-slip vertical walls. In place of (4.3) we have

$$U = \frac{L}{d} \frac{\Lambda}{\sqrt{(2E)}} \left[\overline{(\nabla \times \mathbf{B}') \times \mathbf{B}'} \right]_x, \tag{4.17}$$

which may be interpreted as a balance between the force $\left[\overline{(\nabla \times \mathbf{B}') \times \mathbf{B}'} \right]_x$ accelerating an entire horizontal sheet of fluid in the x-direction and the frictional force produced by the resulting motion at the edges of the sheet, where it meets the fixed vertical walls. The magnetic fields (and fluid motions) necessary to overcome this friction are $O(E^{1/4})$, i.e. much larger than the $O(E^{1/2})$ of scaling (4.1). As a result, the frictional force in the bulk of the fluid is negligible, being $O(E)$ as against the $O(E^{1/2})$ of the Lorentz force; thus the $\nabla^2 \mathbf{U}$ does not appear in (4.3) nor the d^2U/dz^2 in (4.15).

In deriving (4.17), we temporarily revert to dimensional units. When viscosity is omitted from the equation of motion, the force $\mu^{-1} \left[\overline{(\nabla \times \mathbf{B}') \times \mathbf{B}'} \right]_x$ is balanced by the Coriolis force created by a vertical motion, $W(z)\mathbf{1}_z$, in the bulk of the layer, given by

$$W = \frac{1}{2\Omega\rho_0\mu} \left[\overline{(\nabla \times \mathbf{B}') \times \mathbf{B}'} \right]_x.$$

The resulting mass flux WL can be balanced only by an equal but opposite mass flux in the Ekman layers on the vertical walls. Each Ekman layer carries the flux $-(\nu/4\Omega)^{1/2}U$, so that

$$U = \frac{L}{2\Omega\rho_0\mu} \left(\frac{\Omega}{\nu} \right)^{1/2} \left[\overline{(\nabla \times \mathbf{B}') \times \mathbf{B}'} \right]_x,$$

which is the dimensional form of (4.17).

The scaling replacing (4.1) is now

$$\begin{aligned} T &= -z + cE^{1/4}T', & p &= P + cE^{1/4}p', \\ \mathbf{u} &= \mathbf{U} + cE^{1/4}\mathbf{u}', & \mathbf{B} &= \mathbf{1}_z + cE^{1/4}\mathbf{B}', \end{aligned} \tag{4.18}$$

where $\frac{1}{2}c^2$ is the aspect ratio of the duct:

$$c = \left(\frac{d\sqrt{2}}{L}\right)^{1/2}.$$

The vector equations (4.4) - (4.8) and their scalar consequences (4.12) - (4.14) follow as before, but (4.15) is replace by the scaled form of (4.17), i.e.

$$U = -\frac{1}{2(k^2+l^2)}\frac{d}{dz}\left\{l^2(u_z B^* + u_z^* B) + ik^3\Lambda\left(B\frac{dB^*}{dz} - B^*\frac{dB}{dz}\right)\right\}. \qquad (4.19)$$

The mainstream geostrophic flow satisfies (4.10) but neither of the conditions (4.9); thin viscous layers are required in which the flow can adjust to the no-slip or stress-free conditions at the horizontal boundaries.

5. THE RIGID DUCT

The adjective "rigid" in the title of this section indicates that only the case of sticky vertical walls will be investigated here, these walls being (as always) perfect electrical conductors and perfect thermal insulators. As already mentioned, the results will not depend on the mechanical conditions at the horizontal boundaries. We shall focus mainly on the case of electrically insulating horizontal boundaries, although we shall briefly also consider the simpler case in which (2.41) apply.

The results of numerical integrations of (4.12) - (4.14) and (4.20) are presented in Figures 2 and 3. In both these sets of figures, $\Lambda = 6$, $k = 1.117$ and $l = 1.668$, these wavenumbers being those minimizing the Rayleigh number for marginal convection in an infinite layer when $\Lambda = 6$. To fit this solution into the duct, the duct must extend horizontally from $y = 0$ to $y = \pi/l \approx 1.883$, in units in which the layer depth is 1. The choice $\Lambda = 6$ is large enough (> 4) to ensure that the oblique rolls ($l \neq 0$) are preferred over the rolls aligned with the rotation axis ($l = 0$). The critical value of the Rayleigh number, r, for $\Lambda = 6$ is 43.637, so that the case depicted in Figs. 2 is only mildly supercritical. In the Boussinesq approximation, the frequency, ω, is zero for all marginal solutions, $|u_z|$, $|B_z|$ and $|T|$ are all symmetric about the central horizontal plane, $z = \frac{1}{2}$, and the geostrophic flow, U, is antisymmetric. In fact only steady solutions with these symmetries seem to be relevant in the case of a rigid duct, even for finite amplitude states.

The fields u_z, B and T are shown in Figures 2 and 3 through their amplitudes and phases:

$$u_z(z) = \alpha(z)e^{i\theta(z)}, \qquad B(z) = \beta(z)e^{i\phi(z)}, \qquad T(z) = \gamma(z)e^{i\psi(z)}. \qquad (5.1)$$

In Fig.2(b), , $\alpha/\alpha_{\max}$, $\beta/\beta_{\max}$ and $\gamma/\gamma_{\max}$ are shown, where $\alpha_{\max} \approx 3.055$, $\beta_{\max} \approx 0.351$ and $\gamma_{\max} \approx 11.185$ are the maximum (central) values of α, β and γ. It may be noted that β does not vanish at $z = 0$ and 1, as we have imposed the boundary conditions (3.41) for insulating horizontal walls. The phases, θ, ϕ and ψ of u_z, B and T are shown in Fig.2(c). The variation in phase is rather small in this case; this is not surprising as they would all be exactly in phase in the linear Boussinesq case.

Figure 3 is for a case of very large r, namely $r = 576,503$. As r is increased, an asymptotic limit is approached, and a number of terms in the full equations (4.12) – (4.14) become unimportant (see below). It is then possible to solve the equations using the scaling

$$
\begin{aligned}
z &\to \hat{z}\,\frac{l^{1/2}}{k^{1/2}\left(k^2+l^2\right)^{1/4}}\Lambda^{-1/4}r^{-1/4},\\
u_z &\to \hat{u}_z\,\frac{k^{1/4}\left(k^2+l^2\right)^{7/8}}{l^{7/4}}\Lambda^{3/8}r^{3/8},\\
B &\to \hat{B}\,\frac{\left(k^2+l^2\right)^{3/8}}{k^{3/4}\,l^{3/4}}\Lambda^{-1/8}r^{-1/8},\\
T &\to -\hat{T}\,\frac{\left(k^2+l^2\right)^{3/8}}{k^{3/4}\,l^{3/4}}\Lambda^{-1/8}r^{7/8},\\
U &\to \hat{U}\,\frac{\left(k^2+l^2\right)^{1/2}}{l}\Lambda^{1/2}r^{1/2}.
\end{aligned}
\tag{5.2}
$$

In this scaling the horizontal boundaries are $\hat{z} = 0$ and z_1, where

$$
z_1 = \frac{k^{1/2}\left(k^2+l^2\right)^{1/4}}{l^{1/2}}\Lambda^{1/4}r^{1/4}.
$$

With the stated choice of r, and adopting the same values of Elsasser number and wavenumbers as for Figs.2, we have $z_1 = 50$.

The geostrophic wind remains antisymmetric about $z = \frac{1}{2}$ in the asymptotic limit, and is largest near the boundaries [see Fig. 3(a)]; in the central regions there are relatively weak oscillations, whose amplitude decreases towards the centre of the layer. Similar oscillations are present in the amplitudes of u_z, B and T displayed in Fig. 3(b). Note that, because of our asymptotic scaling (5.2), all these amplitudes can be conveniently plotted on the same figure, without dividing by their maxima for normalization. The phase plots shown in Fig.3(c) are almost identical for all three variables; there is a large variation in phase, so that the solutions correspond to convection with a large number of rolls in the vertical direction.

When (4.12) – (4.14) and (4.20) are scaled as in (5.1) and the limit $r \to \infty$ is taken and the $\hat{}$ is omitted, it is found that

$$\frac{d^2u_z}{dz^2} = i(U-\omega)u_z - T, \tag{5.3}$$

$$\frac{d^2B}{dz^2} = i(U-\omega)B - u_z, \tag{5.4}$$

$$\frac{d^2T}{dz^2} = \frac{i(U-\omega)}{q}T - W, \tag{5.5}$$

$$U = -\frac{1}{2}\frac{d}{dz}\left(u_zB^* + u_z^*B\right). \tag{5.6}$$

For the case of the rigid duct considered in this section, we may set $\omega = 0$ in (5.3) - (5.5).

Equations (5.3) - (5.6) for the asymptotic state are solved with particular ease when $q = 1$ (the only case considered here) and the illustrative conditions (4.22) apply. For then by assuming that

$$u_z = B = T \tag{5.7}$$

for all z, we reduce both equations and boundary conditions to the single second order equation,

$$\frac{d^2B}{dz^2} = -i\frac{d}{dz}(BB^*)B - B, \tag{5.8}$$

which must be solved subject to the two conditions

$$B = 0, \qquad \text{at} \quad z = 0, z_1. \tag{5.9}$$

Let us again adopt the polar representation (3.26):

$$B(z) = \beta(z)e^{i\phi(z)}, \tag{5.10}$$

substitute into (5.8) and (5.9), and equate real and imaginary parts. We obtain

$$\frac{d\phi}{dz} = -\frac{1}{2}\beta^2, \tag{5.11}$$

and

$$\frac{d^2\beta}{dz^2} = \frac{1}{4}\beta^5 - \beta, \tag{5.12}$$

which must be solved subject to

$$\beta = 0, \qquad \text{at} \quad z = 0, z_1. \tag{5.13}$$

The relevant solution of (5.12) and (5.13) is

$$z = \frac{2\sqrt{3}}{\beta_0^2}\int_0^{\beta/\beta_0} \frac{dv}{\sqrt{[(1-v^2)(V-v^2-v^4)]}}, \tag{5.14}$$

where

$$V = \frac{12}{\beta_0^4} - 1.$$

According to (5.14), β increases monotonically with z up to a maximum of β_0 ($\leq \sqrt{2}$) at $z = \frac{1}{2}z_1$, where

$$z_1 = \frac{4\sqrt{3}}{\beta_0^2}\int_0^1 \frac{dv}{\sqrt{[(1-v^2)(V-v^2-v^4)]}}. \tag{5.15}$$

Since $\beta(z) = \beta(z_1 - z)$, β decreases symmetrically to zero as z increases from $\frac{1}{2}z_1$ to z_1.

When β differs only slightly from $\sqrt{2}$, β is approximately constant (and equal to β_0) in a mainstream away from the walls, and matches to conditions (5.13) in thermal boundary

layers whose thicknesses, in the original z variable, are $O(r^{-1/4})$; see (5.1). The boundary layer solution is easily obtained by setting $\beta_0 = \sqrt{2}$ in (5.14), so obtaining

$$e^{-2z} = \frac{\sqrt{2}-\beta}{\sqrt{2}+\beta}\left[\frac{\sqrt{[3(\beta^2+4)]}+2\sqrt{2}+\beta}{\sqrt{[3(\beta^2+4)]}+2\sqrt{2}-\beta}\right]. \tag{5.16}$$

When solving (5.3) – (5.5) subject to the more realistic conditions (3.41), corresponding to electrically insulating walls, it is at once clear from (3.41) that (5.7) is untrue, but

$$T = u_z, \tag{5.17}$$

is still admissible. We are then faced with solving (5.3) and (5.4), i.e.

$$\frac{d^2u_z}{dz^2} = -\frac{i}{2}u_z\frac{d}{dz}(u_zB^* + u_z^*B) - u_z, \tag{5.18}$$

$$\frac{d^2B}{dz^2} = -\frac{i}{2}B\frac{d}{dz}(u_zB^* + u_z^*B) - u_z, \tag{5.19}$$

subject to

$$u_z = \frac{\partial B}{\partial z} \pm \sqrt{(k^2+l^2)}\,B = 0, \quad \text{at} \quad z = \tfrac{1}{2} \pm \tfrac{1}{2}. \tag{5.20}$$

To leading order, (5.7) remains true outside the boundary layers, and

$$u_z \sim B \sim \beta_0 e^{-iz}, \tag{5.21}$$

but the numerical solutions shown in Fig 3 have significant oscillations superimposed on these leading order parts. This is slightly surprising, as the Rayleigh number used for Fig 3 is very large, and one might expect the leading to dominate completely. To study these, oscillations we introduce the difference,

$$\xi = u_z - B, \tag{5.22}$$

between u_z and B in the expectation that ξ will be vanishingly small in the limit $r \to \infty$ but will become $O(1)$ as either boundary is approached. By (5.21),

$$\frac{d}{dz}(u_zB^* + u_z^*B) = O(\xi), \tag{5.23}$$

and by (5.18) and (5.19), we have

$$\frac{d^2\xi}{dz^2} = -\frac{i}{2}\xi\frac{d}{dz}(u_zB^* + u_z^*B). \tag{5.24}$$

It follows from (5.23) that to leading order the right-hand side of (5.24) can be neglected, so that $\xi \approx A_0 + A_1 z$. Since however the solution should remain near $\xi = 0$, it follows that the constant A_1 is zero.

In the next approximation, A_0 is a slowly varying function of z, and we therefore write

$$\xi = \epsilon A_0(\zeta) + \epsilon^2 f + \epsilon^3 g + \ldots, \tag{5.25}$$

where ϵ is a measure of the amplitude of ξ and $\zeta = \epsilon z$ is a stretched coordinate. Now refine (5.21) by writing

$$\begin{aligned} u_z &= \beta_0 e^{-iz} + w, \\ B &= \beta_0 e^{-iz} + w - \epsilon A_0, \end{aligned} \tag{5.26}$$

where $w = O(\epsilon)$. On substituting (5.26) into (5.18) and (5.19), and retaining terms of order ϵ, we find

$$\frac{d^2w}{dz^2} + w = \beta_0^2 \left\{ \left[w - \frac{1}{2}\epsilon A_0 - i\frac{dw}{dz} \right] - e^{-2iz} \left[w^* - \frac{1}{2}\epsilon A_0^* + i\frac{dw^*}{dz} \right] \right\}. \tag{5.27}$$

This admits a solution of the form

$$w = k_1 + k_2 e^{-2iz},$$

and after evaluating the constants k_1 and k_2 we find that (5.26) is in fact

$$\begin{aligned} u_z &= \beta_0 e^{-iz} + \frac{3\epsilon\beta_0^2}{8\beta_0^2 - 6} A_0 + \frac{\epsilon\beta_0^2}{8\beta_0^2 - 6} A_0^* e^{-2iz}, \\ B &= \beta_0 e^{-iz} + \frac{\epsilon(6 - 5\beta_0^2)}{8\beta_0^2 - 6} A_0 + \frac{\epsilon\beta_0^2}{8\beta_0^2 - 6} A_0^* e^{-2iz}. \end{aligned} \tag{5.28}$$

Substituting these and (5.25) into (5.24), working to order ϵ^2, and integrating once, we obtain

$$f = -\frac{3\beta_0\epsilon^2}{8\beta_0^2 - 6} A_0 \left[A_0 e^{iz} - A_0^* e^{-iz} \right].$$

We are now in a position to work to order ϵ^3, and, by picking out the secularity of that order in (5.24), to find the slow variation of A_0. We obtain

$$\frac{d^2A_0}{d\zeta^2} = 2\left(\frac{3\beta_0}{8\beta_0^2 - 6} \right)^2 |A_0|^2 A_0. \tag{5.29}$$

The relevant solution to (5.29) is real, and an integration of (5.29) gives

$$\left(\frac{dA_0}{d\zeta} \right)^2 = \left(\frac{3\beta_0}{8\beta_0^2 - 6} \right)^2 A_0^4 + k_3. \tag{5.30}$$

We recall here that we are interested in providing an explanation of the deviation in B from u_z as z increases from the boundary layer at $z = 0$, this increase being accompanied

by a decrease in $|\xi|$. We therefore seek a non-oscillatory solution of (5.30), and so take $k_3 = 0$ in (5.30) and integrate once more to obtain

$$A_0 = \frac{8\beta_0^2 - 6}{3\beta_0(\zeta_0 + \epsilon z)}, \tag{5.31}$$

where ζ_0 is an O(1) constant. Substituting this result into (5.28) we find that

$$\begin{aligned} u_z &= \beta_0 e^{-iz} + \frac{\beta_0}{3(z - \zeta_0/\epsilon)}(3 + e^{-2iz}), \\ B &= \beta_0 e^{-iz} + \frac{1}{3\beta_0(z - \zeta_0/\epsilon)}(6 - 5\beta_0^2 + \beta_0^2 e^{-2iz}). \end{aligned} \tag{5.32}$$

This theory is unable to decide on the value of the constant ζ_0/ϵ, but numerical integrations can be used to determine it approximately. For large r, the forms (5.32) then agree with the numerical results over a wide range of z. This analysis indicates why the oscillations persist at such large values of r: the oscillatory terms decay at only the slow rate $1/z$ as $z \to \infty$, and z itself is scaled only on $r^{1/4}$.

6. THE FREE DUCT

The adjective "free" in the title of this section indicates that only the case of slippery vertical walls will be investigated here, these walls being (as always) perfect electrical conductors and perfect thermal insulators. As already mentioned, the results will not depend on the mechanical conditions at the horizontal boundaries. We shall consider only the case of electrically insulating horizontal boundaries.

The results of numerical integrations of (4.12) – (4.14) and (4.16f), i.e.

$$U = \frac{1}{2(k^2 + l^2)} \int_0^z \left\{ l^2 (u_z B^* + u_z^* B) + ik^3 \Lambda \left(B \frac{dB^*}{dz} - B^* \frac{dB}{dz} \right) \right\} dz + C, \tag{6.1}$$

(where the constant C is chosen so that the mean value of U is zero) are presented in Figures 4 – 7. Fig. 4 displays an essential difference between the free duct and the rigid duct (§5), namely the occurrence of a symmetry-breaking bifurcation in the case of a free duct. In the case of a rigid duct, all solutions were steady and $f = u_z$, B and T all satisfied $f(z) = -f^*(1 - z)$, while the geostrophic wind was antisymmetric: $U(z) = -U(1 - z)$.

In Fig. 4, in which $\Lambda = 6$, $k = 1.117$ and $l = 1.668$ as before, the solution emerging from the bifurcation point, B_1, at $r = 43.637$ is steady and symmetric. But, from the symmetry-breaking bifurcation, B_3, at $r = 304.378$ two time-dependent solutions emerge which are asymmetric in the sense that $f(z) \neq -f^*(1 - z)$, although $f_1(z) = -f_2^*(1 - z)$ where $_1$ and $_2$ refer to the different solutions. Typically, one solution corresponds to convection that occurs primarily in the upper half of the layer, while the other corresponds to convection that mainly takes place in the lower half of the layer. Both solutions travel as waves with equal and opposite phase velocities. After undergoing the bifurcation B_3, the original time-independent branch turns round at a saddle-node bifurcation B_4, and

then continues down to connect with the zero solution at B_2. Here B_2 corresponds to a linear solution with two rolls in the vertical direction and a critical Rayleigh number given by (3.16) with π^2 replaced by $4\pi^2$.

The amplitude shown in Fig.4 is based on the vertical velocity, and is constructed in the following way. We decompose u_z into its real and imaginary parts, u_z^r and u_z^i, and further divide u_z^r and u_z^i into parts that are symmetric and antisymmetric about $z = \frac{1}{2}$, so that

$$u_z = u_z^{rs} + u_z^{ra} + i\left(u_z^{is} + u_z^{ia}\right).$$

Steady solutions ($\omega = 0$) have the property that, with the correct choice of phase, $u_z^{ra} = u_z^{is} = 0$. Near the bifurcation point B_1 (a one cell solution), u_z^{ia} is zero, while near the bifurcation point B_2 (a two cell solution), u_z^{rs} is zero. We define

$$a_1 = \int_0^{1/2} u_z^{rs} dz, \qquad a_2 = \int_0^{1/2} u_z^{ra} dz, \qquad a_3 = \int_0^{1/2} u_z^{is} dz, \qquad a_4 = \int_0^{1/2} u_z^{ia} dz. \tag{6.2}$$

For steady solutions $a_2 = a_3 = 0$. All four are in general nonzero for time-dependent solutions; the two solutions for the same Rayleigh number are related by

$$\omega \sim -\omega, \qquad u_z^{rs} \sim u_z^{rs}, \qquad u_z^{ra} \sim -u_z^{ra}, \qquad u_z^{is} \sim -u_z^{is}, \qquad u_z^{ia} \sim u_z^{ia},$$

so that by (6.2)

$$a_1 \sim a_1, \qquad a_2 \sim -a_2, \qquad a_3 \sim -a_3, \qquad a_4 \sim a_4.$$

The amplitude used in Fig.4 is defined by

$$a = a_1 - a_2 + a_3 - a_4.$$

Although in principle any measure of the amplitude suffices, in practice some care must be exercised. If a does not contain any contribution from a_3 and a_4, the two branches emerging from B_3 will coincide in the (r, a)-plane; if the symmetric part of a does not contain a contribution from both a_1 and a_4, the bifurcation diagram will not necessarily show the correct $(r - r_c)^{1/2}$ behaviour near the bifurcation points B_1 and B_2.

In Figs.5, solutions are plotted in a manner completely analogous to that used in Figs.2. Apart from a slight change in the form of the geostrophic wind, the mildly supercritical cases $r = 50$ for rigid and free ducts are very similar. Figure 6 is for $r = 320$, and shows the solution shortly after it has undergone the symmetry-breaing bifurcation at B_3. These figures are scaled in the same manner as were Figs. 2 and 5. The geostrophic wind is no longer antisymmetric, but is larger in amplitude at one boundary ($z = 0$ in the case shown) than at the other. The value of ω in our dimensionless units is 4.932, so that the wave propagates in the negative x-direction. For the corresponding solution from the other branch, $\omega = -4.932$ (it therefore propagates in the positive x-direction), and has a geostrophic velocity U that is larger in absolute value near $z = 1$ than near $z = 0$. The amplitude peaks are shifted nearer to $z = 1$ where the geostrophic wind is strongest.

Figure 7 presents the solutions for $r = 576,503$, again scaled in the way suggested by the asymptotic theory, in which it is convenient to replace (5.2) by

$$\begin{aligned} z &\to \hat{z}\,\frac{l^{1/2}}{k^{1/2}\left(k^2+l^2\right)^{1/4}}\Lambda^{-1/4}r^{-1/4}, \\ u_z &\to \hat{u}_z\,\frac{k^{3/4}\left(k^2+l^2\right)^{9/8}}{l^{9/4}}\Lambda^{5/8}r^{5/8}, \\ B &\to \hat{B}\,\frac{\left(k^2+l^2\right)^{5/8}}{k^{1/4}\,l^{5/4}}\Lambda^{1/8}r^{1/8}, \\ T &\to -\hat{T}\,\frac{\left(k^2+l^2\right)^{5/8}}{k^{1/4}\,l^{5/4}}\Lambda^{1/8}r^{9/8}, \\ U &\to \hat{U}\,\frac{\left(k^2+l^2\right)^{1/2}}{l}\Lambda^{1/2}r^{1/2}. \end{aligned} \tag{6.3}$$

These scalings reduce (4.12) - (4.14) again to (5.3) - (5.5), where now ω is nonzero after the symmetry is broken, together with

$$U = \frac{1}{2}\int_0^z \left(u_z B^* + u_z^* B\right) dz + C. \tag{6.4}$$

Only the z scaling is the same as in (5.1), and this means that the position of the horizontal boundaries scales as in §5, i.e. they are at $\hat{z} = 0$ and z_1 as before. The advantage of scaling (6.2) is that, when the limit $r \to \infty$ is taken and the $\hat{}$ is omitted, (5.3) - (5.5) are recovered from (4.12) - (4.14); only (5.6) is replaced by the scaled form of (6.1). We shall not attempt to develop here an asymptotic, $r \to \infty$, theory along the lines of that presented in §5.

The nature of the solutions shown in Figs.7 is remarkable: the convection is almost entirely confined to a boundary layer of thickness $O(r^{-1/4})$. The frequency is $\omega = 1.0433$ in these units, which means that the critical level, at which the Doppler-shifted frequency $\omega_D \equiv \omega + kU$ vanishes, lies within the boundary layer. In the mainstream, ω_D is large, and this is why the amplitude of the convection is so small there; the wave is moving too rapidly through the fluid for significant convection to occur. There is, of course, an analogous solution to that shown in Figs.7, in which ω is negative, corresponding to wave motion in the positive x-direction, and in which convection occurs only in a boundary layer near the bottom boundary, $z = 1$.

We conjecture that these solutions are unlikely to be stable; disturbances that have a large amplitude in the mainstream and which travel with the mainstream geostrophic velocity will probably be unstable at such large Rayleigh numbers.

7. THE FREE COMPRESSIBLE DUCT

We now return to the subject which formed the starting point of this investigation, the extension of the linear theory of compressible rotating magnetoconvection developed in

paper I into the nonlinear regime. Because we have in mind astrophysical applications, it is inappropriate to analyse the case of rigid boundaries, and we shall consider here only the free duct, in which the horizontally averaged Lorentz force in the direction of the field is balanced by the viscous shear associated with the geostrophic flow. In application to the solar convection zone, viscous shears are normally modelled by a turbulent eddy transport of momentum, a concept that lacks some precision (see, for example, Rüdiger, 1989).

The linear theory of paper I showed that the critical wavenumbers determining the minimum Rayleigh number were only slightly altered by the introduction of compressibility, even when the density varied over many scale heights within the layer. The only important exception to this was the $l \rightarrow 0$ limit (corresponding to pure banana cells in the solar convection zone) which was markedly affected by compressibility. Since we are primarily interested in situations where the field strongly affects the dynamics, and since then the wavenumbers k and l are both nonzero, we have, in the work described below, concentrated on the same values of Λ, k and l as we used in studying the Boussinesq limit. This seemed preferable to introducing the slight changes that would occur had we selected the k and l that minimized r in the compressible case.

An important distinction, reported in paper I, between the linear compressible and linear Boussinesq problems is that compressible convection always occurs as a travelling wave, not as steady convection. In consequence, the Boussinesq symmetry between the waves that propagate in the positive and negative x-directions is lost from the outset. In fact, waves propagating in the positive x-direction are associated with convection that occurs mainly in the lower part of the layer. When the layer is polytropic, this has a very different structure from the tenuous upper part of the layer, in which the convection associated with waves moving in the negative x-direction are principally concentrated.

The vector form of the equations in the compressible case has been given equations (2.23) to (2.28) above. As in paper I, a convenient set of dependent variables is $w = \rho u_z$, B_z and T. The equations satisfied by these are

$$\left(\frac{d^2}{dz^2} - k^2 - l^2\right) w = i(\omega + kU)\left[w - \frac{\Lambda^2 k^4}{l^2 \zeta^m} B\right] + \frac{\Lambda^2 k^4}{l^2 \zeta^{2m}} w - \frac{ik w \Lambda}{(z_0 + \frac{1}{2})\zeta^{m+1}}\left[m + \frac{(m+1)(k^2+l^2)}{l^2}\right] + \Lambda k^2 \frac{dU}{dz} B + \frac{\Lambda k^2 (k^2 + l^2)}{l^2 \zeta} T, \tag{7.1}$$

$$\left(\frac{d^2}{dz^2} - k^2 - l^2\right) B = i(\omega + kU) B - \frac{w}{\zeta^m}, \tag{7.2}$$

$$\left(\frac{d^2}{dz^2} - k^2 - l^2\right) T = \frac{i(\omega + kU)\zeta^m}{q} T + \frac{(\omega + kU)}{kq(z_0 + \frac{1}{2})} w + rw. \tag{7.3}$$

The equation for the geostrophic wind is the same as in the Boussinesq case: (4.15) since we assume the vertical walls are stress-free.

Even though compressible convection occurs as waves, it was found in paper I that the eigenfunctions are not totally dissimilar from those of the Boussinesq model. We therefore

expect that the symmetry-breaking bifurcation of the Boussinesq model (see Fig. 4) will be unfolded, and that one of the branches emerging from that pitchfork bifurcation will be smoothly connected to the linear solution appearing at the lowest critical Rayleigh number (B_1 on Fig. 4), while the other branch will emerge from the second lowest critical Rayleigh number (B_2 on Fig. 4). This behaviour can be seen in Figure 8, where the bifurcation diagram is shown for three cases: the Boussinesq case ($z_0 \to \infty$), a slightly compressible case ($z_0 = 1.0$), and a strongly compressible case ($z_0 = 0.1$). The definition of the amplitude is the same as in §6, but with w replacing u_x. Although this diagram shows how complicated the situation can become as z_0 is decreased, the behaviour of the solutions can be understood in general terms.

We see in Fig. 8 that when $z_0 = 1.0$, the case closest to Boussinesq, the primary branch behaves much as expected: the solution consisting of one series of rolls filling the vertical extent of the layer (as distinct from the solution at β_2, in which there are two horizontal layers of rolls, one lying above the other) evolves smoothly into a solution in which that one roll concentrates towards the lower, denser part of the layer. The behaviour of the secondary mode is more complicated. As compressibility is gradually imposed, the secondary branch first "pinches off" near B_3, and then "loops" near B_3. This is because, in the Boussinesq case, the asymmetric branch has, just below B_3 in Fig. 4, a smaller Rayleigh number than does the symmetric solution. As we move further from B_3, the situation is reversed, because the asymmetric branch has, at the same amplitude, a larger Rayleigh number than does the symmetric branch. Consequently there has to be a loop on the secondary branch. At $z_0 = 1.0$, this loop is just visible in Fig. 8, although it is very tiny. Two saddle-node bifurcations are associated with this phenomenon, labelled β_5 and β_6.

There are also two further saddle-node bifurcations on this secondary branch, β_3 and β_4. The origin of these is not so clear, but they seem to be associated with the change in the pattern of the eigenfunctions. At β_2, the mode has two horizontal layers of rolls of roughly similar size and strength. As we move along the secondary branch past β_3 and β_4 the roll in the upper half of the layer increases in strength, while that in the lower half decreases. If we now move to the strongly compressible case, $z_0 = 0.1$, we see that the primary branch, now bifurcating from the zero solution at b_1, is not greatly changed. The only new feature is that the critical Rayleigh number for b_1 is significantly greater than for the Boussinesq B_1. The loop where the secondary branch pinched off from B_3 has disappeared, so that no bifurcations corresponding to β_5 and β_6 exist. As z_0 is reduced from 1 to 0.1 these two bifurcations coalesce. There are, however, still two saddle-node bifurcations corresponding to β_3 and β_4 which are labelled b_3 and b_4. The secondary branch now bifurcates off from the zero solution at b_2.

In Figures 9 and 10 compressible eigenfunctions are plotted in the same format as for Figure 3. Figure 9 is for the primary branch in the strongly compressible case, with $r = 700$, and this can be compared with Figure 10 which is for the secondary branch but at the same parameter values as Figure 9. In constructing these figures, it should be noted that the zero linear momentum condition takes the form

$$\int_0^1 \rho \mathbf{U}\, dz = 0, \tag{7.4}$$

which replaces (4.10). This has the effect of making the geostrophic wind much greater in the tenuous upper regions of the layer than in the lower part of the zone.

Although the equations (7.1) to (7.3) were solved using w, in Figures (9) and (10) u_z is plotted, consistent with the practice of paper I. The value of ω in the primary mode case is -18.022 and in the secondary mode case is 21.669. The depth at which the wavespeed equals the fluid speed is therefore much greater in the primary branch than the secondary branch. The geostrophic wind is rather small at large depth in the secondary mode, but the wavespeed is not, so these regions are being disrupted by the shear: this accounts for the small amplitudes at the base of the zone in Figure 10b. The corresponding amplitudes are much larger in figure 9b, because the wave speed and fluid speed are there much closer at the base of the layer. It might be expected that the geostrophic wind would be smaller near the top of the zone in the primary mode than it is (see Fig. 9a). The geostrophic wind is driven by B_z and u_z, not w; although w is quite small near the top of the layer u_z is considerably larger, because of the density factor. If the horizontal momentum, rather than wind speed, were plotted, there would be more symmetry between the two modes. The phases, shown in Figures 9c and 10c, are quite similar in the two cases: however, it is interesting to note that in the primary mode particularly, a substantial phase difference develops between the vertical velocity and the temperature. This feature was noted in the linear theory of paper I.

8. DISCUSSION

Perhaps the most surprising finding of this investigation is the difference between the original Roberts-Stewartson problem where the rotation is parallel to gravity and the case considered here, when rotation and gravity are perpendicular. The linear theory of these two cases is not strikingly different, but a comparison of this work with that of Soward (1986) and Soward and Skinner (1989) shows that in the nonlinear regime marked differences appear. These are connected with the "anti-Taylor" inequalities developed in §3, which apparently have no analogue in the Roberts-Stewartson problem. The nonlinear behaviour is strongly dependent on whether a Taylor state emerges or not.

We first review the case where a Taylor state occurs at some value, r_T, of r as, for example, in the Roberts-Stewartson problem: we assume the Ekman number is small. At values of $r < r_T$, the amplitude of the convection is controlled by the geostrophic wind and is held to a value proportional to a positive power of the Ekman number. The precise value of this power depends on the boundary conditions.

As $r \rightarrow r_T$ the amplitude of convection rises sharply and new nonlinearities become important: in the present problem the advection of temperature and magnetic field described by $\mathbf{u}.\nabla T$ and $\mathbf{u}.\nabla\mathbf{B}$ will dominate. For $r < r_T$ only the geostrophic velocity $\mathbf{U}$, which is purely azimuthal, makes a significant contribution to these advection processes: when $r > r_T$, however, the convective velocities become sufficiently large to affect the amplitude of convection. Advection of temperature is of course the dominant nonlinear mechanism by which the amplitude is controlled in moderate or high Prandtl number Rayleigh-Bénard convection: in this sense, then, when $r > r_T$ rapidly rotating magnetoconvection has a nonlinear limiting mechanism similar to that of "ordinary" convection, although the fluid motions are still highly constrained by the rotation and the magnetic field. By "ordinary"

convection we here refer to convection in which the Taylor and Chandrasekhar numbers are moderate or small. Although the dominant nonlinear mechanism in large T and Q convection is the same as in ordinary convection, there is still an important difference: in ordinary convection viscosity is always important, and enters in the definition of the Rayleigh number, whereas in convection at high T and Q the solutions are independent of viscosity once r has exceeded r_T.

The whole picture is changed if there is no Taylor state, as in the problem we have investigated. The dominant nonlinearity is now always provided by the geostrophic flow, since the convective velocities are always smaller than the geostrophic flow by a factor proportional to some positive power of the viscosity. The geostrophic flow controls the convection by shearing it and hence inhibiting its growth, a very different mechanism from the advection of heat.

In most of the numerical simulations that have been conducted in spherical geometry the Taylor and Chandrasekhar numbers have been quite modest. In consequence, the viscous terms in the equation of motion have been of the same order of magnitude as the Lorentz and Coriolis terms, so that the differential rotation is usually of the same order of magnitude as the convective velocities, and the regime we describe here has not properly been reached.

The analysis here presupposed that E is small. In fact, the limit $E \rightarrow 0$ was taken for fixed r, and only subsequently was the limit $r \rightarrow \infty$ considered. A natural question to ask is what happens if the order of these limits is reversed, i.e. if it is assumed that E is fixed initially at a small nonzero value, and r is increased. Eventually, as r becomes very large the amplitude of the solution increases and the advection terms will begin to become significant. In the rigid boundary case, the scalings (4.18) and (5.2) imply that the $(\mathbf{u}'.\nabla)T'$ term is of order $E^{1/2}r^{3/2}$ whereas the terms retained in (4.14) are order $E^{1/4}r^{11/8}$. In consequence, we expect the advection terms to become significant when $r \sim E^{-2}$. (Similar considerations apply to the advection terms in the induction equation.) In the free boundary case, scalings (4.1) and (6.3) give $r \sim E^{-4/3}$. For values of r exceeding this, the nonlinear mechanism of advection of temperature will start to become important again, as it is in ordinary convection. The mathematical problem then becomes much more difficult, as this nonlinearity couples together different horizontal modes, so that the solutions no longer have exp $i(kx + ly)$ dependence.

The main application of the theory of rapidly rotating magnetoconvection has been to geodynamo theory: see, for example, Fearn, Roberts and Soward (1988). It is generally accepted that, in the outer core of the Earth, Coriolis and Lorentz forces are of comparable strength, and that the viscous terms in the interior are considerably less (small Ekman number, E). The most significant application of our results to the geodynamo problem concerns the non-appearance of Taylor states, in contrast to the cases studied by Soward (1986) and Soward and Skinner (1989). In the second of these papers, rotation and gravity are still parallel, but the geometry is that of a cylinder rather than that of a plane layer. The significant difference between their models and ours seems to be the angle between the rotation vector and gravity. What happens in full spherical geometry is an interesting but so far unresolved question: in cases where the convection is predominantly near the equatorial zone, as for example in the Braginsky (1978) model-Z dynamo, the configuration

of gravity, rotation and field used in this paper would appear to be more relevant.

Another application of the theory is to the dynamics of the solar convection zone (e.g. Jones and Galloway 1988, and paper I). The situation here is not so clear cut, however, as it is not certain that the Lorentz force plays an important role in the dynamics of solar convection. Between the photosphere and a depth of a few thousand kilometres, the Lorentz force is, of course, vital in the neighbourhood of sunspots, but it is not significant on a large scale outside these active regions; the field appears to be expelled by the vigorous convective eddies, and its role is confined to rather narrow flux tubes. The situation at greater depths is uncertain. Earlier models of the dynamics of the convection zone ignored the magnetic field, but this may have been due more to a desire to avoid the mathematical complexities of rotating magnetoconvection than to a belief that the magnetic field was irrelevant. The idea that the magnetic field might be significant in controlling the pattern of convection has been given further impetus by the suggestion by Ribes et al (1985) that the convection pattern is more in the form of doughnut cells than in the form of banana cells. A further argument is made plausible by the large-scale coherence of the solar cycle, which suggests that, at least in the regions where the toroidal field is generated, convection is not sufficiently strong to disrupt and redistribute the field as happens near the photosphere. We might expect the field in these regions (which may well lie near the base of the convection zone) to vary only on a fairly long length scale: this will then restrict large-scale convective velocities to the rate at which fluid can diffuse through the field.

These considerations lead us to a picture of the astrophysical circumstances under which our assumptions about the relative strength of the terms in the governing equations may be justified. First, we require that the Ekman number $\nu/2\Omega d^2$ be small: here d is the length scale on which the convection is occuring. If ν is a turbulent viscosity, $\nu \sim u'l$, where u' is the turbulent velocity and l is the correlation length. If, as is generally assumed in the mixing length approach, u' is similar to the convective velocity u and l is similar to d, then small Ekman number is equivalent to small Rossby number $u/2\Omega d$. The Rossby number is large near the solar photosphere, but fairly small in the deeper solar convection zone, and is very small in the convection zones of rapidly rotating stars.

Second we require there to be a magnetic field of a suitable strength present. If this is generated by dynamo action, it is likely that the field strength will rise to a value at which the Lorentz force is comparable with the Coriolis force: the induction equation is linear in $\mathbf{B}$, so an amplifying field will grow until the nonlinear Lorentz force makes itself felt. Also the convection itself is most efficient when the Elsasser number of $O(1)$, since then the preferred modes have wavelengths which fill the volume available. This second requirement is therefore quite likely to be fulfilled if dynamo action occurs in a low Rossby number regime.

Third we require that the flux not be expelled into thin flux tubes. If it is, the fluid between the tubes can convect in a manner which is relatively unimpeded by the fluid, and our assumptions are no longer justified. Two fields of the same mean flux density could have very different effects on convection if one is uniform and the other is condensed into thin tubes. Whether the flux in the deeper convection zone is in the form of thin tubes is not known. It certainly is near the surface, but rotation is unimportant near the surface, so that magnetic field can only impede convection. It is perhaps therefore not

surprising that the convection expels the flux into tubes in order to boost its efficiency. In a rotating system at small Ekman (or Rossby) number, however, magnetic field can help release the Taylor-Proudman constraint, and hence actually promote convection (see e.g. Fearn, Roberts and Soward, 1988). Under these circumstances it is less clear that flux expulsion will occur.

In view of their considerations we believe that our model may have some relevance to the deep solar convection zone: our plane geometry and simplified polytropic structure require us to be cautious in applying our results. Nevertheless, we should draw attention to the symmetry breaking bifurcations that occur when the rigid lid is removed (see §§6 and 7 above). In almost all previous investigations of linear and nonlinear compressible convection, with magnetic field and rotation (as in paper I) or without them, the preferred mode of convection involved just one roll in the vertical direction. The only exceptions were models in which two or more rolls were induced in the vertical by an inhomogeneity in the equilibrium model: for example, in the two-zone models of paper I, in which the polytropic layer was divided into a weakly superadiabatic zone at the bottom of the layer and a strongly superadiabatic zone at the top of the layer, two modes of convection were found, each dominating in one of the zones. In the nonlinear model discussed here, however, convection divides *naturally* into modes which exist primarily in the lower part of the zone and modes which are concentrated mainly in the upper part. This unusual behaviour is a consequence of the geostrophic shear (differential rotation) being the controlling nonlinearity. As the shear increases in magnitude, the convection becomes localized in the vertical direction to reduce the disruptive effect of the shear. This localization of the convection is an essentially Boussinesq effect, and should not be confused with the localization of convection into horizontal layers based on the local pressure scale height (an idea essentially deriving from the mixing length theory) which is an entirely compressible effect.

ACKNOWLEDGEMENTS

One of us (CAJ) is grateful to the U.S. National Science Foundation for support under grant DMS88-22287; the other of us (PHR) thanks the U.S. Office of Naval Research for support under grant N00014-86-K-0641.

REFERENCES

Abdel-Aziz, M.M. and Jones, C.A. "$\alpha\omega$-dynamos and Taylor's constraint", *Geophys. Astrophys. Fluid Dynam.* **44**, 117-139 (1988).

Beckers, J.M. "Observations of solar rotation and meridional flows at the Sacramento Peak Observatory", pp 166 – 177 in *Proceedings of the Workshop on solar Rotation*, Catania, 26 – 29 September, 1978. Eds. G. Belvedere and L. Paterno (1978).

Braginsky, S.I. "Nearly axially symmetric model of the hydromagnetic dynamo of the Earth: I", *Geomag. Aeron.* **15**, 122 – 128 (1975).

Braginsky, S.I. "Nearly axially symmetric model of the hydromagnetic dynamo of the Earth", *Geomag. Aeron.* **18**, 225-231 (1978).

Braginsky, S.I. and Roberts, P.H. "A model-Z geodynamo", *Geophys. Astrophys. Fluid Dynam.* **38**, 327 – 349 (1988).

Condi, F.J. "Sidewall boundary layers in rapidly rotating convection", Woods Hole Oceanographic Institution Technical Report WHOI-78-67, vol II, pp 18 – 24 (1978).
Eltayeb, I.A. "Hydromagnetic convection in a rapidly rotating fluid layer", *Proc. R. Soc. Lond.* **A326**, 229–254 (1972).
Fearn, D.R. "Boundary conditions for a rapidly rotating hydromagnetic system in a cylindrical container", *Geophys. Astrophys. Fluid Dynam.* **25**, 65 – 75 (1983).
Fearn, D.R., Roberts, P.H. and Soward, A.M. "Convection, stability and the dynamo ", pp 60–324 in *Energy, Stability and Convection*, ed. G.P. Galdi and B. Straughan, Longmans (1988).
Gilman, P.A. "Dynamically consistent nonlinear dynamos driven by convection in a rotating spherical shell: II. Dynamos with cycles and strong feedbacks", *Astrophys. J. Supp.* **53**, 243–268 (1983).
Glatzmaier, G.A. "Numerical simulations of stellar convective dynamos: I. The model and the method", *J. Comp. Phys.* **55**, 461 – 484 (1984).
Glatzmaier, G.A. "Numerical simulations of stellar convective dynamos: II. Field propagation in the convection zone", *Astrophys. J.* **291**, 300 – 307 (1985a).
Glatzmaier, G.A. "Numerical simulations of stellar convective dynamos: III. At the base of the convection zone", *Geophys. Astrophys. Fluid Dynam.* **31**, 137 – 150 (1985b).
Jones, C.A. and Galloway, D.J. "The pattern of large-scale convection in the Sun" pp 97–108 in *Secular Solar and Geomagnetic Variations in the last 10,000 Years*, eds. F. R. Stephenson and A. W. Wolfendale, NATO ASI series, Kluwer Academic publishers (1988).
Jones, C.A., Roberts, P.H. and Galloway, D.J. "Compressible convection in the presence of rotation and a magnetic field" *Geophys. Astrophys. Fluid Dynam.*, to appear (1990). This paper was referred to as 'Paper I' above.
Malkus, W.V.R. and Proctor, M.R.E. "The macrodynamics of α-effect dynamos in rotating fluids, *J. Fluid Mech.* **67**, 417 – 443 (1975).
Merryfield, W.J. "Azimuthal convective rolls and the subsurface magnetic field", to appear in *Inside the Sun*; IAU Colloquium 121 (1990).
Ribes, E., Mein, P. and Mangeney, A. "A large-scale meridional circulation in the convective zone", *Nature* **318**, 170 – 171 (1985).
Roberts, P.H. "From Taylor state to model-Z?" *Geophys. Astrophys. Fluid Dynam.*, **49**, to appear (1989).
Roberts, P.H. and Stewartson, K. "On finite amplitude convection in a rotating magnetic system", *Phil. Trans. R. Soc. Lond.* **A277**, 287 – 315 (1974).
Roberts, P.H. and Stewartson, K. "Double roll convection in a rotating magnetic system", *J. Fluid Mech.* **68**, 447 – 466 (1975).
Rüdiger, G. *Differential Rotation and stellar Convection. Sun and solar-type Stars.* New York: Gordon and Breach (1989).
Skinner, P.H. and Soward, A.M. "Convection in a rotating magnetic system and Taylor's constraint", *Geophys. Astrophys. Fluid Dynam.* **44**, 91 – 117 (1989).
Soward, A.M. "Finite-amplitude thermal convection and geostrophic flow in a rotating magnetic system", *J. Fluid Mech.* **98**, 449 – 471 (1980).
Soward, A.M. "Non-linear marginal convection in a rotating magnetic system", *Geophys. Astrophys. Fluid Dynam.* **35**, 329 – 371 (1986).

Soward, A.M. and Jones, C.A. "α^2-dynamos and Taylor's constraint", *Geophys. Astrophys. Fluid Dynam.* **27**, 87 – 122 (1985b).
Taylor, J. B. "The magneto-hydrodynamics of a rotating fluid and the Earth's dynamo problem", *Proc. R. Soc. Lond.* **A274**, 274 – 283 (1963).
Wilson, P.R. "The solar dynamo and the convective rolls", *Solar Phys.* **117**, 217 – 226 (1988).
Zhang, K.-K. "A study of buoyancy-driven flows and magnetic field generation in rotating spherical shells". Ph.D. thesis in Geophysics and Space Physics, UCLA (1987).
Zhang, K.-K. and Busse, F.H. "Finite amplitude convection and magnetic field generation in a rotating spherical shells", *Geophys. Astrophys. Fluid Dynam.* **44**, 33 – 53 (1988).

FIGURE CAPTIONS

Figure 1. The location of Taylor States in the (Λ, r)-plane for $\Lambda < 4$. The solid curve shows the critical Rayleigh number of linear Boussinesq theory, i.e. that corresponding to the minimizing values of k and l. The curve consists of two segments, the left-hand one corresponding to cases in which $l = 0$ modes provide the minimum r; the right-hand one for that in which the minimizing l is nonzero. These segments are continued as dashed lines beyond their point of intersection. The dashed curve labelled r_T gives the Rayleigh numbers of Taylor states; here the same wavenumbers were used as gave, for $l \neq 0$, the smallest r on linear Boussinesq theory.

Figure 2. Solutions for the rigid duct in the case $\Lambda = 6$ and $r = 50$ and the wavenumbers $k = 1.117$ and $l = 1.668$ that minimize r on linear Boussinesq theory.

(a) the geostrophic velocity;
(b) the amplitudes $\alpha/\alpha_{\max}$, $\beta/\beta_{\max}$ and $\gamma/\gamma_{\max}$ of u_z, B, and T;
(c) the phases θ, ϕ and ψ of u_z, B, and T.

Here $\alpha_{\max} = 3.055$, $\beta_{\max} = 0.3508$ and $\gamma_{\max} = 11.186$.

Figure 3. Solutions for the rigid duct in the case $\Lambda = 6$ and $r = 576,503$ and the wavenumbers $k = 1.117$ and $l = 1.668$ that minimize r on linear Boussinesq theory.

(a) the geostrophic velocity;
(b) the amplitudes α, β and γ of u_z, B, and T;
(c) the phases ϕ and ψ of B, and T.

Here z, U, α, β and γ are scaled as in (5.2). The phase of u_z is too close to that of T to be shown in (c).

Figure 4. Bifurcation diagram for the free duct ($\Lambda = 6$), showing the symmetry-breaking bifurcation, B_3. Also shown in this (r, a) plot are the marginal states of the first two modes that arise on linear Boussinesq theory for $k = 1.117$ and $l = 1.668$, and also the saddle-node bifurcation, B_4.

Figure 5. Solutions for the free duct in the case $\Lambda = 6$ and $r = 50$ and the wavenumbers $k = 1.117$ and $l = 1.668$ that minimize r on linear Boussinesq theory.

(a) the geostrophic velocity;
(b) the amplitudes $\alpha/\alpha_{\max}$, $\beta/\beta_{\max}$ and $\gamma/\gamma_{\max}$ of u_z, B, and T;
(c) the phases θ, ϕ and ψ of u_z, B, and T.

Here $\alpha_{\max} = 9.928$, $\beta_{\max} = 1.123$ and $\gamma_{\max} = 35.947$. Since $r < r_3$, the solutions possess the expected $z \leftrightarrow 1 - z$ symmetry.

Figure 6. Solutions for the free duct in the case $\Lambda = 6$ and $r = 320 > r_3$ and the wavenumbers $k = 1.117$ and $l = 1.668$ that minimize r on linear Boussinesq theory.

(a) the geostrophic velocity;
(b) the amplitudes $\alpha/\alpha_{\max}$, $\beta/\beta_{\max}$ and $\gamma/\gamma_{\max}$ of u_z, B, and T;
(c) the phases θ, ϕ and ψ of u_z, B, and T.

Here $\alpha_{\max} = 153.42$, $\beta_{\max} = 3.365$ and $\gamma_{\max} = 1126.5$. Since $r > r_3$, the solutions do not possess $z \leftrightarrow 1 - z$ symmetry.

Figure 7. Solutions for the free duct in the case $\Lambda = 6$ and $r = 576,503$ and the wavenumbers $k = 1.117$ and $l = 1.668$ that minimize r on linear Boussinesq theory.

(a) the geostrophic velocity;
(b) the amplitudes α, β and γ of u_z, B, and T;
(c) the phases ϕ and ψ of B, and T. The phase of u_z is too close to that of T to be shown in (c).

Here z, U, α, β and γ are scaled as in (6.2).

Figure 8. Bifurcation diagrams for the free compressible duct in three cases:

(a) the Boussinesq limit ($z_0 \to \infty$);
(b) a slightly compressible case ($z_0 = 1.0$);
(c) a highly compressible case ($z_0 = 0.1$).

The unfolding of the symmetry-breaking bifurcation, B_3, of (a) as z_0 is decreased is evident.

Figure 9. Solutions on the primary branch for convection in the free compressible duct for the case $z_0 = 0.1$, $\Lambda = 6$, $r = 700$ and the wavenumbers $k = 1.117$ and $l = 1.668$ that minimize r on linear Boussinesq theory for $\Lambda = 6$.

(a) the geostrophic velocity;
(b) the amplitudes $\alpha/\alpha_{\max}$, $\beta/\beta_{\max}$ and $\gamma/\gamma_{\max}$ of u_z, B, and T;
(c) the phases θ, ϕ and ψ of u_z, B, and T.

Here $\alpha_{\max} = 373.07$, $\beta_{\max} = 2.911$ and $\gamma_{\max} = 2848.0$.

Figure 10. Solutions on the secondary branch for convection in the free compressible duct for the case $z_0 = 0.1$, $\Lambda = 6$, $r = 700$ and the wavenumbers $k = 1.117$ and $l = 1.668$ that minimize r on linear Boussinesq theory.

(a) the geostrophic velocity;
(b) the amplitudes $\alpha/\alpha_{\max}$, $\beta/\beta_{\max}$ and $\gamma/\gamma_{\max}$ of u_z, B, and T;
(c) the phases θ, ϕ and ψ of u_z, B, and T.

Here $\alpha_{\max} = 673.42$, $\beta_{\max} = 4.358$ and $\gamma_{\max} = 1690.5$.

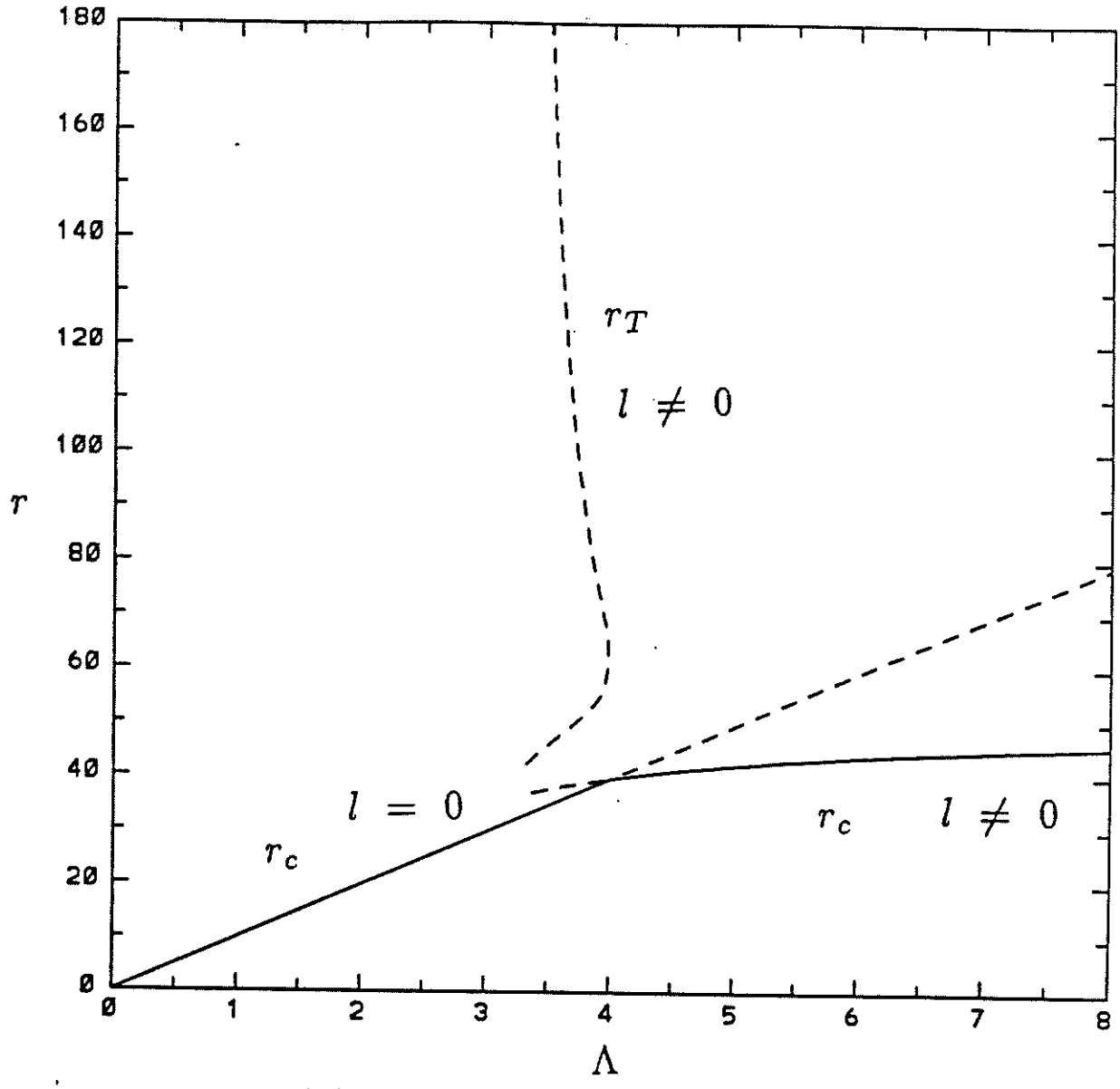

Figure 1. The location of Taylor States in the (Λ, r)-plane for $\Lambda < 4$. The solid curve shows the critical Rayleigh number of linear Boussinesq theory, i.e. that corresponding to the minimizing values of k and l. The curve consists of two segments, the left-hand one corresponding to cases in which $l = 0$ modes provide the minimum r; the right-hand one for that in which the minimizing l is nonzero. These segments are continued as dashed lines beyond their point of intersection. The dashed curve labelled r_T gives the Rayleigh numbers of Taylor states; here the same wavenumbers were used as gave, for $l \neq 0$, the smallest r on linear Boussinesq theory.

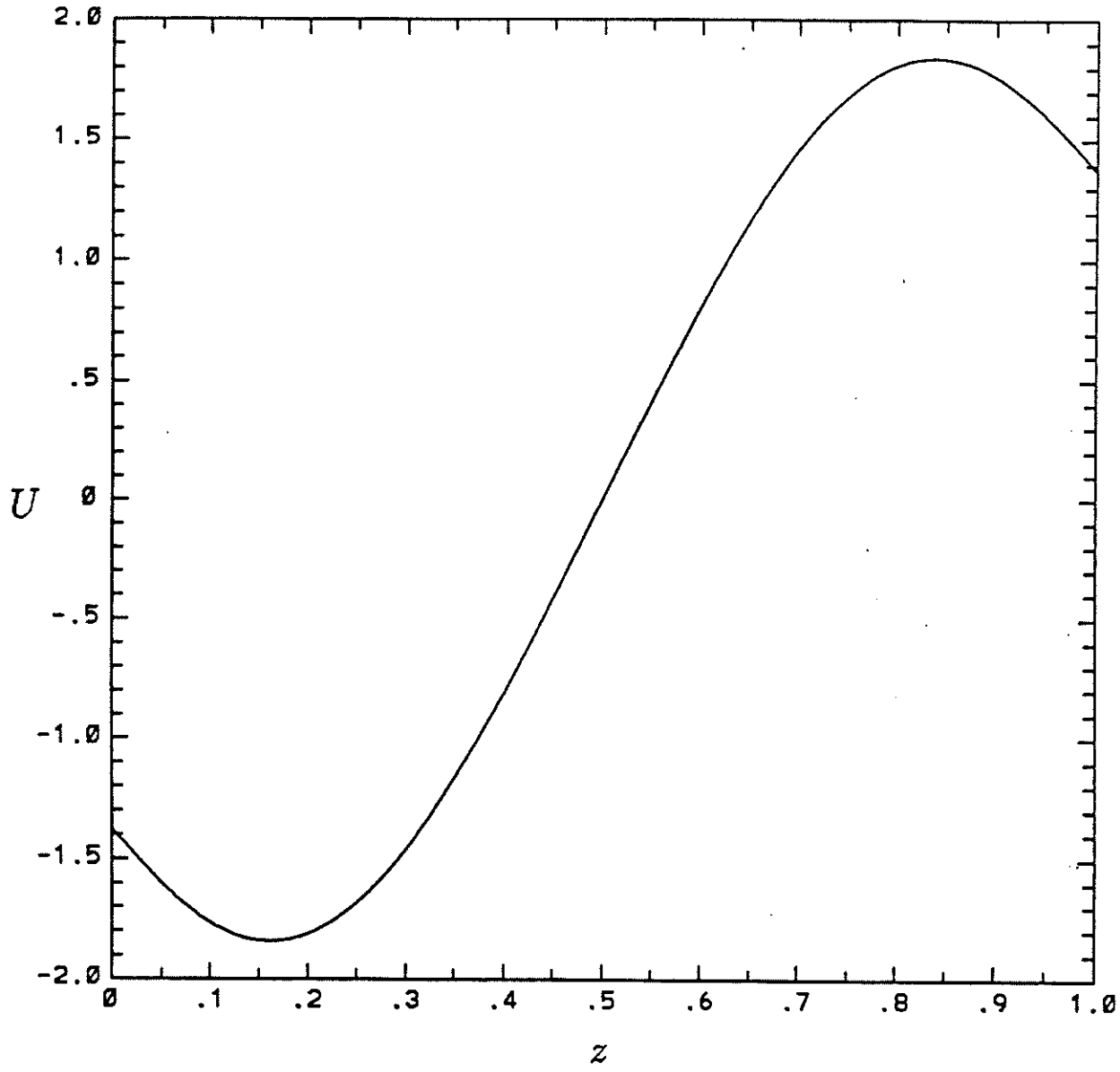

Figure 2(a). The geostrophic velocity for the rigid duct in the case $\Lambda = 6$ and $r = 50$ and the wavenumbers $k = 1.117$ and $l = 1.668$ that minimize r on linear Boussinesq theory.

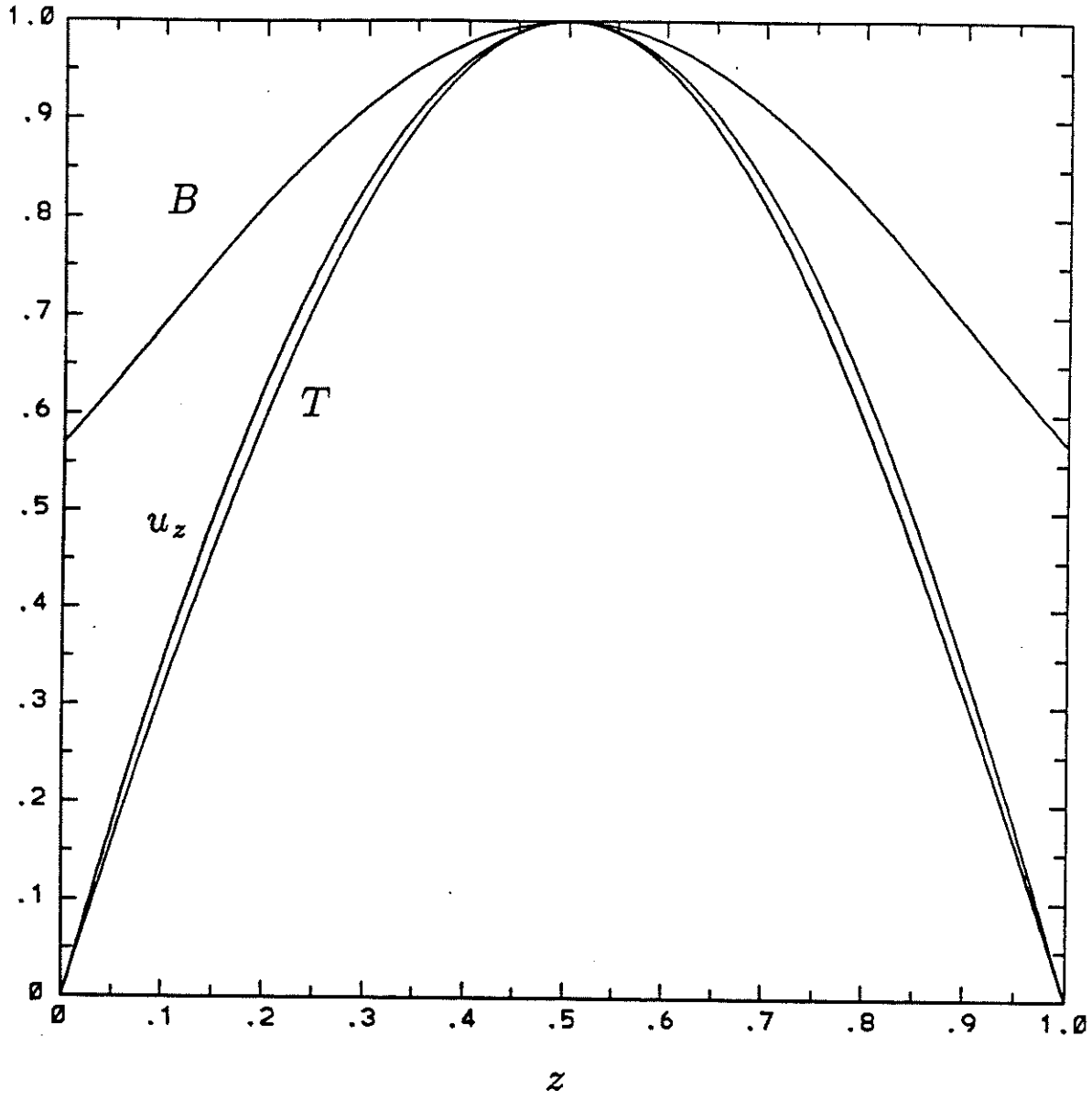

Figure 2(b). The amplitudes $\alpha/\alpha_{\max}$, $\beta/\beta_{\max}$ and $\gamma/\gamma_{\max}$ of u_z, B, and T for the rigid duct in the case $\Lambda = 6$ and $r = 50$ and the wavenumbers $k = 1.117$ and $l = 1.668$ that minimize r on linear Boussinesq theory. Here $\alpha_{\max} = 3.055$, $\beta_{\max} = 0.3508$ and $\gamma_{\max} = 11.186$.

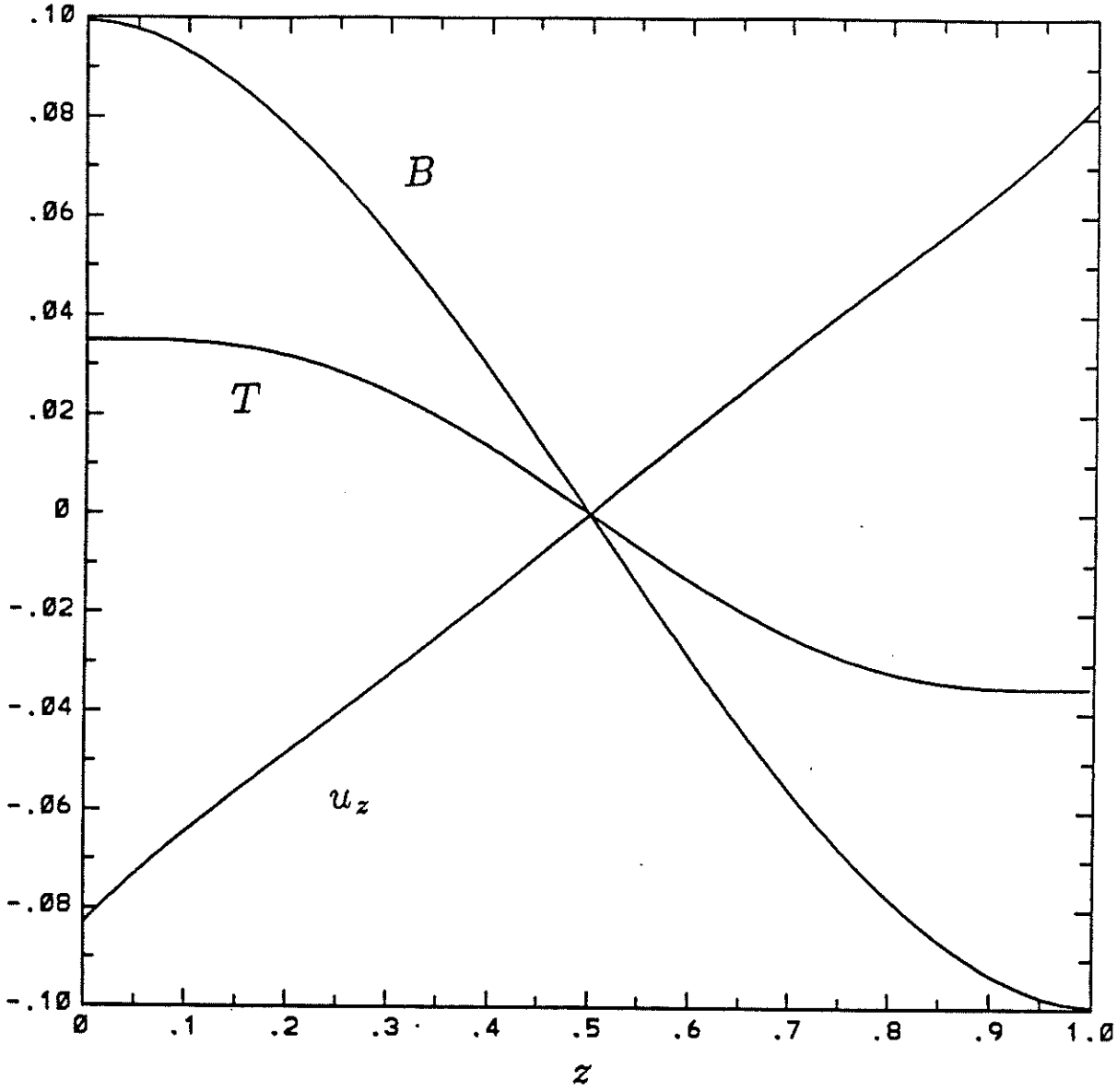

Figure 2(c). The phases θ, ϕ and ψ of u_z, B, and T for the rigid duct in the case $\Lambda = 6$ and $r = 50$ and the wavenumbers $k = 1.117$ and $l = 1.668$ that minimize r on linear Boussinesq theory.

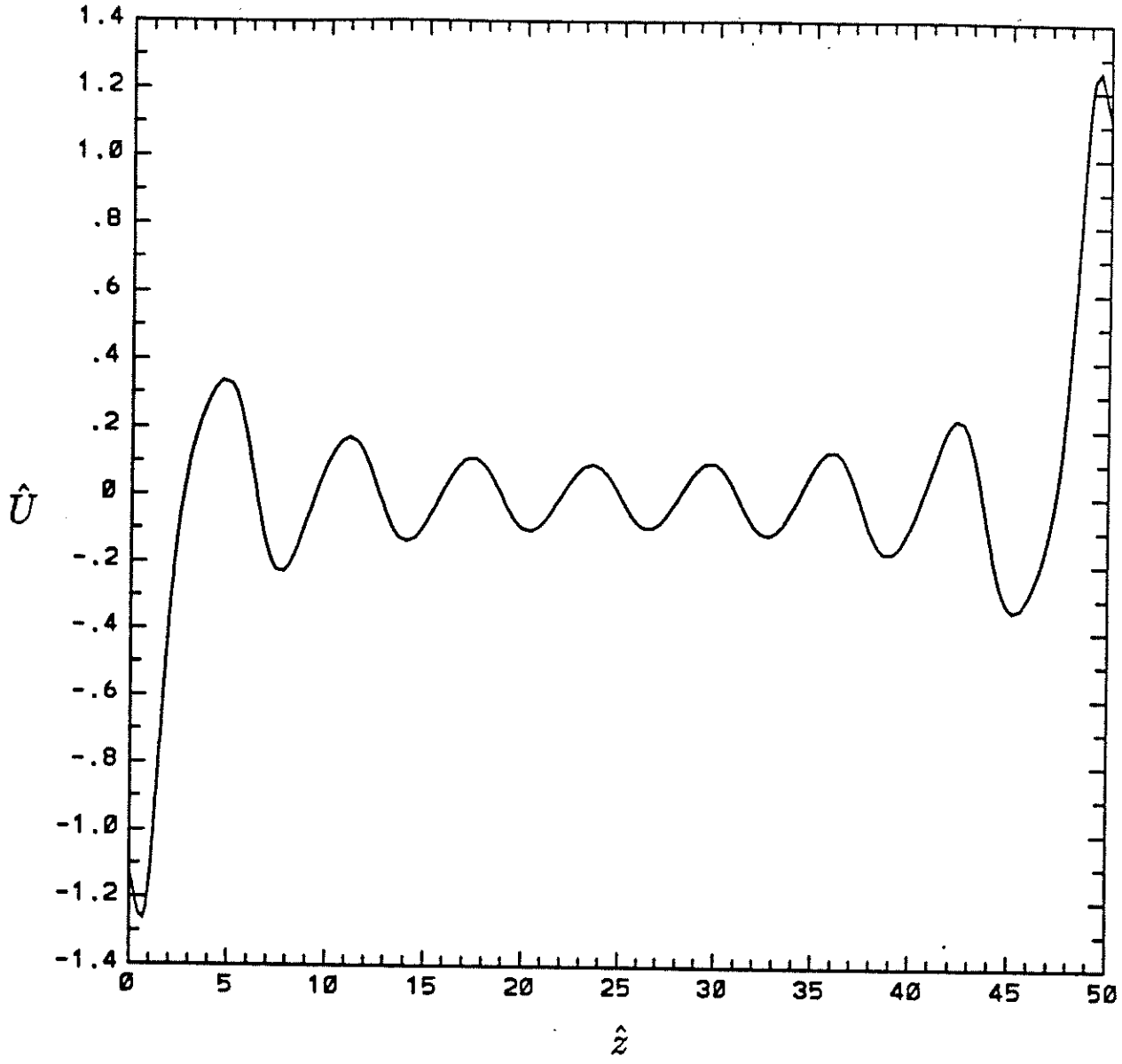

Figure 3(a). The geostrophic velocity for the rigid duct in the case $\Lambda = 6$ and $r = 576,503$ and the wavenumbers $k = 1.117$ and $l = 1.668$ that minimize r on linear Boussinesq theory. Here z and U are scaled as in (5.2).

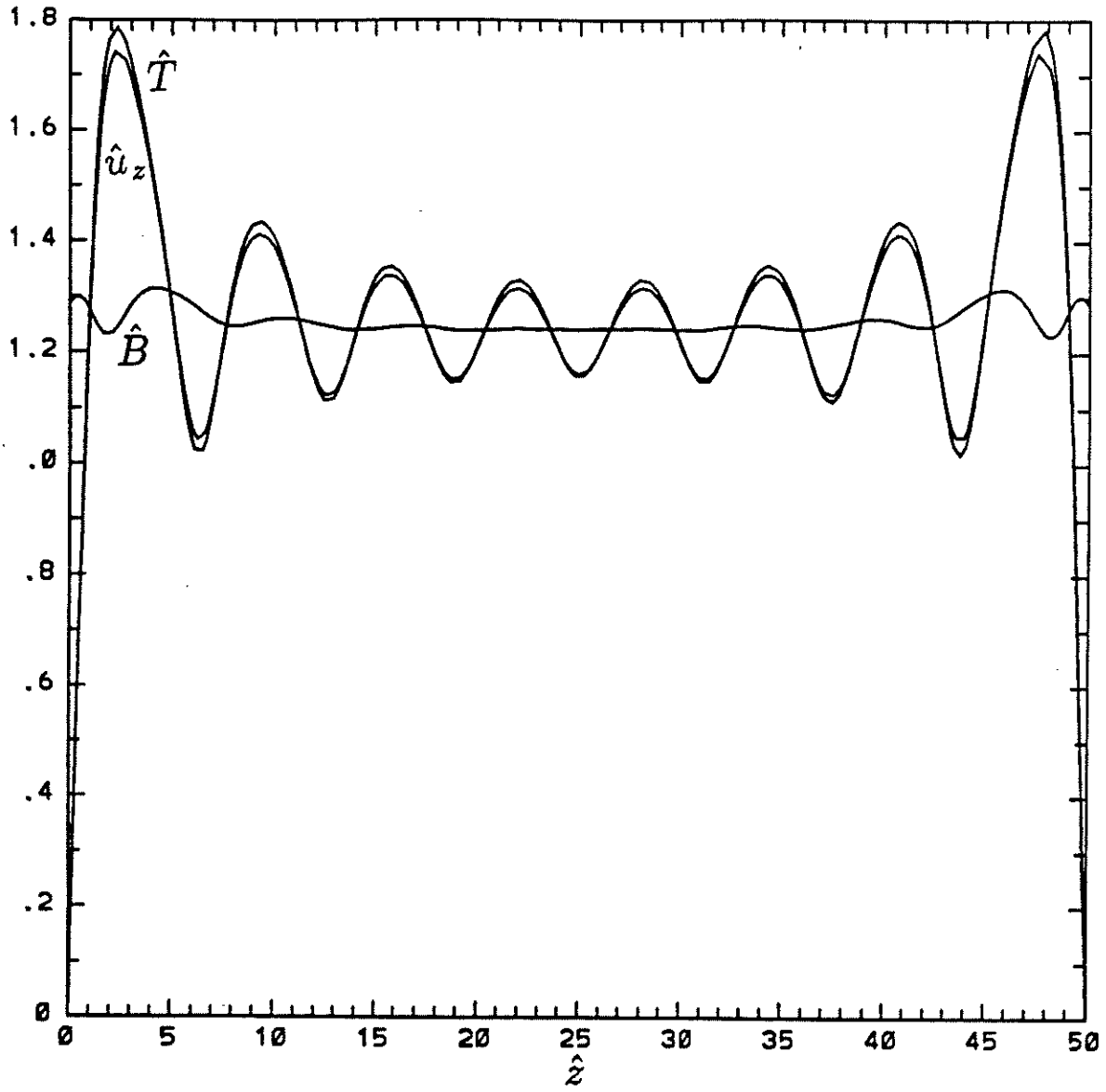

Figure 3(b). The amplitudes α, β and γ of u_z, B, and T for the rigid duct in the case $\Lambda = 6$ and $r = 576,503$ and the wavenumbers $k = 1.117$ and $l = 1.668$ that minimize r on linear Boussinesq theory. Here α, β and γ are scaled as in (5.2).

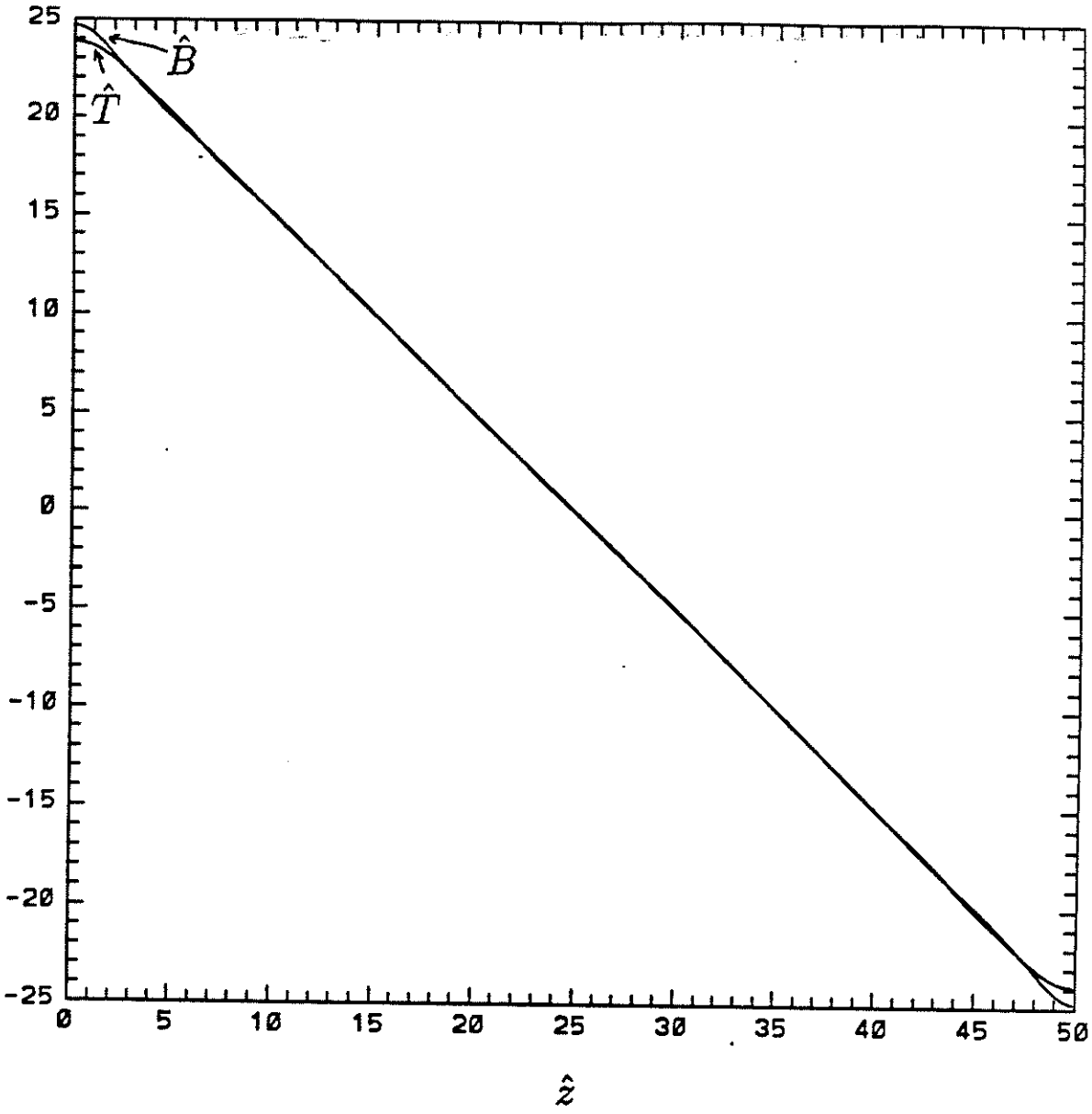

Figure 3(c). The phases ϕ and ψ of B, and T. for the rigid duct in the case $\Lambda = 6$ and $r = 576,503$ and the wavenumbers $k = 1.117$ and $l = 1.668$ that minimize r on linear Boussinesq theory. The phase of u_z is too close to that of T to be shown.

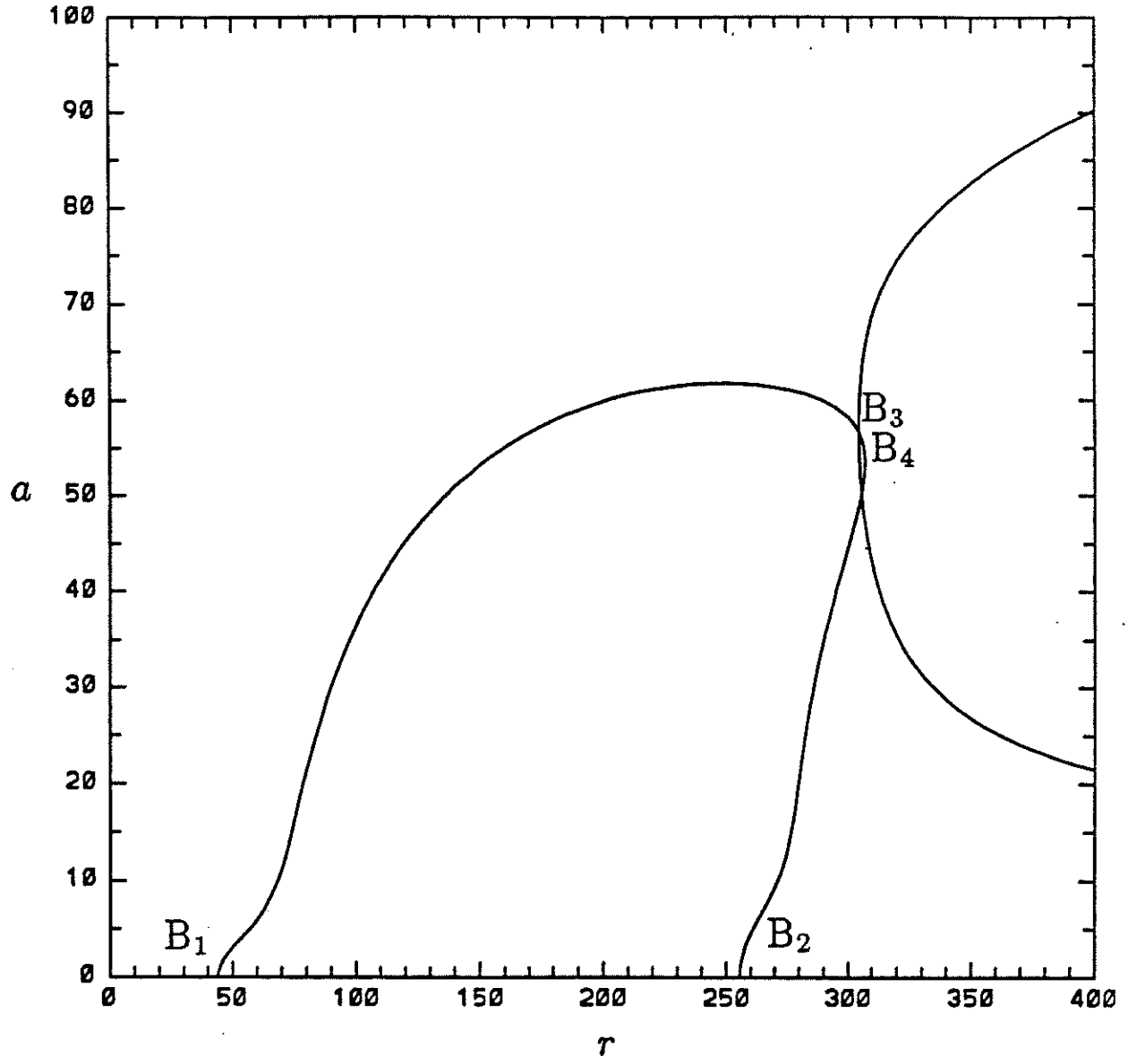

Figure 4. Bifurcation diagram for the free duct ($\Lambda = 6$), showing the symmetry-breaking bifurcation, B_3. Also shown in this (r, a) plot are the marginal states of the first two modes that arise on linear Boussinesq theory for $k = 1.117$ and $l = 1.668$, and also the saddle-node bifurcation, B_4.

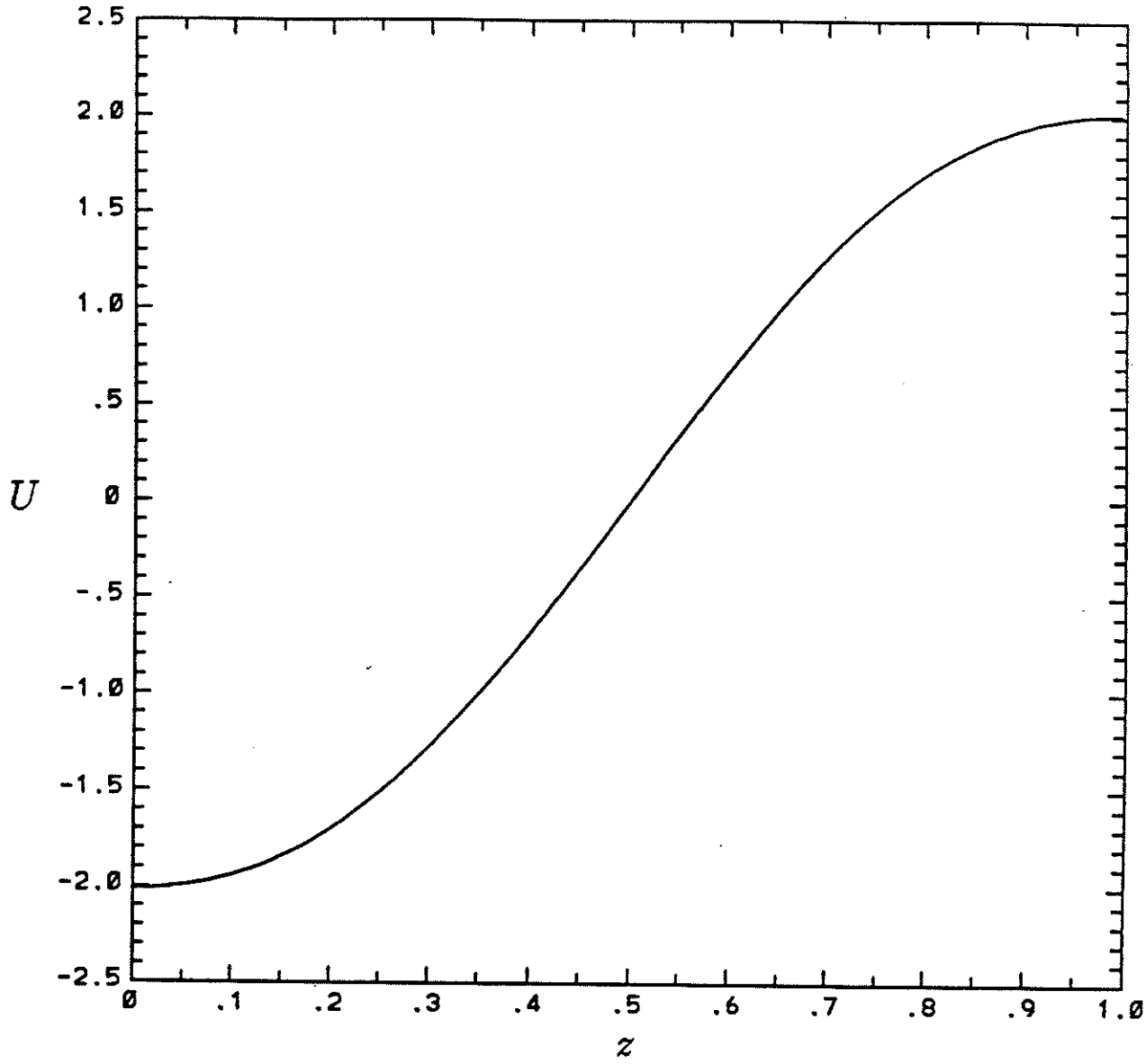

Figure 5(a). The geostrophic velocity for the free duct in the case $\Lambda = 6$ and $r = 50$ and the wavenumbers $k = 1.117$ and $l = 1.668$ that minimize r on linear Boussinesq theory. Since $r < r_3$, the solution possesses the expected $z \leftrightarrow 1 - z$ symmetry.

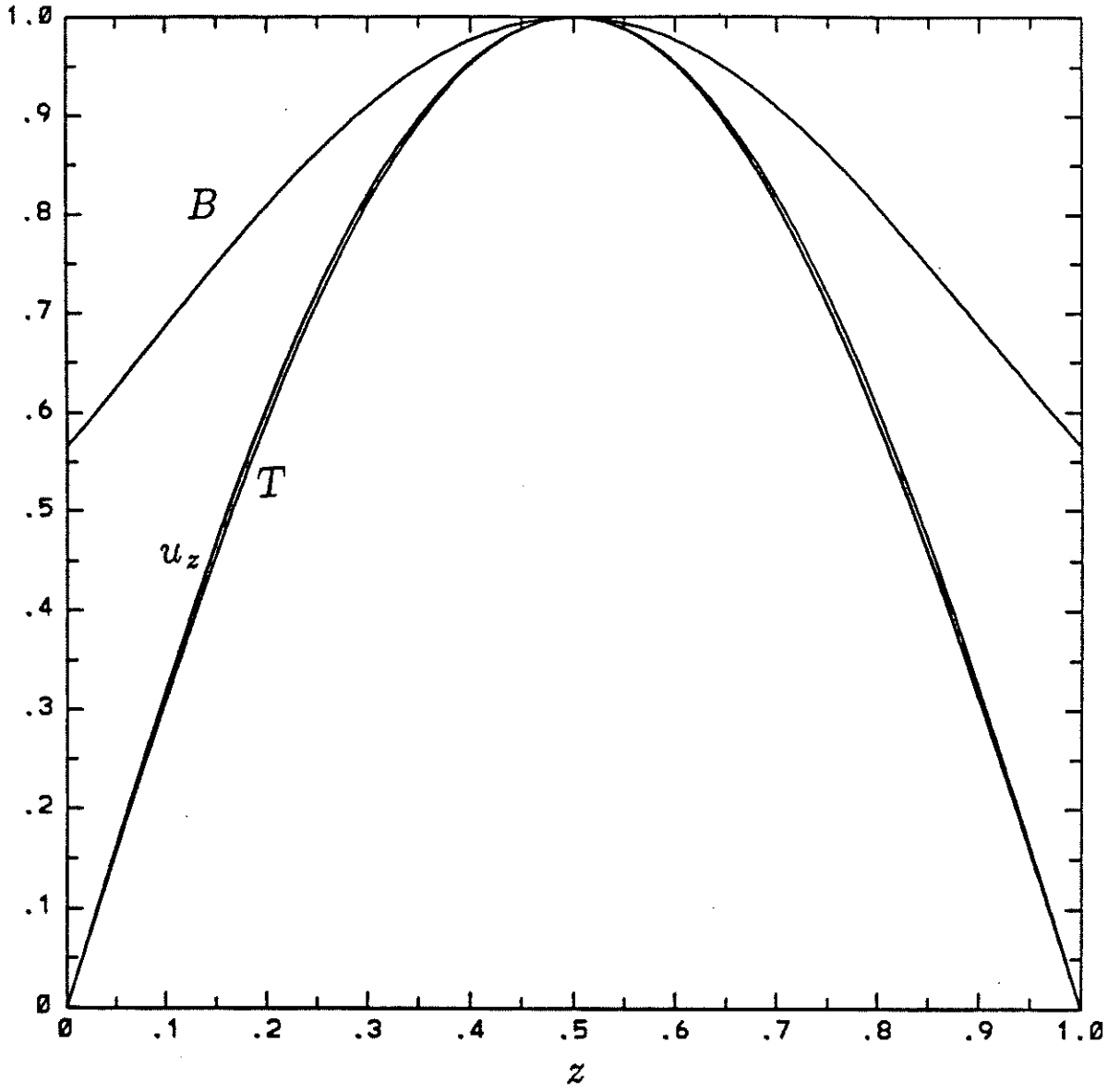

Figure 5(b). The amplitudes $\alpha/\alpha_{\max}$, $\beta/\beta_{\max}$ and $\gamma/\gamma_{\max}$ of u_z, B, and T for the free duct in the case $\Lambda = 6$ and $r = 50$ and the wavenumbers $k = 1.117$ and $l = 1.668$ that minimize r on linear Boussinesq theory. Here $\alpha_{\max} = 9.928$, $\beta_{\max} = 1.123$ and $\gamma_{\max} = 35.947$. Since $r < r_{\frac{1}{2}}$, the solutions possess the expected $z \leftrightarrow 1 - z$ symmetry.

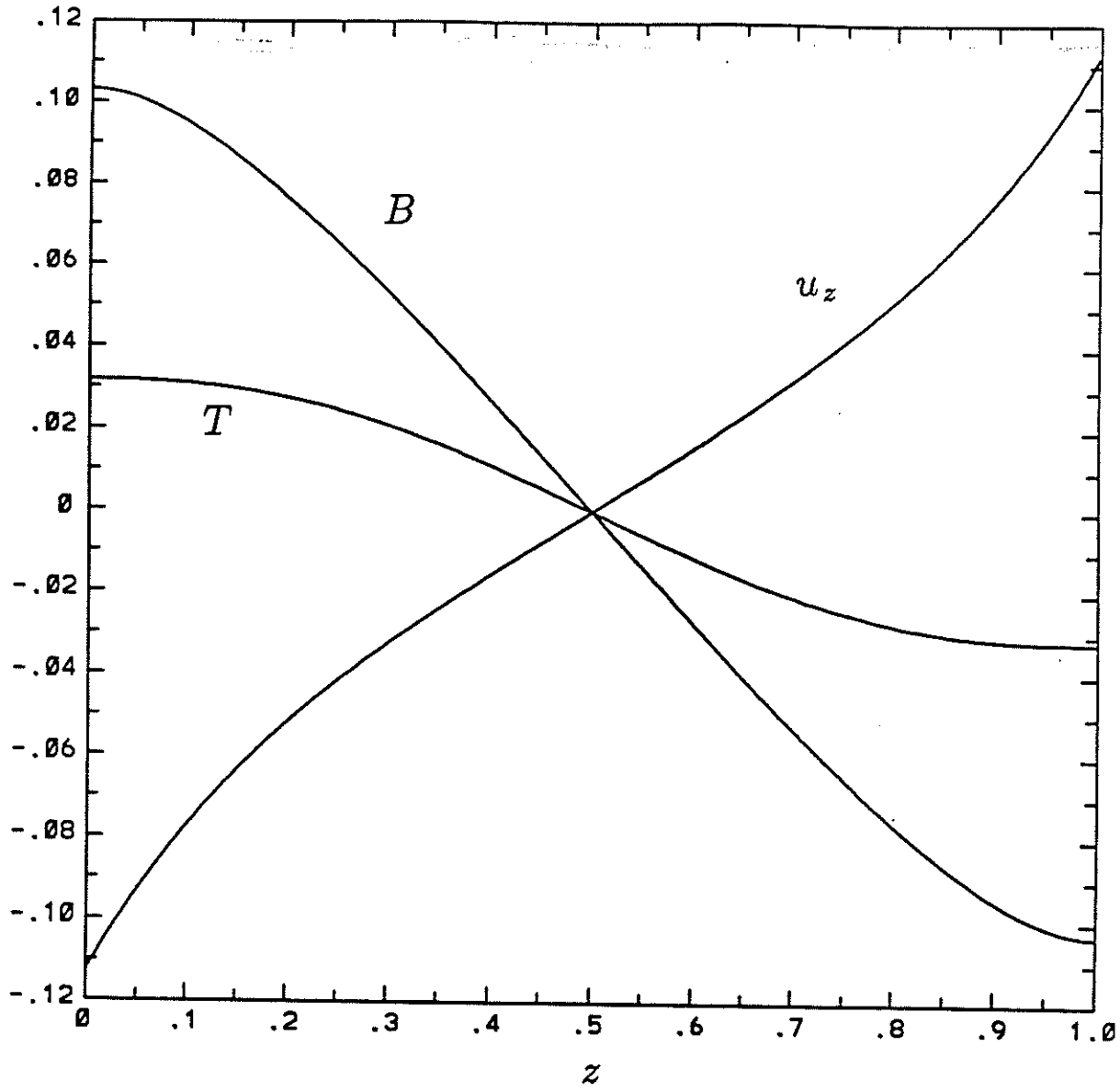

Figure 5(c). The phases θ, ϕ and ψ of u_z, B, and T for the free duct in the case $\Lambda = 6$ and $r = 50$ and the wavenumbers $k = 1.117$ and $l = 1.668$ that minimize r on linear Boussinesq theory. Since $r < r_3$, the solutions possess the expected $z \leftrightarrow 1 - z$ symmetry.

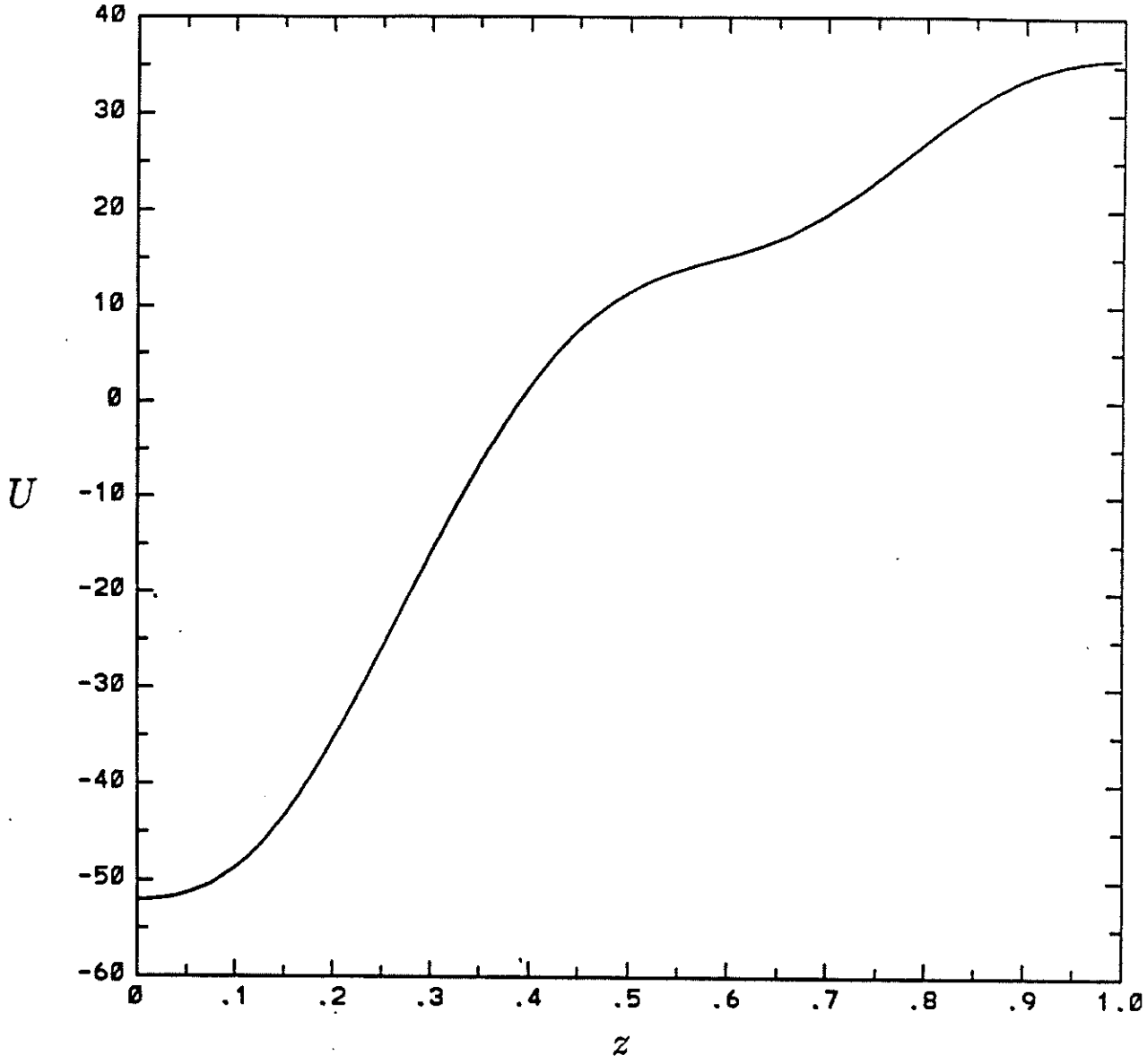

Figure 6(a). The geostrophic velocity for the free duct in the case $\Lambda = 6$ and $r = 320 > r_3$ and the wavenumbers $k = 1.117$ and $l = 1.668$ that minimize r on linear Boussinesq theory. Since $r > r_3$, the solution does not possess $z \leftrightarrow 1 - z$ symmetry.

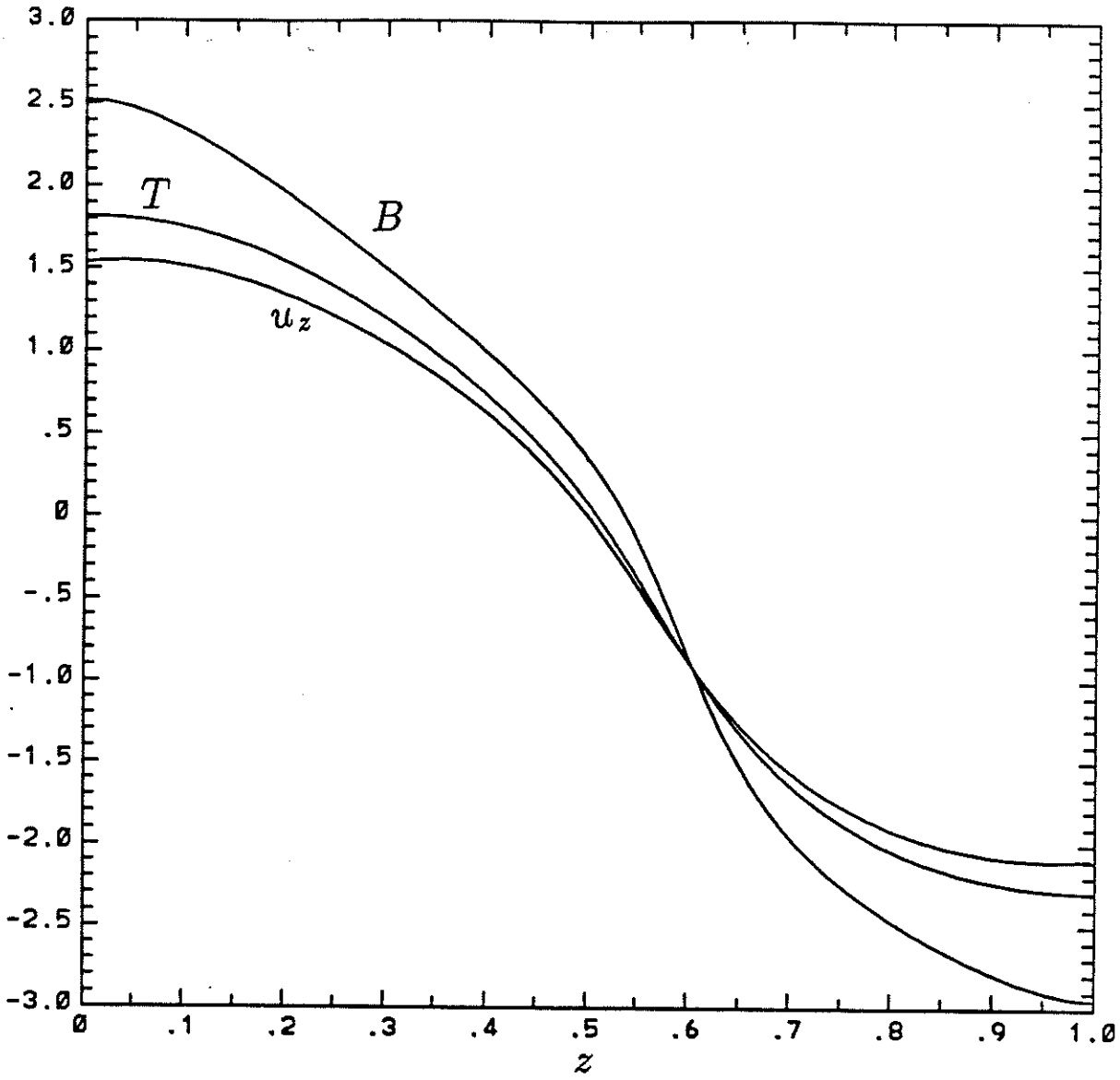

Figure 6(b). The amplitudes $\alpha/\alpha_{\max}$, $\beta/\beta_{\max}$ and $\gamma/\gamma_{\max}$ of u_z, B, and T for the free duct in the case $\Lambda = 6$ and $r = 320 > r_3$ and the wavenumbers $k = 1.117$ and $l = 1.668$ that minimize r on linear Boussinesq theory. Here $\alpha_{\max} = 153.42$, $\beta_{\max} = 3.365$ and $\gamma_{\max} = 1126.5$. Since $r > r_3$, the solutions do not possess $z \leftrightarrow 1 - z$ symmetry.

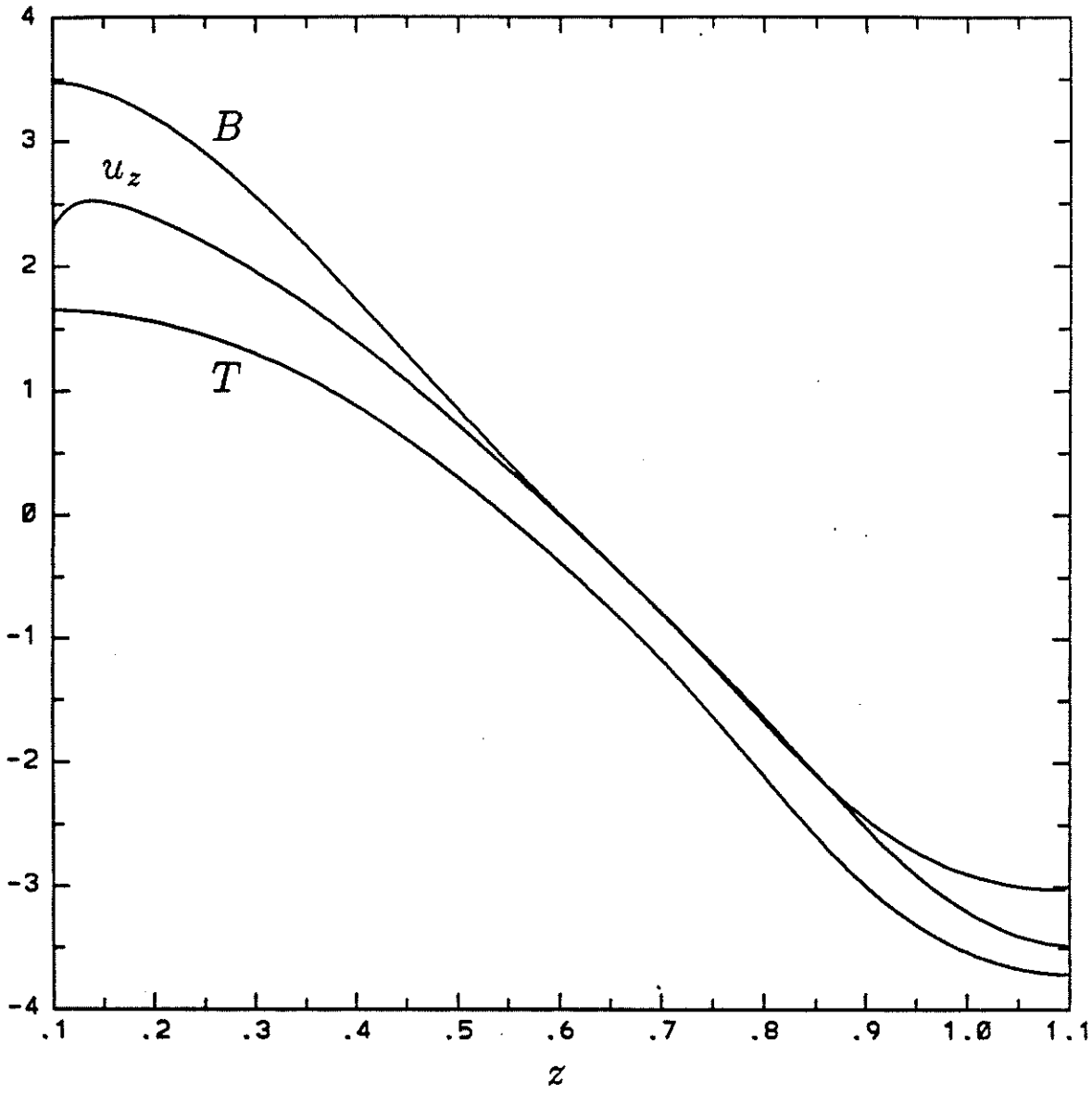

Figure 6(c). The phases θ, ϕ and ψ of u_z, B, and T for the free duct in the case $\Lambda = 6$ and $r = 320 > r_3$ and the wavenumbers $k = 1.117$ and $l = 1.668$ that minimize r on linear Boussinesq theory. Since $r > r_3$, the solutions do not possess $z \leftrightarrow 1 - z$ symmetry.

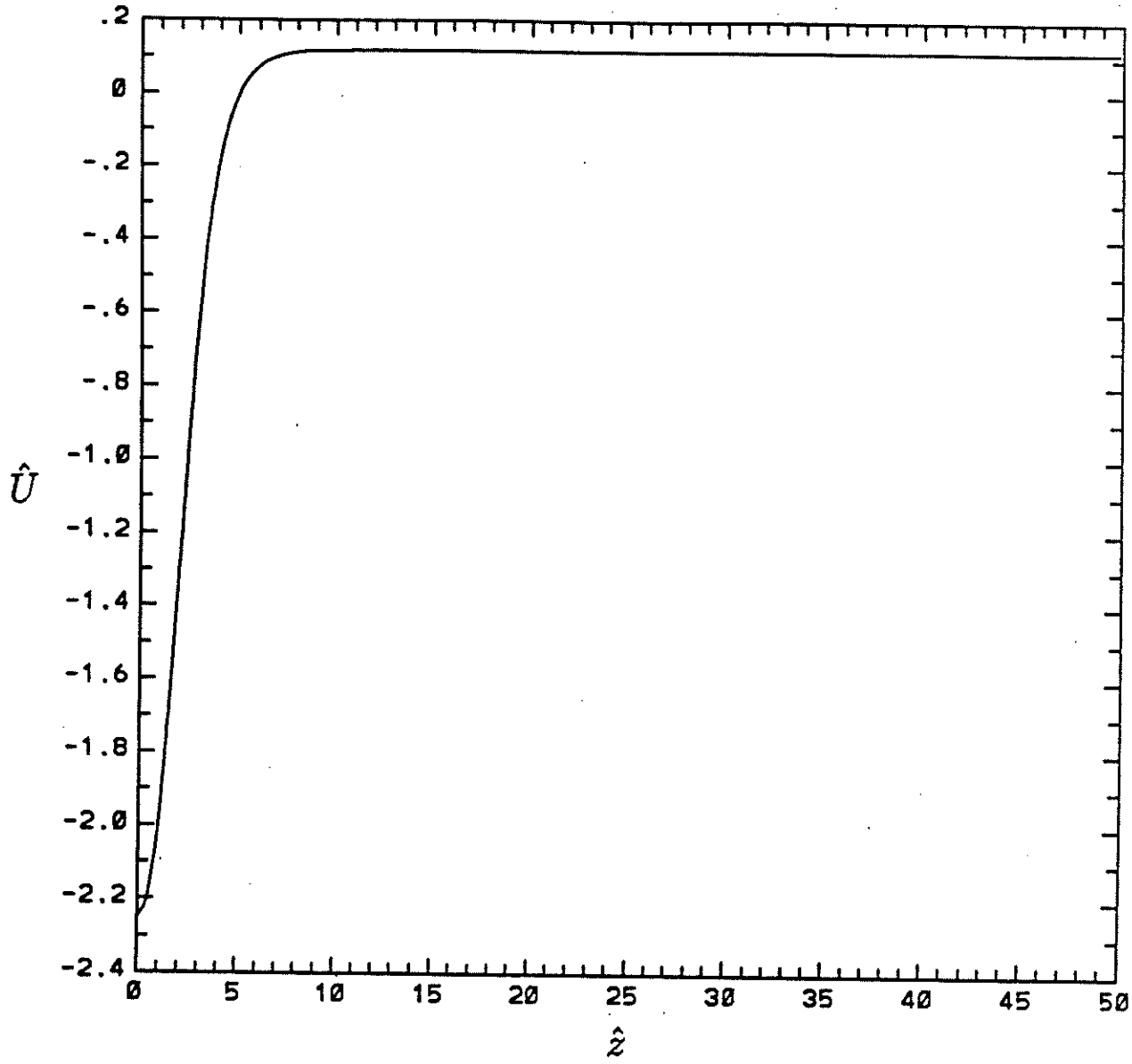

Figure 7(a). The geostrophic velocity for the free duct in the case $\Lambda = 6$ and $r = 576,503$ and the wavenumbers $k = 1.117$ and $l = 1.668$ that minimize r on linear Boussinesq theory. Here z and U, are scaled as in (6.2).

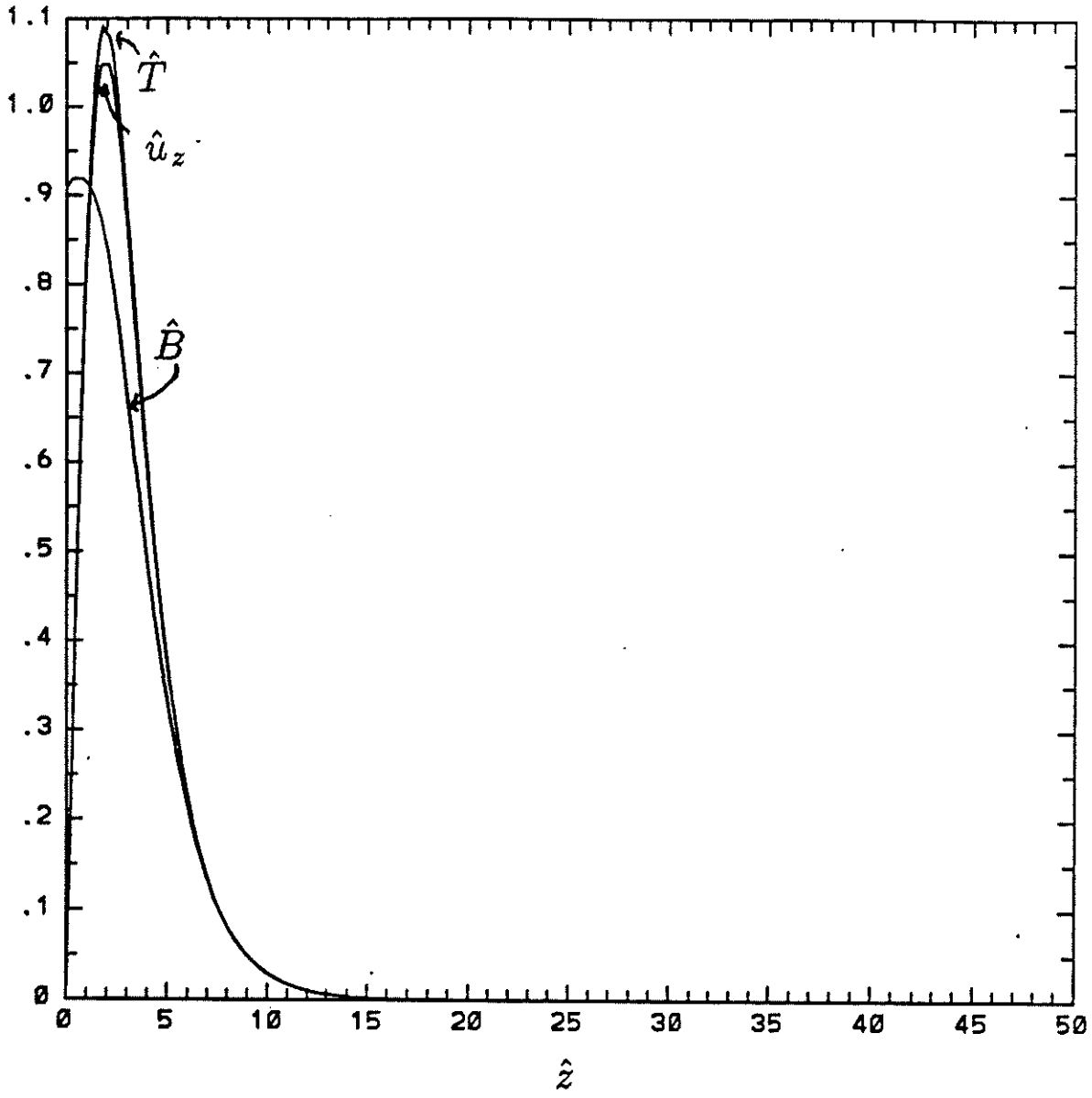

Figure 7(b). The amplitudes α, β and γ of u_z, B, and T for the free duct in the case $\Lambda = 6$ and $r = 576,503$ and the wavenumbers $k = 1.117$ and $l = 1.668$ that minimize r on linear Boussinesq theory. Here z, α, β and γ are scaled as in (6.2).

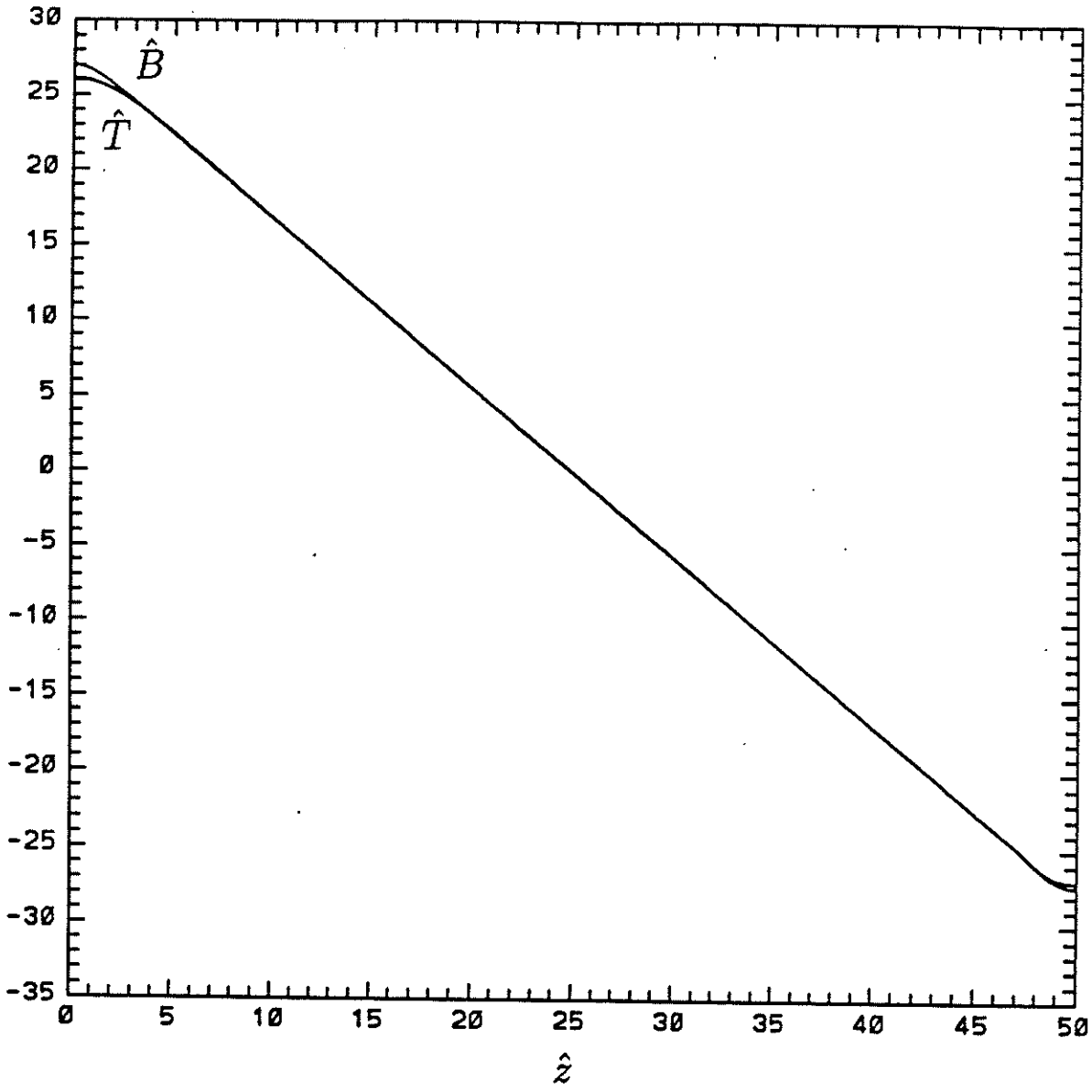

Figure 7(c). The phases ϕ and ψ of B, and T for the free duct in the case $\Lambda = 6$ and $r = 576,503$ and the wavenumbers $k = 1.117$ and $l = 1.668$ that minimize r on linear Boussinesq theory. The phase of u_z is too close to that of T to be shown in (c).

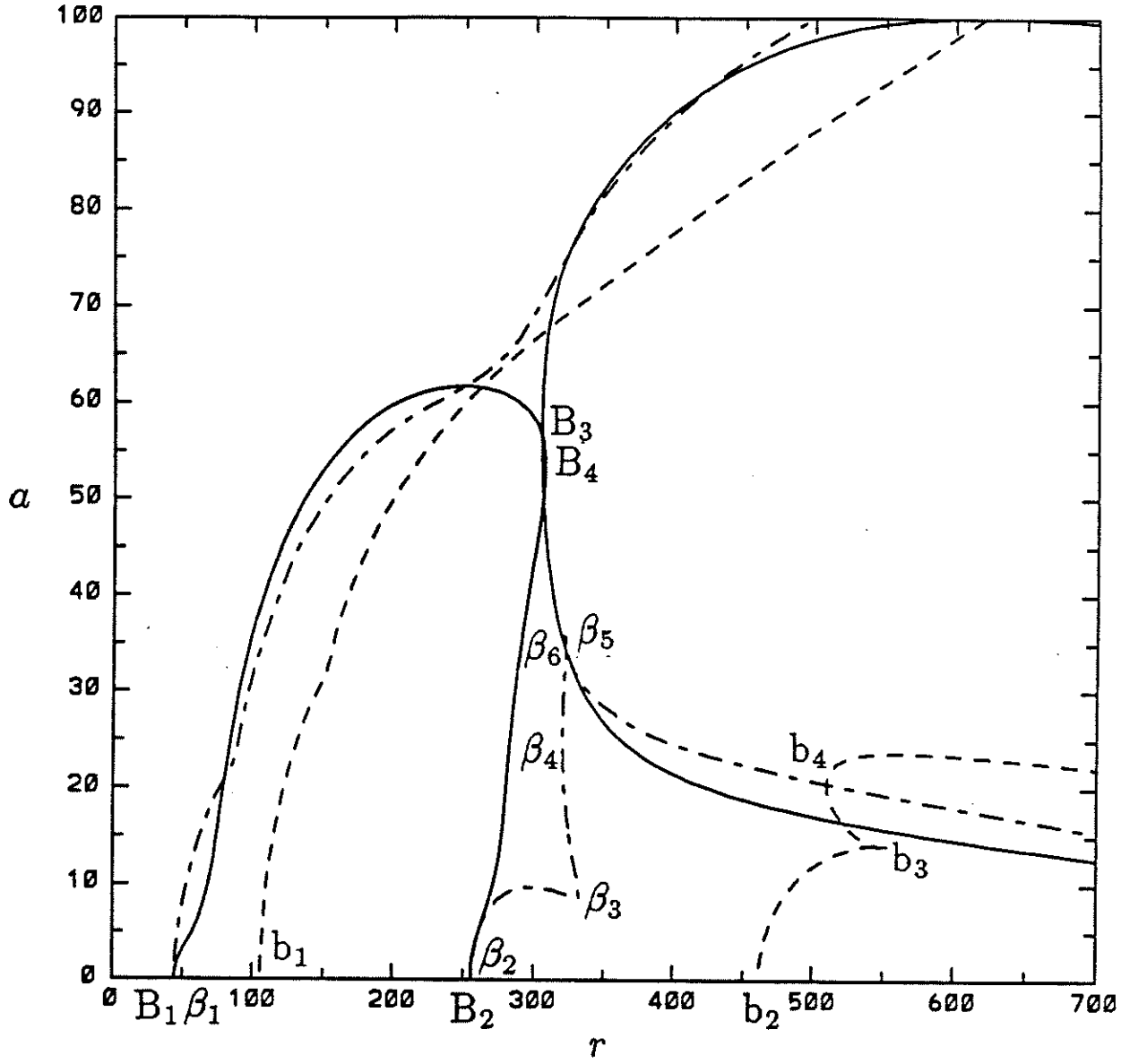

Figure 8. Bifurcation diagrams for the free compressible duct in three cases:

(a) the Boussinesq limit ($z_0 \to \infty$);
(b) a slightly compressible case ($z_0 = 1.0$);
(c) a highly compressible case ($z_0 = 0.1$).

The unfolding of the symmetry-breaking bifurcation, B_3, of (a) as z_0 is decreased is evident.

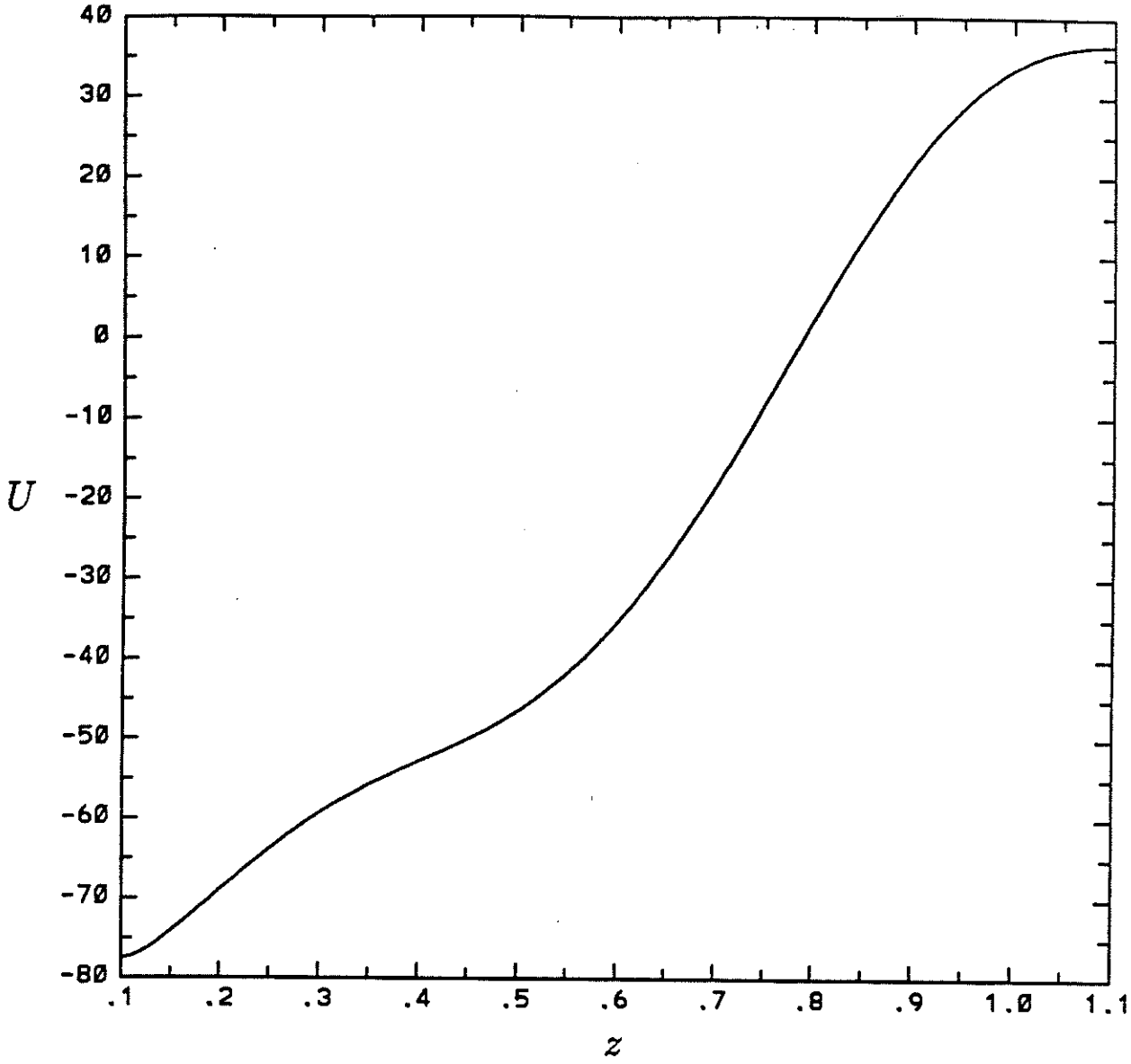

Figure 9(a). The geostrophic velocity on the primary branch for convection in the free compressible duct for the case $z_0 = 0.1$, $\Lambda = 6$, $r = 700$ and the wavenumbers $k = 1.117$ and $l = 1.668$ that minimize r on linear Boussinesq theory for $\Lambda = 6$.

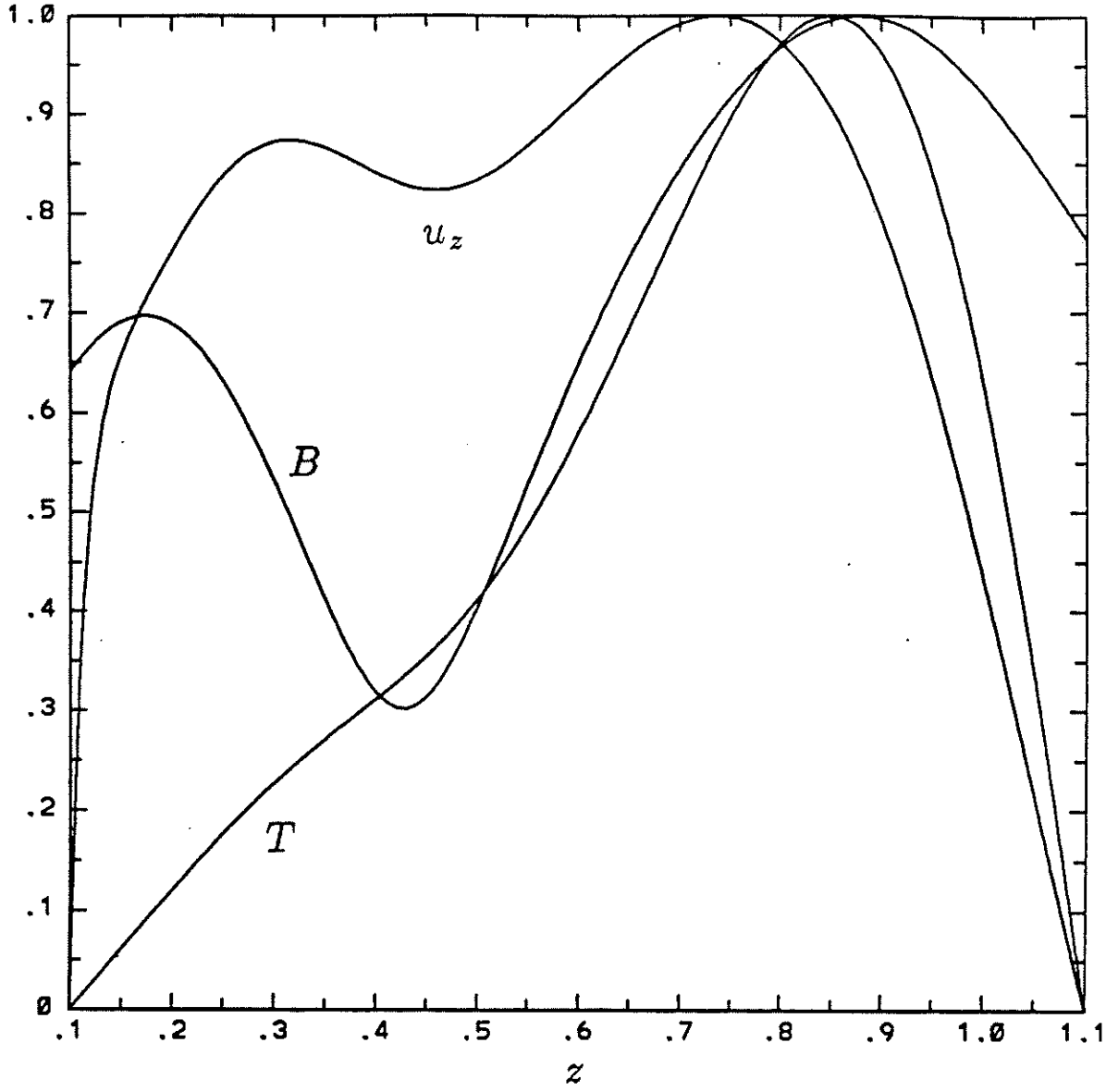

Figure 9(b). The amplitudes $\alpha/\alpha_{\max}$, $\beta/\beta_{\max}$ and $\gamma/\gamma_{\max}$ of u_z, B, and T on the primary branch for convection in the free compressible duct for the case $z_0 = 0.1, \Lambda = 6, r = 700$ and the wavenumbers $k = 1.117$ and $l = 1.668$ that minimize r on linear Boussinesq theory for $\Lambda = 6$. Here $\alpha_{\max} = 373.07$, $\beta_{\max} = 2.911$ and $\gamma_{\max} = 2848.0$.

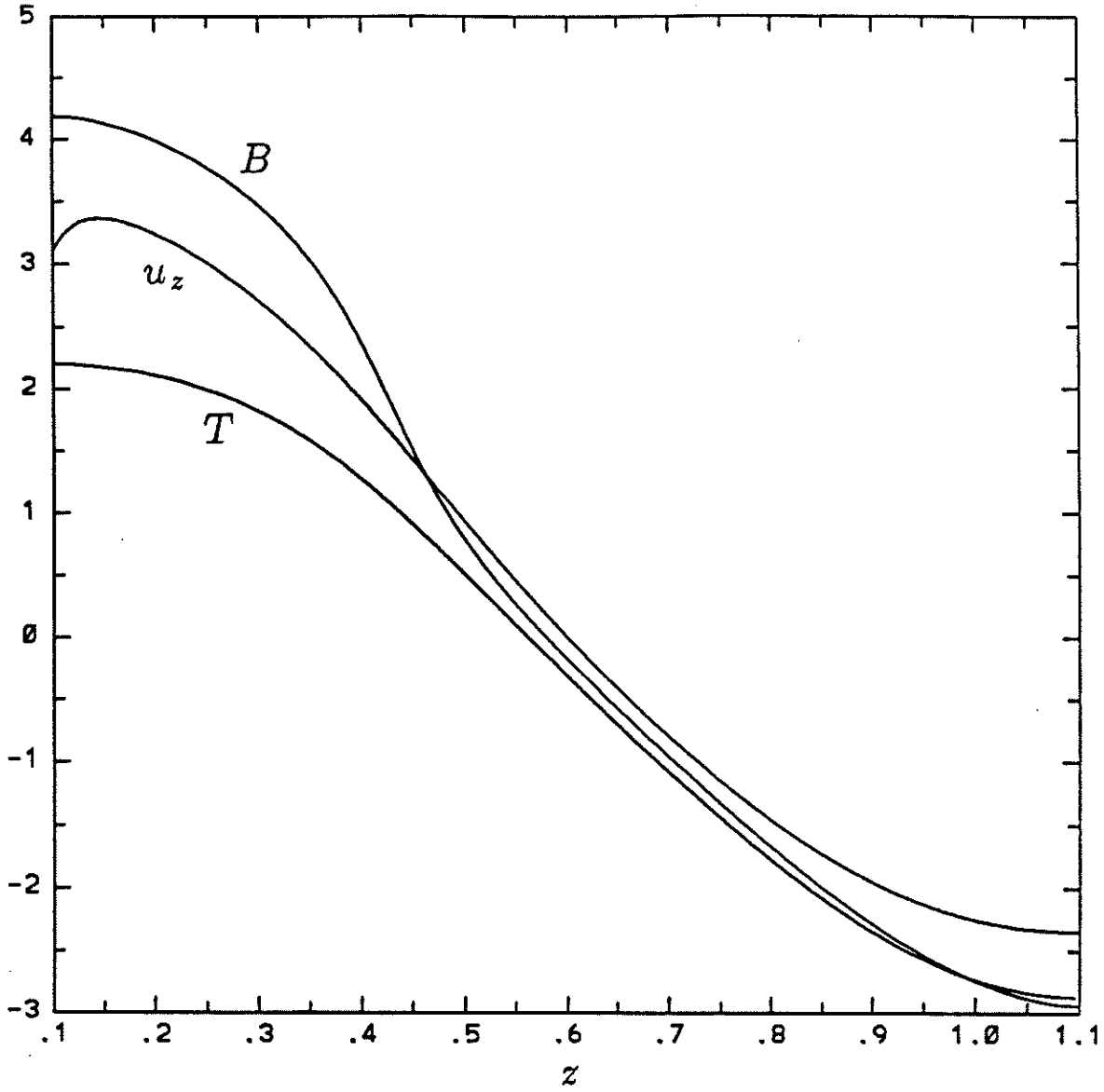

Figure 9(c). The phases θ, ϕ and ψ of u_z, B, and T on the primary branch for convection in the free compressible duct for the case $z_0 = 0.1$, $\Lambda = 6$, $r = 700$ and the wavenumbers $k = 1.117$ and $l = 1.668$ that minimize r on linear Boussinesq theory for $\Lambda = 6$.

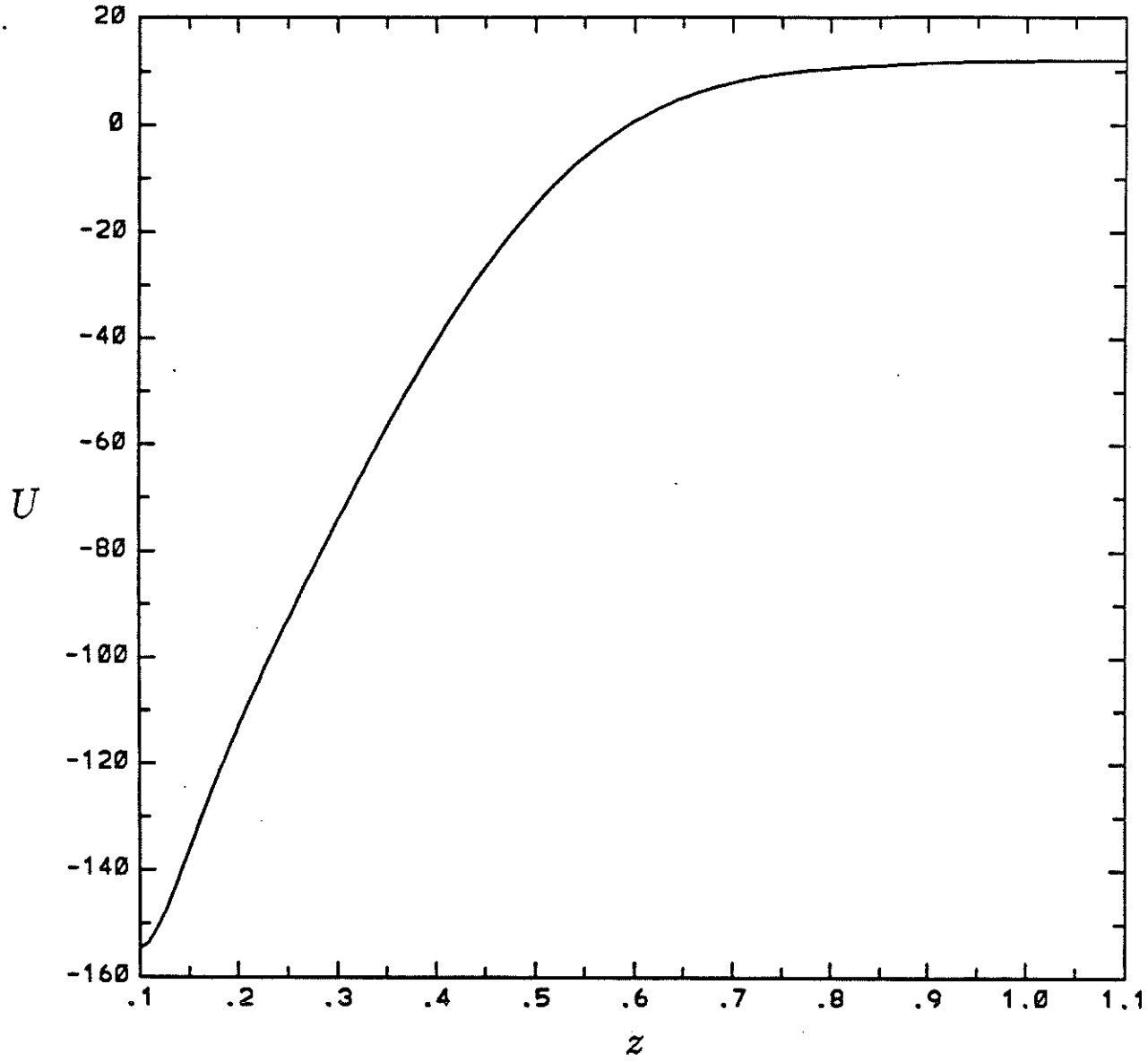

Figure 10(a). The geostrophic velocity on the secondary branch for convection in the free compressible duct for the case $z_0 = 0.1$, $\Lambda = 6$, $r = 700$ and the wavenumbers $k = 1.117$ and $l = 1.668$ that minimize r on linear Boussinesq theory.

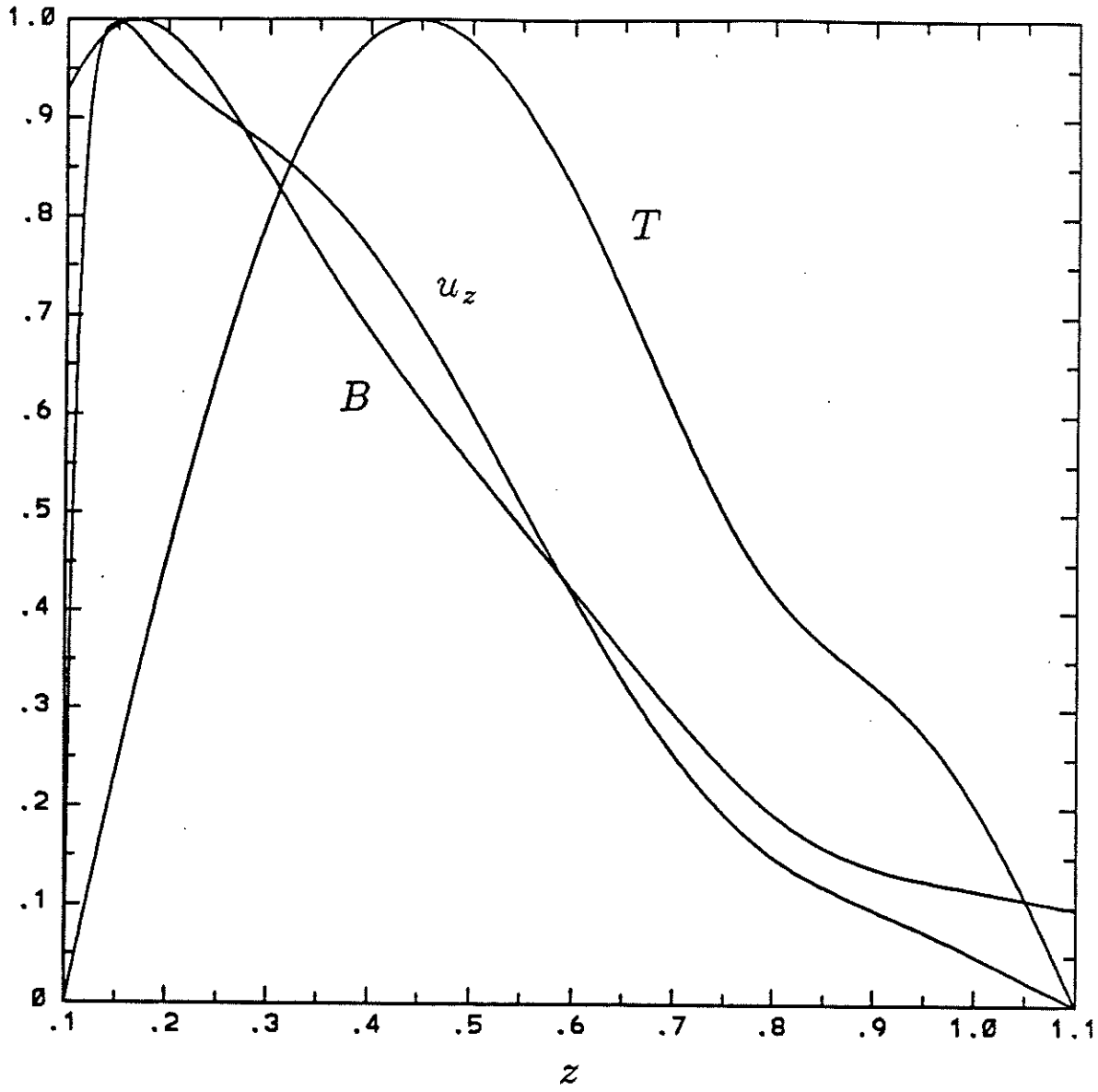

Figure 10(b). The amplitudes $\alpha/\alpha_{\max}$, $\beta/\beta_{\max}$ and $\gamma/\gamma_{\max}$ of u_z, B, and T on the secondary branch for convection in the free compressible duct for the case $z_0 = 0.1$, $\Lambda = 6$, $r = 700$ and the wavenumbers $k = 1.117$ and $l = 1.668$ that minimize r on linear Boussinesq theory. Here $\alpha_{\max} = 673.42$, $\beta_{\max} = 4.358$ and $\gamma_{\max} = 1690.5$.

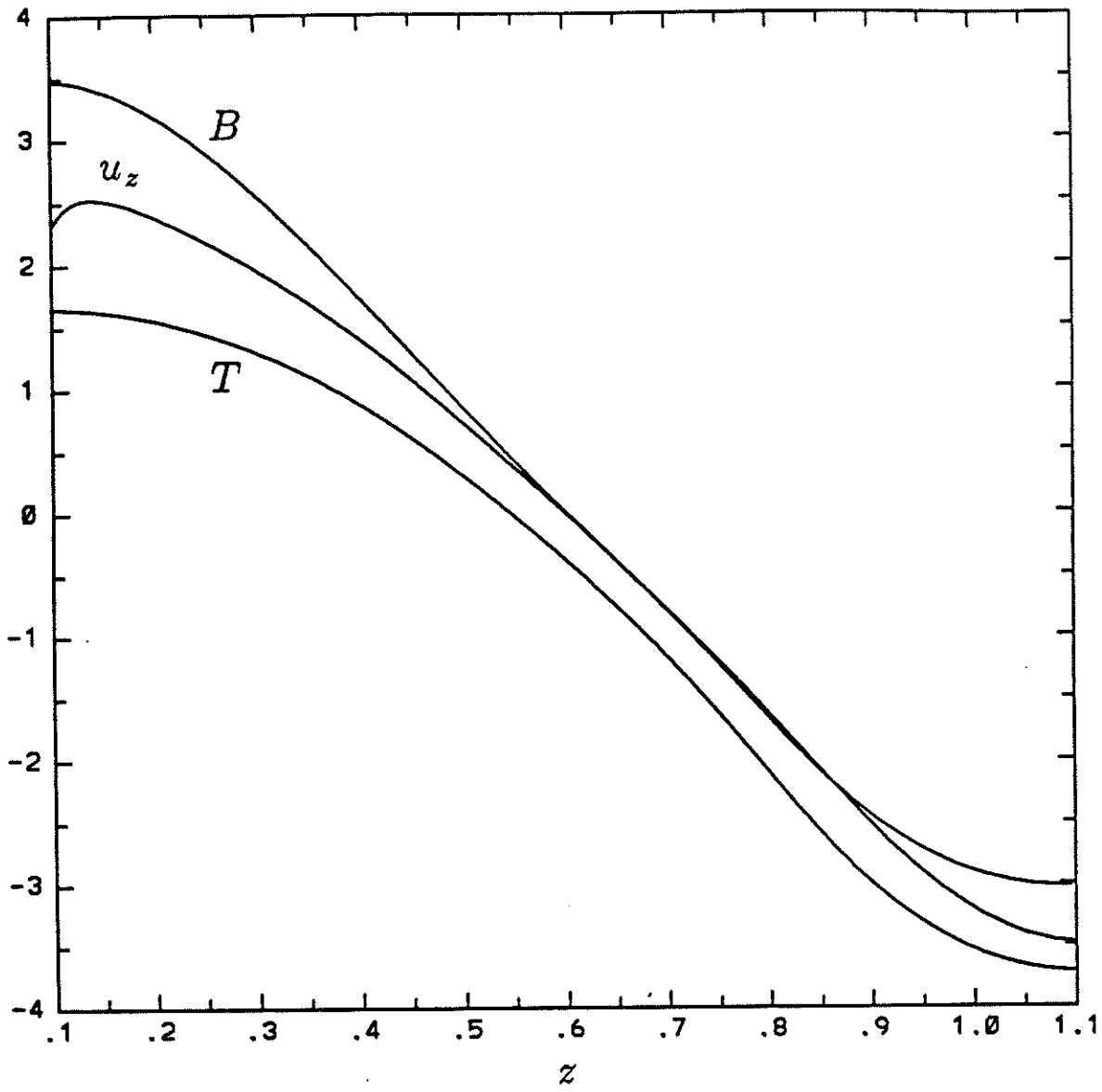

Figure 10(c). The phases θ, ϕ and ψ of u_z, B, and T on the secondary branch for convection in the free compressible duct for the case $z_0 = 0.1, \Lambda = 6, r = 700$ and the wavenumbers $k = 1.117$ and $l = 1.668$ that minimize r on linear Boussinesq theory.